University of New Mexico
UNM Digital Repository

Electrical and Computer Engineering ETDs Engineering ETDs

Spring 5-13-2017

Thermoreflectance Technique for Thermal Properties Measurement of Micro/Nanoscale Cantilever Beams

Mirza M. Elahi
University of New Mexico

Follow this and additional works at: https://digitalrepository.unm.edu/ece_etds

Part of the Electrical and Computer Engineering Commons

Recommended Citation
Elahi, Mirza M.. "Thermoreflectance Technique for Thermal Properties Measurement of Micro/Nanoscale Cantilever Beams." (2017). https://digitalrepository.unm.edu/ece_etds/346

This Dissertation is brought to you for free and open access by the Engineering ETDs at UNM Digital Repository. It has been accepted for inclusion in Electrical and Computer Engineering ETDs by an authorized administrator of UNM Digital Repository. For more information, please contact disc@unm.edu.

Mirza Mohammad Mahbube Elahi

Candidate

Electrical and Computer Engineering

Department

This dissertation is approved, and it is acceptable in quality and form for publication:

Approved by the Dissertation Committee:

Dr. Ashwani Sharma, Chairperson

Dr. Ganesh Balakrishnan, Committee Member

Dr. Mark Gilmore, Committee Member

Dr. Naz Islam, Committee Member

Thermoreflectance Technique for Thermal Properties Measurement of Micro/Nanoscale Cantilever Beams

by

MIRZA MOHAMMAD MAHBUBE ELAHI

B.Sc., Electrical and Electronic Engg., Islamic Univ. of Tech., 2007
M.Sc., Electrical Engineering, University of New Mexico, 2011

DISSERTATION

Submitted in Partial Fulfillment of the
Requirements for the Degree of

Doctor of Philosophy
Engineering

The University of New Mexico
Albuquerque, New Mexico

May, 2017

DEDICATION

I dedicate this dissertation to my wife (Zakia Afrin), newborn daughter (Sanaaz Afrin Elahi), my parents (Md. Fozle Elahi and Latifa Begum), my brothers (Mirza Mohammad Lutfe Elahi, Mirza Mohammad Monzure Elahi and Mirza Mohammad Maqbule Elahi), my parents in law (ATM Ashraf and Selina Ashraf), my brother in law (Ferdous Mohammad Aktab) and to my late best friend Abeedur Rahim for their continuous support and motivations in my bad and good days throughout my graduate studies. Without my wife's help and understanding, I would not be able to reach this stage right now and my parents were always been the motivator of my life who raised me, taught me to be a good person and always supported me however they can. My elder brother was always been the beacon of my life to guide me in the path that I needed to travel with hope and courage. They always encouraged me, helped me in difficulties which I will not be able to ever re-pay. I would like to thank them from my bottom of my heart for their sacrifice and well wishes.

ACKNOWLEDGMENTS

So many people has their contributions to fulfilling my quest to achieve the degree what I always revered for, their help and continuous support always motivated me to wake up next morning and keep working thorough out my graduate studies. I would like to thank first of all University of New Mexico and Department of Electrical and Computer Engineering for giving me an opportunity to have a quality education with lot of diversity and their continuous support thorough out the years. Also Manufacturing Training and Technologies Center, for giving me the opportunity to have experience in the field I always liked. I also like to thank Dr. Ashwani Sharma and Dr. Ganesh Balakrishnan for their continuous support and motivation to achieve the degree. Without the help of all of my colleges and the Bangladeshi students here at Albuquerque who had their impact in their own way to live a social and educational life which ease my goal to achieve. I am proud being a student of UNM and honored to have such good friends and colleagues throughout the years.

I would like to thank my wife, parents, brothers, parents in law and brother in law to have trust in me and supporting me during all the years. Without their support and motivation I would not be able come this far. And for most I want to thank Allah for giving me the strength, intellect and will power to pursue my dream and showing me the path of hope in all difficulties.

Thermoreflectance Technique for Thermal Properties Measurement of Micro/Nanoscale Cantilever Beams

by

Mirza Mohammad Mahbube Elahi

B.Sc., Electrical and Electronic Engineering, Islamic Univ. of Tech., Bangladesh, 2007

M.Sc., Electrical Engineering, University of New Mexico, USA, 2011

Ph.D., Engineering, University of New Mexico, USA, 2017

ABSTRACT

Thermal property analysis of thin film materials on a semi-infinite substrate is a very important area of research in last few decades due to the deviation of their properties from its bulk values and measurement technique plays very important role to be free from the effect of interface conductance, surface impurities, convective and radiative losses and fabrication tolerances. Non-contact optical measurement technique drew attention to be applicable to measure thermal properties using pump-probe thermoreflectance where short pulse Laser beam applied to the film to avoid heat loss with the inclusion of the interfacial conductance and extract thermal diffusivity which is coupled to the thermal conductivity and the heat capacity of the film. This work extends the technique using Continuous Wave laser to freestanding cantilever beams for thermal properties measurement more accurately and without having any affect from interfacial conductance where heat flow is dominantly driven by 1-D heat conduction due to the device structure and experimental conditions. The pump beam applies a constant flux to the free end of the cantilever thereby inducing a

thermal gradient along its length which is measured by the probe beam. Measurement of the thermal gradient allows for determination of the thermal conductivity of the material. First of all, the cantilever beam structure was chosen due to its 1D structure and free from the effect of the interface conductance and convective and radiative heat losses are minimized by performing the experiment at high vacuum and removing the substrate underneath the beam. Specific heat capacity of the cantilever beam also can be extracted by applying harmonic signal of the pump flux at the free end of the beam, furthermore the specific heat capacity verified using transient analysis of the heat flux using probe laser thermoreflectance. We demonstrate the technique by measuring the thermal conductivity of a 1.29 μm thick piece of Si. The sample demonstrated ~30% reduction in thermal conductivity when compared to the bulk value and the specific heat capacity ~ $760JKg^{-1}K^{-1}$, does not have much change from its bulk.

Table of Contents

Chapter 1 1

1.1 Heat transport in solids due to conduction 3

1.2 Thermal Properties Measurement: 5

1.3 Thermal Conductivity Measurement Technique: 7

1.3.1 Cross Plane Measurement Technique: 7

1.4 Size Effect: 10

1.5 Heat Capacity: 13

1.6 Thermoreflectance Measurement: 14

1.6.1 Temperature and Thermoreflectance Correlation: 15

1.6.2 Transient Thermoreflectance Method: 17

1.6.3 Time Domain Thermoreflectance: 20

1.6.4 Frequency Domain Thermoreflectance: 23

Chapter 2 27

2.1: Cantilever Beam Structure: 27

2.2: Device Fabrication: 27

i. Cantilever Beam: 27

ii. Semi-infinite Sample: 33

Chapter 3 34

3.1 Theory: 34

3.1.1 Measurement of Thermoreflectance Coefficient of Aluminum for Semi-infinite Structure: 35

3.1.2 Steady State Analysis for Cantilever Beam: 36

3.2 Experimental Setup: 36

3.2.1 Spot Size Measurement: 38

3.2.2 Vacuum Chamber Fabrication: 40

3.2.3 Topside probing: 41

3.2.4 Thermal Gradient Probing: 44

3.3 Results: 46

3.4.1 Thermorfeflectance Coefficient of Aluminum Measurement: 46

3.4.2 Cantilever beam tip temperature measurement: 47

3.4.3. Change of reflectance along the beam measurement: 47

3.4.4 Measurement of Thermoreflectance Coefficient of Si: 48

3.4.5 Thermal Gradient profile extraction along the beam: 49

3.4.6 Thermal Conductivity of Si cantilever Beam: 50

3.5 Constraint Validation: 51

3.5.1 1D Heat Transfer Validation: 51

3.5.2 Temperature Boundary condition Validation 52

3.6 Validation of only Conduction 53

3.6.1 Convective Loss: 53

3.6.2 Radiative Loss: 55

Chapter 4 56

4.1 Theory: 56

4.1.1 Semi Infinite Frequency Domain Thermoreflectance Analysis: 56

4.1.2 1D Harmonic Thermoreflectance for Free Standing Structure: 57

4.2 Experimental Setup: 59

4.3 Results: 64

4.3.1: Semi Infinite Sample Result validation: 65

4.3.2 Cantilever Beam Phase Response: 66

Chapter 5 68

5.1 Theory 68

5.2 Experimental Setup: 69

5.3 Results: 70

Chapter 6 72

1. Analysis of thermal Conductivity with Various Film Thickness: 73

2. Measurement at Cryogenic: 73

3. Phononic Crystal Structure Measurement: 75

References 77

Appendix 81

Appendix A: Fabrication Process Flow 81

Appendix B: Supporting Experimental Data 85

Appendix C: Matlab Script 89

1. Steady State: 89

2. Hermonic Analysis: 93

3. Transient Analysis: 96

List of Figures:

Figure 1.1: Schematic cross section of the 3ω sample geometry for cross plane thermal conductivity measurement.[21] 8

Figure 1.2: Cross section of an in-plane thermal conductivity measurement setup. 10

Figure 1.3: Dependence of thermal conductivity of Si on the film thickness........ 12

Figure 1.4: Phonon mean free path variation contribution to the accumulated thermal conductivity due to size effect.[3] 12

Figure 1.5: Al film heat capacity for different temperature and thickness. 13

Figure 1.6: Thermoreflectance coefficient vs. illumination wavelength for various materials.[39] 17

Figure 1.7 Transient Thermoreflectance Technique 19

Figure 1.8: (a) Modulated pump beam (b) The surface temperature of the sample (c) Probe pulses reflected back to a detector after a certain delay (d) Measured probe signal and reference signal.[12] 22

Figure 1.9: Frequency Domain Thermoreflectance steup[6] 24

Figure 2.1: Photoresist pattern of cantilever beam 28

Figure 2.2: Microscopic image after RIE etch 29

Figure 2.3: Microscopic Al pad deposition and lift off 30

Figure 2.4: (a) Fabrication Steps; (b) Device Structure; (c) SEM images; (d) cleaved sample 33

Figure 3.1: Basic Steady State Thermoreflectance Measurement Setup 38

Figure 3.2: Spot size imaging setup 39

Figure 3.3: Spot Size Imaging Setup; (b) Spot size image 40

Figure 3.4: High Pressure small vacuum chamber for thermoreflectance measurement; the cross section of the chamber is shown in (a) and chamber with a handle to be attached to the optical stage is shown in (b).. 41

Figure 3.5: Top side measurement beam incident on cantilever beam............................ 43

Figure 3.6: Transducer side thermoreflectance measurement setup for Semi-infinite and cantilever beam at tip The front side thermoreflectance technique is used to measure the thermoreflectance coefficient of Al film deposited on the semi-infinite Si wafer and the change of reflectivity from Al pad tip of the cantilever beam... 43

Figure 3.7: Thermal gradient measurement architecture along the cantilever beam........ 44

Figure 3.8: Thermal gradient measurement setup for thermoreflectance along the cantilever beam. 45

Figure 3.9: Aluminum Thermoreflectance Coefficient for different incident power level 47

Figure 3.10: Change of reflectance along the beam length of a cantilever beam from the free end to the anchored side. Different power level of incident pump beam is shown to illustrate how the profile is changing.. 48

Figure 3.11: Temperature profile along the beam length extracted from the thermoreflectance measurement. 49

Figure 3.12: Thermal Conductivity of at different power levels of the incident pump beam.. 50

Figure 3.13: Heat flux FEM simulation results for slab structure; (b) heat flux FEM simulation results for isotherm analysis of cantilever beam.. 51

Figure 3.14: Thermoreflectance from cantilever beam tip for varying power, higher incident power induces non continuity of the linear response of thermoreflectance........ 53

Figure 3.15: Thermoreflectance response of a constact pump and probe beam displacement for a 2.4 mm cantilever beam from atmospheric pressure to $1X10^{-7}$ Torr. 54

Figure 4.1: Analytical and Numerical analysis result of cantilever beam in harmonic case from the frequency ranging from 10 Hz to 100Hz 59

Figure 4.2: Modulated Incident pump beam and thermally modulated reflected probe beam for harmonic analysis 60

Figure 4.3: Harmonic analysis setup for topside thermoreflectance measurement 63

Figure 4.4: Setup for harmonic analysis setup for backside thermoreflectance 64

Figure 4.5: Semi-infinite sample result validation with malen et at. [6]............................. 65

Figure 4.6: Semi-infinite result fit with the analytical analysis 66

Figure 4.7: Cantilever beam phase response between 400µm and 600µm from the center of the Aluminum pad of the free end of the cantilever beam. 67

Figure 5.1: Setup for harmonic analysis setup for backside thermoreflectance 69

Figure 5.2: Transient temperature response using pump probe technique on cantilever beam 71

Figure 5.3: Analysis of rise and fall time with different incident laser power 71

Figure 6.1: Thermal conductivity variation with film thickness extracted from different author and comparison to our analysis 73

Figure 6.2: Cryogenic setup design for low temperature application 74

Figure 6.3: installation of Cryogenic Setup for low temperature measurement application 75

Figure 6.4: Phononic Crystals along the slab of cantilever beam to compare thermal conductivity variation with their slab counterpart. 76

Chapter 1

Introduction and Background

The design of thin film and miniaturized semiconductors electronic devices for specialized application has drawn considerable attention in recent years. Thus the measurement and analysis of thin films properties, including its thermal characteristics, is of importance since the material parameters may deviate from the bulk values. As the dimensions shrink, specifically as the mean free path of phonon becomes comparable to the device's dimensions, the measurement techniques will also play an important role in the extraction of such properties as thermal conductivity and heat capacity etc. In addition heat transfer analysis becomes a challenge for thin films deposited on semi-infinite structures, mainly due to interface conductance, surface impurities, convective and radiative losses and fabrication tolerances. This is especially true for materials used for low temperature applications where a small change in temperature may cause a change in the phonon mean free path, thus affecting the material's thermal properties.[1–5] In last few decades, pump-probe thermoreflectance measurement technique is an area of growing interest for thermal properties measurement of thin film materials due to the nature of no-contact optical measurement, accurately applicable co-relating with the thermal decay and change in refractive index due to temperature change.[6–12]. In recent past, pump probe technique has been developed using femto second laser pulse heating and measurement with the inclusion of interfacial conductance with the substrate materials, expensive laser usage due to fact that convection can be avoided by measuring beyond nano second pulse heat. These are

one of the obstruction of the pump-probe measurement which also requires high precision measurement without effecting varying thermal induced material properties.

In our study, pump-probe technique to be applied on a cantilever beam structure which forces the heat to be transport by only 1-D heat conduction as the width and thickness are very small comparing with the length of the device. Due to the device structure, we can apply steady state heat conduction to extract the thermal conductivity of the material which is free from any interfacial conductance of the substrate materials, it does not require expensive femto second laser. The measurement were taken installing the device in high vacuum chamber to avoid any kind of heat loss due to convection and the radiation is eliminated by cleaving the surface underneath of the cantilever beam. Then the experiment is conducted for harmonic and transient analysis for the measurement of heat capacity of the material. We will be able to show in this study how the thermal conductivity of material varies due to effect of film thickness and heat capacity follows literature value and does not have thickness varying effect on the measurement.

The classical form of heat transport was first published by Jean Baptiste Joseph Fourier in 1807 in the theoretical framework of transient heat conduction equation with the consideration of the differential form of the heat conduction equation which develops the basics of how thermal energy flows in bulk materials and governed by the temperature gradient and the heat flux boundary conditions.

$$\nabla^2 T + \frac{Q}{\kappa} = \frac{1}{\alpha}\frac{\partial T}{\partial t} \tag{1.1}$$

Heat flow is solely dependent on the geometry of the experiment and the thermal properties of its heat carrier, comprised of thermal conductivity, κ, density, ρ, and heat capacity, C. These are the parameter defines the nature of heat flow with the inclusion of any generation term inside the material. The terms Q is the internally generated thermal power and the α is thermal diffusivity, respectively, where $\alpha = \frac{\kappa}{\rho C}$. The variable t represents time. Thermal conductivity is the material property which can be easily identified using Fourier's law of heat flux but it contains lot of information of the materials itself which are understood using complex set of analysis and relationships between energy transport via quantized packets, carrier of heat either by phonon (lattice vibration) or electron or both. Considering the heat carrier, boundary condition and the initial condition of the system the whole picture of thermal energy transport can be understood and can be applied on thin film materials considering the phonon mean free path way smaller than the dimension of the structure. This dissertation focuses on the measurement of thermal properties measurement technique and their variation from the bulk values which governs the role in heat conduction through solid, semiconductor materials fabricated on the nanoscale.[13–16]

1.1 Heat transport in solids due to conduction

Heat transport mechanism is mainly governed by three mechanism which are conduction, convection and radiation, these are commonly characterized through measurement of the spatially dependent thermal potential energy, k_bT, defined through temperature, T. Conduction is the dominant heat transfer mechanism in solid materials. Convective heat transport can be eliminated due to fact that lack of mass transport prevents it to occur and radiative effects are negligible. If a homogeneous and axisymmetric material is heated in

one end and the other end is kept at cold or ground then the 1D material has a temperature gradient along the length. For a steady state condition of such material, the thermal conductivity of the solid is determined using Fourier's law of heat conduction for one dimension,

$$q'' = -\kappa \frac{\partial T}{\partial x} \quad (1.2)$$

where the heat flux, q'', per unit area, A is generated along the length of the 1D system due to the temperature gradient, $\frac{\partial T}{\partial x}$ sustained by the material with the relative magnitudes determined by the thermal conductivity, κ.

Heat Conduction Equation correlates the 1st order time derivative and 2nd order spatial derivative of temperature with a constant of thermal diffusivity, $\alpha = \frac{\kappa}{\rho C}$. Thermal diffusivity depends on the thermal property where κ is C is the specific heat capacity and ρ is the density of the material.

$$\frac{\partial T}{\partial t} = \alpha \frac{\partial^2 T}{\partial x^2} \quad (1.3)$$

Heat conduction equation can be proven using Fourier’s empirical law of heat transfer shown in eqn. 1.1 and the Integral Conservation Law shown in eqn. 1.4.

$$\frac{\partial e}{\partial t} = -\frac{\partial q''}{\partial x} + Q \quad (1.4)$$

$$e(x,t) = \rho(x)C(x)T(x,t) \quad (1.5)$$

The rate of heat transfer is defined by not by the thermal energy differential, ΔT, but by the gradient, implies that heat transport is a diffusion limited process. Integral Conservation Law of heat transfer correlates the time derivative of thermal energy density and spatial

derivative of heat flux with the internal generation (Q) term in eqn. 1.4. And the thermal energy density also defined as in eqn. 1.4 which is dependent on the density, specific heat capacity and the temperature at that point and time. Heat conduction equation with no internal generation term can be proved (eqn. 1.3) using all the eqns. 1.2, 1.4 and 1.5.

Thermal conductivity of a solid material is a material property and it correlates the relationship with its energy-carrying quasi particles using classical kinetic theory of gases and can be approximated as,[2,17,18]

$$k = \frac{1}{3} C v \lambda \tag{1.6}$$

where the values of heat capacity, C, velocity, v, and mean free path, λ, are identical for all particles. The average distance traveled by a particle before it collides with other one or the wall of the system is known as the phonon mean free path. In this approximation heat conduction is contributed by all particles which are equal and indistinguishable. The normalized product of Cvλ with three degrees of freedom implies that the thermal conductivity must be taken as an average value for a particular direction. It is well known that thermal energy in solids is transported by phonons and electrons, such that $k = k_{ph} + k_e$. In case of metals, $k_e \gg k_{ph}$ and $k \approx k_e$; for dielectrics $k_{ph} \gg k_e$and $k \approx k_{ph}$and for semiconductor $k_e \approx k_{ph}$ in this case both the thermal conductivity of phonon and electron contribute to the cumulative thermal conductivity of the material.

1.2 Thermal Properties Measurement:

Different measurement technique of thermal diffusivity, $\alpha = \frac{\kappa}{\rho C}$ have been applied in recent years to extract thermal conductivity of thin film or bulk materials. The measurement technique can be involved in spatially and periodically to extract the properties with appropriate boundary conditions and experimentally feasible measuring parameters.

1. Steady-state measurement: Steady state measurement involves using Fourier's law heat conduction (eqn. 1.2) where heat capacity does not have any role to play and thermal conductivity is the free parameter to be measured. Temperature difference for a particular spatial difference can be measured using temperature sensor or other sensing methods and heat flux to be known in this equation.
2. Transient Measurement: Transient measurement of thermal properties involves in measurement using transient heat source with a temperature probe that can be localized spatially. Thermal conductivity and diffusivity can be highly sensitivity to the frequency of ac heat source. And frequency dependent measurement technique became very popular recent years to be able apply with accuracy.
3. Transient and Spatially: Transient and spatially varying T is a measurement technique with their linear superposition that commonly uses analogy between electrical and thermal transport qualitatively classify the various heat transfer regimes. In electrical analogy, Ohm's law $I = \frac{\Delta V}{R}$ is compared with Fourier's law of heat transfer in 1 D, $= \frac{\Delta T}{K}$, where K is the thermal resistance of the material. The following equivalencies can be made,
   i. $\sigma \approx k$
   ii. $I \approx P$
   iii. $\Delta V \approx \Delta T$

The formulation of Fourier's law of steady-state heat conduction can then be derived from Ohm's law,

$$I = \Delta V \left[\frac{L}{\sigma A}\right]^{-1} \approx P = \Delta T \left[\frac{L}{kA}\right]^{-1} \quad (1.7)$$

1.3 Thermal Conductivity Measurement Technique:

Thermal conductivity measurement technique can be divided among several conditions like depending on the direction of heat flow either it is cross plane or in plane thermal conductivity. It also can be divided among the nature of the measurement technique such as is it a contact method or an optical method etc. Below are some different measurement technique described in details.

1.3.1 Cross Plane Measurement Technique:

Cross plane thermal conductivity measurement using the flash method is one of the basic mechanism implemented by Parker, et al. In this technique a modulated heat lamp was used to impart a thermal pulse on the front side of axially symmetric sample and a thermocouple is used to monitor the subsequent heating on the back.[19] In this method the one dimensional heat was maintained through the thickness of the sample. A method developed by Birge and Nagel to measure the specific heat of liquids,[20] and the most widely used thermal measurement techniques is the 3ω method for solids, based on was first introduced by Cahill to measure the thermal conductivity of solids,[21] 3ω method utilizes a long, narrow metal line deposited on the surface of the sample which simultaneously acts as a heater and thermometer. A Sinusoidal AC heating is induced in the metal line through Joule heating

through an electrical current at angular frequency $\omega = 2\pi f$ .The current signal is rectified by the Joule heating term, which drives a temperature dependent resistance change of the metal line at 2ω. By monitored the voltage at 3ω which arises from the 1ω and 2ω resistance variation.

$$I \approx \exp(i\omega t), \qquad P \approx \exp(i2\omega t) \tag{1.8}$$

$$\Delta T \approx \exp(i2\omega t), \qquad \Delta R \approx \exp(i2\omega t) \tag{1.9}$$

$$\Delta V \approx I\Delta R \approx \exp(i3\omega t) \tag{1.10}$$

By manufacturing the heater width with respect to the film, the heat conduction equation can be formulated and the heat diffusivity of the film can be formulated. A schematic of 3ω method for thermal conductivity measurement is shown in fig 1.1

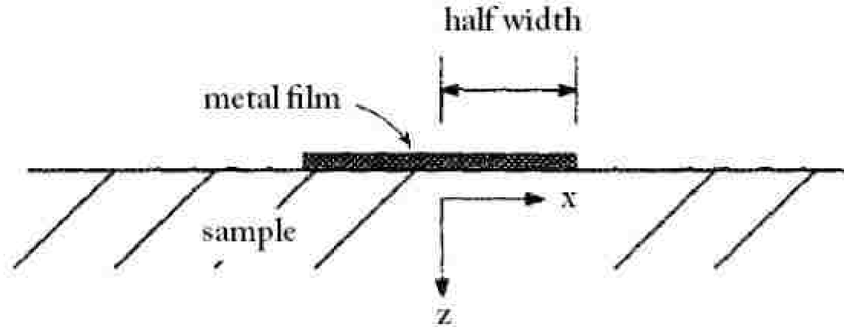

Figure 1.1: Schematic cross section of the 3ω sample geometry for cross plane thermal conductivity measurement.[21]

Considering the geometry and implementation issues associated with 3ω technique, Paddock and Easley[22] pioneered a technique "Time-domain thermoreflectance (TDTR)" which can measure predominantly the cross-plane thermal conductivity of any sample that has a smooth, reflective surface and is at least a few tens of nanometers thick. In principle, the rate at which the heat escapes into the bulk sample can be correlated by fitting to the

solution of heat conduction equation. In this process a pump laser is used capable of generating high power (excimer laser pulse) where the width of the pulse is on the order of picoseconds for the heating of the surface of the film and the optical energy is absorbed in an area of few square microns. A transducer layer of metal thin film is deposited on the surface for uniform heating as well as good reflection at probe wavelength. The change temperature of the surface is used to probe using a probe laser via change in the reflectance. The temperature dependence of the refractive index of the material which is known as thermoreflectance, by measuring how fast the heat diffuses across the plane the thermal properties of the material can be correlated solving heat diffusion equation with proper boundary condition. Thus directly measuring the thermal conductivity of a thin film, irrespective of substrate can be obtained without the limitations in the 3ω technique. [1,23–27]

1.3.2 In-plane Thermal Conductivity:

One of the important thin film thermal conductivity measurement technique is to measure the In-plane thermal conductivity of the material. This technique is designed in such a way that the thermal conductivity of the thin film is very large than the thermal conductivity of the substrate. It is very important in this technique that decoupling the thermal conductivity of the film from its substrate where the temperature profile can be measured without any effect of the substrate. The best way to design this experiment is using SOI wafer where Si device layer deposited on buried oxide layer. This technique can be implemented using measurement of two distinct point's temperature using electrical resistance thermometry. Due to the change in electrical resistant of that two point the temperature variation can be measured. For the heating of the thin film metal film is deposited which can behave as the

heater by joule heating. With or without the Si device layer, the metal heater is deposited on a suspended bridge. And also for the characterization, sensor's thermal contact has to be taken in to account for precise measurement. As heat conduction equation accommodates both the cross plane (k_{cp}) and the in-plane (k_{ip}) thermal conductivity and has the effect in the measurement simultaneously. By improving the 3ω technique, some more corrections and by manipulating the device structure the cross-plane thermal conductivity the in-plane thermal conductivity can be. A cross section of an in-plane thermal conductivity measurement setup is shown in fig 1.2.[11,26]

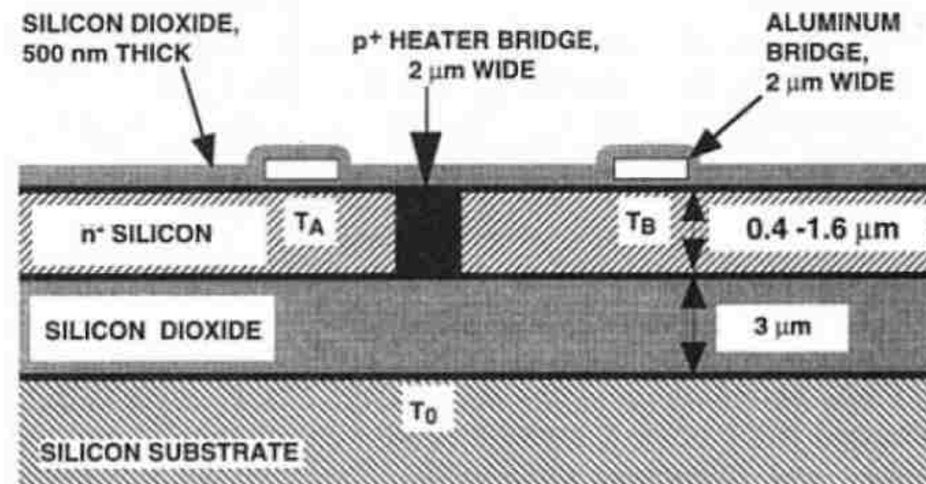

Figure 1.2: Cross section of an in-plane thermal conductivity measurement setup.

Measurement of In-plane thermal conductivity can also be implemented using thermoreflectance technique by measuring the in phase and out of phase voltage reflected from the sample and correlate with the constituent's thermal properties of the material.

1.4 Size Effect:

Films with thicknesses less than the length scale of their phonon mean free paths due to incoherent boundary scattering of phonons ballistically traversing the film, thermal conductivity can be reduced from the bulk value.[28,29] Phonons behavior analysis became a great challenge due to scattering, grain boundary of the film (for amorphous sample). Manipulation of phonon band structure also area of research in acoustic communication. Measurement technique can be an important factor to measure the thermal conductivity and depending on the structure of the material confining the heat in a certain direction can affect the thermal conductivity value, as the device sizes are shrinking the phonon mean free path gets comparable to the device structure and in turn manipulating the thermal conductivity of material. Variation of thermal conductivity of Si from its bulk has been reported repeatedly from various authors by correlating the phonon mean free path to the heat diffusion. The variation of membrane type film thermal conductivity with the thickness of Si is shown in figure 1.3 and thermal conductivity change with phonon mean free path in fig. 1.4 below.[3,10,28]

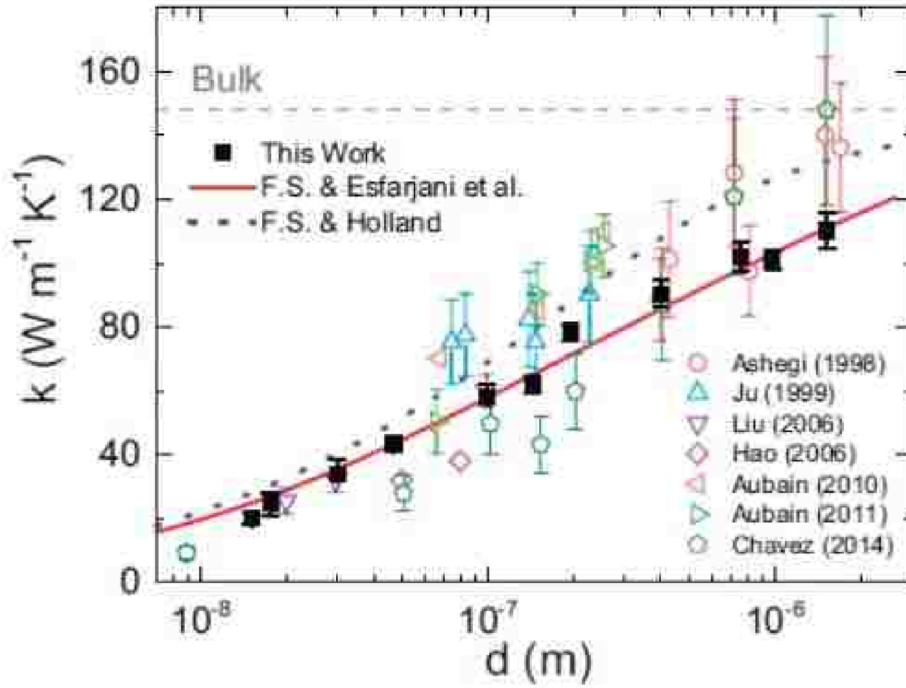

Figure 1.3: Dependence of thermal conductivity of Si on the film thickness

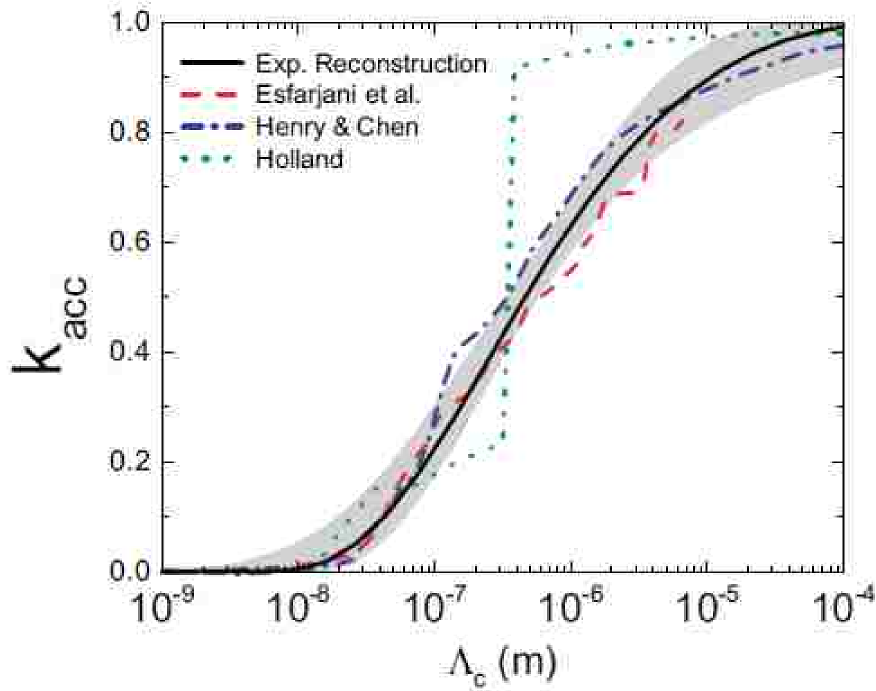

Figure 1.4: Phonon mean free path variation contribution to the accumulated thermal conductivity due to size effect.[3]

Phononic crystal structure where introducing holes in the films are dominantly effected by the size effect due to the fact that scattering starts play role in the heat transfer mechanism and which also effect the thermal conductivity for the entire structure.

1.5 Heat Capacity:

The specific heat capacity is a measure of how much energy is required for temperature to rise 1 degree for a unit mass.

$$C = \frac{Q}{m\Delta T} \tag{1.11}$$

Calorimetry technique is normally used to find heat capacity of macro to micro scale device structure.[30–35] Below is a demonstration of how heat capacity is varying depending on the temperature profile and the film thickness itself.

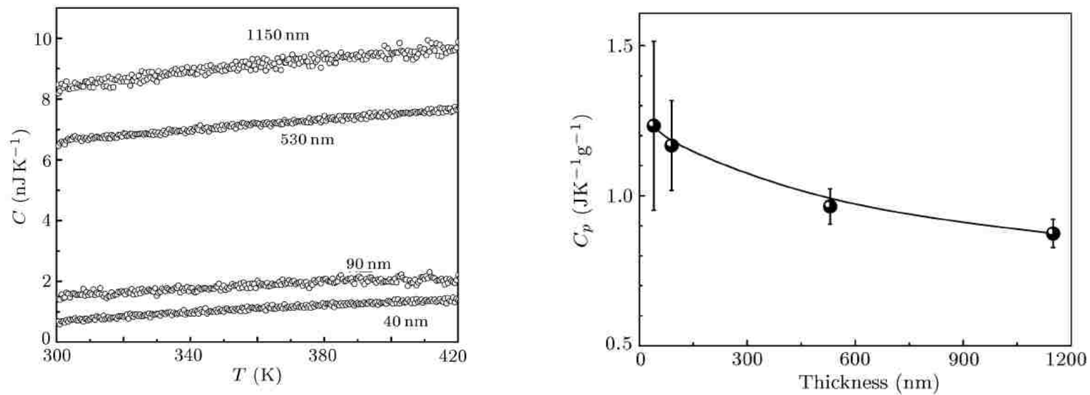

Figure 1.5: Al film heat capacity for different temperature and thickness.

It is a very important area of research because recent studies demonstrates heat capacity is not a parameter depends on the size of the film. As the device sizes are shrinking it needs to make sure how it is effecting the results extracted using the constant value of heat capacity? Our aim would be in this study measuring thermal conductivity using Fourier's law for steady state case which is totally free from the effect of heat capacity and using that

value extract specific heat capacity with harmonic and transient analysis using thermoreflectance technique.

1.6 Thermoreflectance Measurement:

Thermoreflectance measurement technique is a non-contact optical measurement technique that enables the measurement of thermal properties of metal, interface or semiconductor by measuring the change of reflectance or dielectric property with the change in temperature. Applying heat diffusion equation with appropriate initial and boundary condition the thermal conductivity can extracted with more accuracy and avoiding experimental tolerance. The basis of thermorelctance is implemented by deposition of a metal transducer film on top of the film of interest for uniform heating of the material. Heating the metal film using laser source creates shift in the fermi level and that induces band bending in the semiconductor film. Precaution should be taken that the perturbation of reflectivity due to change in temperature should be linearly dependent which means the change of temperature should be small enough that does not vary other material property like thermoreflectance coefficient. It also requires diligent approach to make sure the heating spot and its position at the film, measuring the change of reflectivity with appropriate alignment of the reflected beam and sample itself. When the phenomena of thermoreflectance is implemented to measure temperature, it must be assured that the temperature excursion is relatively small, typically on the order of a few degrees Kelvin, such that the proportionality of change in reflectance to the change in temperature can be approximated as linear. [8]

1.6.1 Temperature and Thermoreflectance Correlation:

The change in refractive index or equivalently the change in dielectric constant due to change in temperature is physical basis of Thermoreflectance Technique. In this part, we will show that the correlation between the change in temperature with reflectivity. For a normally incident electromagnetic wave the reflectivity of a surface of a material in a medium of air ($n_{air} = 1$) can be defined as,

$$R = \left(\frac{\tilde{n} - 1}{\tilde{n} + 1}\right)^2 \tag{1.12}$$

where $\tilde{n}$ is the complex refractive index, it can be represent in terms of the real part of the refractive index, n, and the imaginary part of the refractive index or attenuation constant, k as $\tilde{n} = n + ik$. By expanding eqn. 1.12 with respect to the real part and the imaginary part the reflectivity is expressed as,

$$R = \frac{(n-1)^2 + k^2}{(n+1)^2 + k^2} \tag{1.13}$$

Change in reflectivity due to change in the real and imaginary part can be extracted by differentiating the reflectivity with respect to n and k. And doing some normalization with the reference reflectivity it yields the normalized modulation of R,

$$\frac{\Delta R}{R} = \frac{4(n^2 - k^2 - 1)\Delta n + 8nk\Delta k}{[(n+1)^2 + k^2][(n-1)^2 + k^2]} \tag{1.14}$$

The more simplification of Eqn. 1.14 can be achieved by considering $k \ll n$, for the case of semiconductors near or below the fundamental absorption edge, eqn. 1.14 can be simplified to,

$$\frac{\Delta R}{R} = \frac{4\Delta n}{n^2 - 1} \tag{1.15}$$

Maxwell's equation relates the dielectric constant with refractive index and the complex dielectric constant, $\tilde{\epsilon}$, (in a non-magnetic material) is related to $\tilde{\epsilon}$ such that $\tilde{\epsilon} = \tilde{n}^2$. By separating the real and imaginary parts, the relations are,

$$\epsilon_1 = n^2 + k^2 \tag{1.16}$$

$$\epsilon_2 = 2nk \tag{1.17}$$

solving equations (1.12) and (1.13) for n and k obtains,

$$n = \sqrt{\left[\frac{1}{2}\sqrt{(\epsilon_1^2 + \epsilon_2^2)}\right] + \frac{1}{2}\epsilon_1} \tag{1.18}$$

$$k = \sqrt{\left[\frac{1}{2}\sqrt{(\epsilon_1^2 + \epsilon_2^2)}\right] - \frac{1}{2}\epsilon_1} \tag{1.19}$$

Due to dielectric constant modulation the modulation of reflectivity can be obtained by substituting (1.18) and (1.19) into (1.14), and the equation is,

$$\frac{\Delta R}{R} = \frac{2A}{A^2 + B^2}\Delta\epsilon_1 + \frac{2B}{A^2 + B^2}\Delta\epsilon_2 \tag{1.20}$$

where,

$$A = n(n^2 - 3k^2 - 1) \tag{1.21}$$

$$B = k(3n^2 - k^2 - 1) \tag{1.22}$$

and, if the dielectric constant is a function of temperature,

$$\Delta\tilde{\epsilon} = \frac{\partial\tilde{\epsilon}}{\partial T}\Delta T \tag{1.23}$$

then it establishes the mathematical basis for thermoreflectance.[36,37]

In the case of first order approximation of relationship between change in surface temperature and change in surface reflectivity is given as,[4,36,38]

$$\frac{\Delta R}{R} = \left(\frac{1}{R}\frac{\partial R}{\partial T}\right)\Delta T = C_{TR}\Delta T \tag{1.24}$$

where, T is the surface temperature in units K, R is the reflected illumination intensity from the surface of the sample, and C_{TR} is the thermoreflectance coefficient in the unit of k^{-1}.The thermoreflectance coefficient is a wavelength dependent parameter.[39,40] The variation of thermoreflectance coefficient for different material with respect to wavelength is shown in fig. 1.6. Which is very important in terms of selecting transducer material and their response at different wavelength to get maximum response in an experiment.

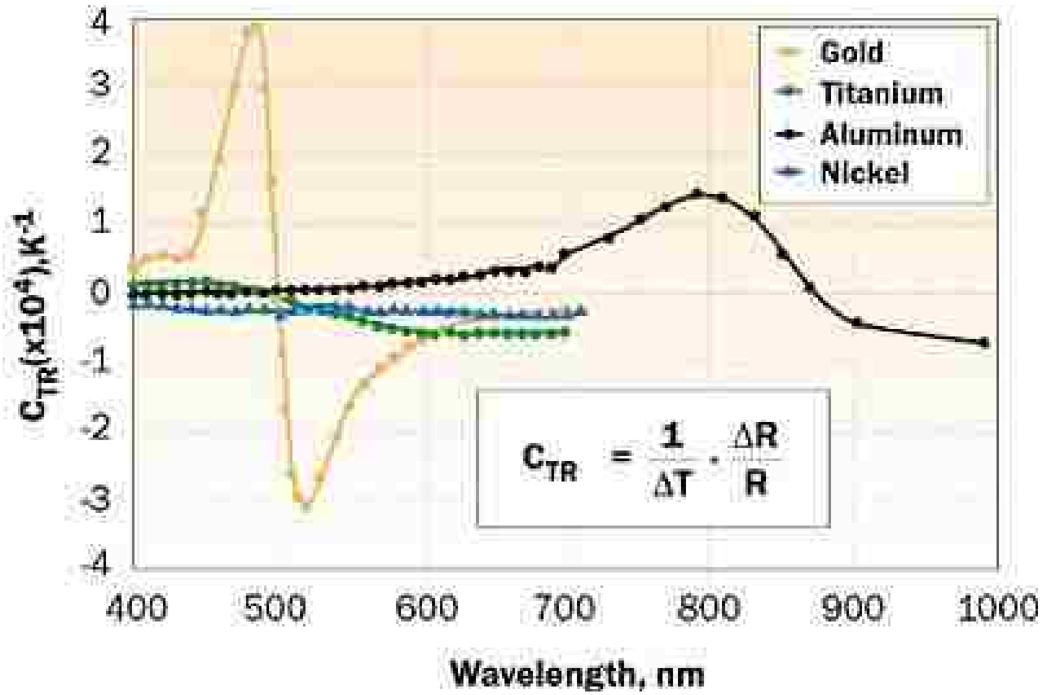

Figure 1.6: Thermoreflectance coefficient vs. illumination wavelength for various materials.[39]

1.6.2 Transient Thermoreflectance Method:

Transient Thermoremectance was first introduced by Eesley et al.[22] to measure thermal properties of metal film using an intense ultrashort laser pulse to generate a transient

thermal heat flux at the metal surface and another laser (probe) was used to monitor the change in reflectance at the surface. The change in reflectivity carries information of the thermal property of the material. Since then transient thermoreflectance method became very popular due to their nature of measurement having no contact with the surface later transient thermo-reflectance method (TTR) is used to determine the thermal conductivity of thin-film and multi-layered materials. The main advantage of the TTR method is that it is a non-contact and nondestructive optical approach, both for heating a sample under test and for probing the variations of its surface temperature. Because the method is non-invasive, it is attractive for the measurement of thermal properties of thin-layer materials whose investigation by invasive methods would present the difficulties of having to fabricate a measuring device into a sample, and then having to isolate and exclude the influence of the measuring device itself. The basic principle of the transient thermal reflectance method is to heat a sample by laser irradiation and probe the changes in the surface reflectivity of the heated material. The source of energy in the TTR method is normally provided by a pulsed laser with short pulse duration. During each pulse, a given volume on the sample surface heats up to a temperature level above ambient due to the laser light energy absorbed into the sample. The heating area is specified by adjusting the pulsing laser aperture and the optics of the system. The depth of the volumetric heating on the other hand, is determined by the optical penetration depth, which is a function of laser wavelength and surface material properties. The heating level through the light penetration depth (dk) obeys an exponential decay law after each laser pulse is completed, the sample begins to cool down to the initial ambient temperature. During this process, the probing CW laser light reflected from the sample surface at the heating spot center (probing spot in

figure) is collected on a photo detector that reads the instantaneous surface reflectivity. The changes in surface reflectivity are linearly proportional to the changes in surface temperature, within a wide but finite temperature range. The influence of a pulsed laser irradiation on a given material depends both on the optical properties of that material as well as on the wavelength and pulse duration of the laser itself. Thus, the wavelength and pulse width are important parameters in the determination of the effectiveness of the TTR method for different materials. [22]

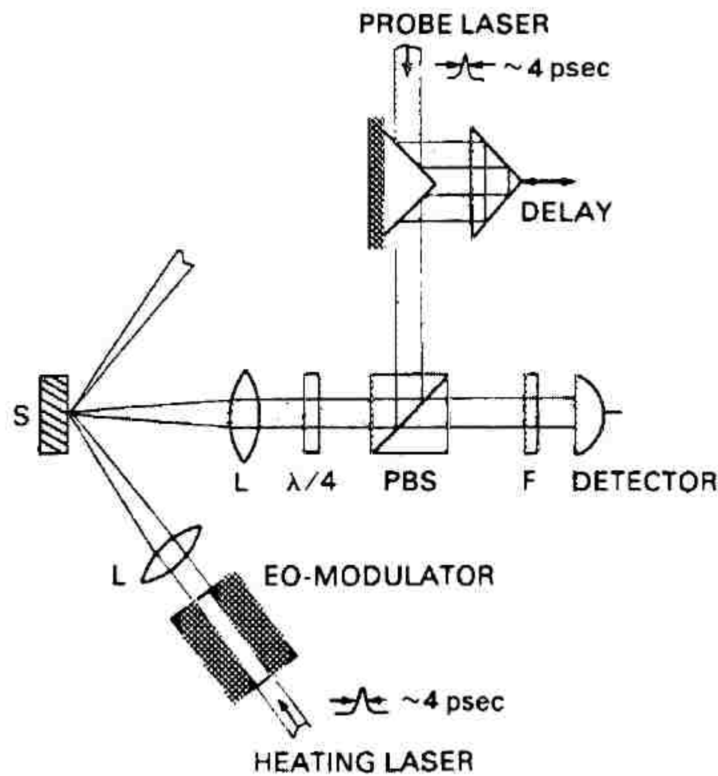

FIG. 1. Schematic diagram of the TTR optical arrangement. L: lens; F: filter; PBS: polarization beamsplitter; $\lambda/4$: quarter-wave retardation plate.

Figure 1.7 Transient Thermoreflectance Technique

The heat transfer within the metal film and the substrate material heated by a short-pulsed laser on a timescale greater than; 100ps is governed by the time dependent heat conduction

equation, which describes the thermal diffusion in the metal film and substrate, respectively:

$$C_f \frac{\partial \theta_f}{\partial t} = k_f \frac{\partial^2 \theta_f}{\partial x^2} \tag{1.25}$$

$$C_s \frac{\partial \theta_s}{\partial t} = k_s \frac{\partial^2 \theta_s}{\partial x^2} \tag{1.26}$$

where θ is the temperature above ambient, C is the thermal capacitance, and k is thermal conductivity. Upon absorption of a laser pulse, there is an immediate temperature gradient in the metal film given by eqn. 1.25 and a negligible temperature rise in the substrate. Therefore, initial conditions for the metal film and the substrate are:

$$\theta_f(x) = \frac{F(1-R)}{C_f \delta} e^{-x/\delta} \tag{1.27}$$

$$\theta_s = 0 \tag{1.28}$$

The time constant, τ, associated with diffusion of heat in the film can be approximated using:

$$\tau \approx \frac{d^2}{\alpha} \tag{1.29}$$

where, α is thermal diffusivity of the metal film and the d is the film thickness.

1.6.3 Time Domain Thermoreflectance:

The time-domain thermoreflectance (TDTR)[12,19,24,36] method is a very well researched area of non-contact optical measurement technique provides insight of material properties due to heat for thin film, multi-layer thin film and also bulk samples. It is basically pump probe technique where two laser beams are incident towards sample from two different beam paths having a delay of Δt between the beams. The sole purpose of pump beam is to heat

up the sample, it is directed onto the surface of the sample and heats up the sample surface. Depending on the properties of the materials either for bulk, film or multi-layer film heat diffusion occurs. On the hand, the probe beam is used to monitor the heat flux in the surface introduced by the pump beam and thermal properties of the material can be extracted by proper heat diffusion analysis enforcing on the surface and the material. The probe beam's intensity changes due to the change is temperature at the surface which eventually change the reflectivity of the sample. This change of reflectivity is correlated with the change in thermal properties and with proper boundary conditions free parameters like thermal conductivity, interfacial conductance of the material are extracted. This experiment also gives the sensitivity of the experiment towards the measured parameters.[12] Time domain thermoreflectance requires very fast pulse laser to measure the thermal properties due to the time constant of the material which is very expensive and requires high precision to implement. This technique can be applied at room temperature without having any vacuum chamber to prevent convective heat due to the very fast laser measurement the convection does not play any role in the heat transfer and also need to maintain low temperature difference that does not affect the temperature dependent parameters of material property. The basic steps of measurement using pump probe laser is shown in fig 1.8. Due to the time difference between the pump and probe laser it is capable of capturing the decay of temperature decay of each pulse. The main advantage or disadvantages of TDTR technique are below,

- Isolate the effect of interface conductance from thermal conductivity of thin layer.
- High time resolution, picoseconds (MHz)
- Equipment is complex

- Accuracy is typically limited to several percent due to uncertainties in the many experimental parameters

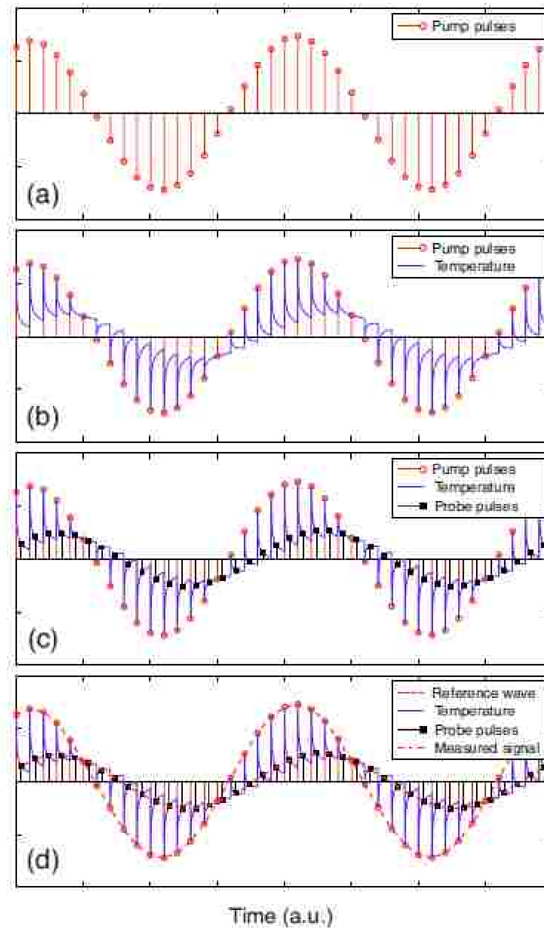

Figure 1.8: (a) Modulated pump beam (b) The surface temperature of the sample (c) Probe pulses reflected back to a detector after a certain delay (d) Measured probe signal and reference signal.[12]

The TDTR method is been applied in different structure, different type of material from metal, semiconductor, dielectric to polymers. This technique is capable of tracking material properties spanning a few nanometers to a few micrometers or millimeters.[8,9,28]

1.6.4 Frequency Domain Thermoreflectance:

Frequency-domain thermoreflectance (FDTR) is a non-contact pump probe optical measurement technique implemented in recent years to find thermal properties of bulk and thin film materials across long range of frequency spectrum. Heat transfer equation in this technique are analyzed in frequency spectrum to extract unknown parameters like thermal conductivity, interfacial thermal conductance etc. In this method a periodically modulated heat source using a pump laser applied on the film and probe beam either modulated or unmodulated tracked reflected from the film to compare with the incident beam. Either from amplitude or phase change from the incident to the reflected are analyzed to measure thermal properties of the material. A typical FDTR setup for thermoreflectance measurement is shown in figure 1.9.[6]

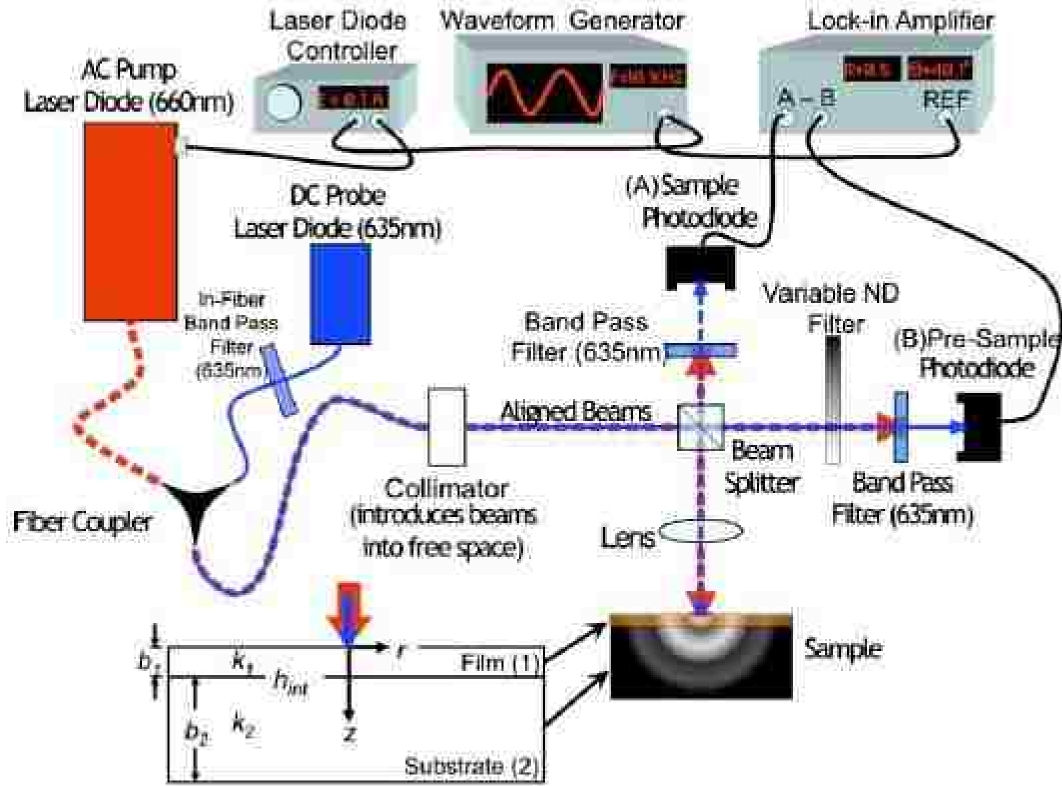

Figure 1.9: Frequency Domain Thermoreflectance steup[6]

FDTR measures the phase lag between a periodic surface heat flux and surface temperature over a wide range of heating frequencies. The metal layer is used in this experiment an a transducer layer which is normally selected for high absorption at the pump wavelength to give a uniform distribution of heat pulse and also to maximize the heating capacity on the other hand it has good reflectance at the probe wavelength to make sure the temperature response is sensitive enough while detecting at the photodiode.[6,7,41]

The advantages of FDTR technique over others are explained below,

- Frequency-domain methods avoid the complexity associated with a mechanical delay stage and the high cost of a pulsed laser system.

- good sensitivity for submicron thin films
- Implementable by CW Laser instead of costly Femto second Laser.
- Sensitivity of TDTR signals to the thermal properties of thin films is given to show the dilemma on appropriate modulation frequency selection; however the FDTR technique can avoid the above mentioned critical challenges. The sensitivity of FDTR signals to the thermal properties of thin films is analyzed with different thicknesses.
- Applicable for low temperature and at high vacuum measurement due to less optical items for the sample stage.
- Simpler optical alignment comparing to TDTR technique.

In this study, micro cantilever beam structures were analyzed for different dimension to avoid any kind of conduction with another material, which can affect the measurement. Non-contact optical measurement technique was established for the thermoreflectance measurement as it has the less probability of including error in the measurement.[6–10] Chapter 2 in this study is comprised of the fabrication of both the cantilever beam and semi-infinite structure for calibration purpose. All the fabrication steps including necessary images are elaborated in this chapter. Steady state measurement of cantilever beam to extract thermal conductivity is described in chapter 3 where temperature profile of the cantilever beam along the beam's length was analyzed using steady state thermoreflectance including all other supporting experiment like validation of 1D heat transfer along the beam length, boundary condition of the input heat flux maintaining infinite heat sink at base of the cantilever beam, effect of pressure of the reflected probe beam in the vacuum chamber.

In chapter 4, analytical and numerical model of harmonic analysis has been established to measure the phase difference along the beam length to calculate the specific heat capacity of Si. In this chapter, validation of the results for bulk and Aluminum on semi-infinite Si are shown and phase response of cantilever beam were performed. Chapter 5 is on the topic of transient analysis and its results to find the time constant of cantilever beam and hence extract specific heat capacity. At the end chapter 6 is explained with the conclusion of the study and future possibilities with these technique to be able apply on size effect on different thickness, phononic crystal structure and as well as at low temperature application to see how phonon mean free path react with other experimental parameters or different device structure.

This study is a platform to analyze thermal properties (thermal conductivity, heat capacity) of thin film materials with the help of cantilever beam device structure for their unique architecture of free standing, free from substrate interfacial conductance and with the implementation of pump probe thermoreflectance technique applicable at high vacuum for precise thermoreflectance measurement. Measurement with more accuracy is the most important factor recent years due to device size reduction from the bulk values. Though we have demonstrated the whole technique for characterization of Si thin film using steady state, harmonic and transient analysis to extract the thermal properties but this technique can be applied to any thin film material for accurate thermal measurement.

Chapter 2

Cantilever Beam Structure and Device Fabrication

2.1: Cantilever Beam Structure:

Cantilever structure is a special type of device structure where one end of the beam is anchored with the substrate and the other side is free of having any contact. Intentionally making the length of the beam greater than the width and thickness heat transport can be manipulated as 1D system and analyze the thermal properties of the material. Design consideration were,

a. Length > 4X Width
b. Length >> thickness
c. Infinite heat sink at the fixed end of cantilever beam
d. Thin film transducer film at the free end for isotropic heat distribution

A metal film of 80nm thickness were deposited at the free end of the cantilever beam for uniform heat absorption at the pump wavelength and good reflection at the probe wavelength. Aluminum was proffered as the metal transducer layer due to their good stiction with Si and relatively simple lift-off process for the fabrication.

2.2: Device Fabrication:

i. Cantilever Beam:

For the cantilever beam fabrication, Silicon on Insulator wafer was selected with a resistivity of the device layer of 1-20 ohm-cm, thickness of 1.291µm, box layer thickness of 1µm. Fabrication of the cantilever beam in SOI wafers is composed of following steps,

1. The fabrication is performed on a SOI (Silicon on Insulator) wafer with device layer of 20-25 μm of Si, Buried Oxide or BOX of 1-2 μm and handle layer of ~500 μm thick Si. Crystal orientation on both the device layer and handle layer were (100). The resistivity of the device layer for the wafers used was 0.01-0.02 Ohm-cm. The resistivity of the handle layer for the wafers used was 10 Ohm-cm. The lower resistivity on the device layer provides good electrical path on a MEMS device surface and a higher resistivity (less dopant) on the handle layer prevents higher residual stress in the wafer from buckling the freestanding beams upon release

2. Photomask was designed using AutoCAD and the designed Cantilever beam is patterned using AZ1518 photoresist, soft baked, exposed and developed tuning the photoresist profile.

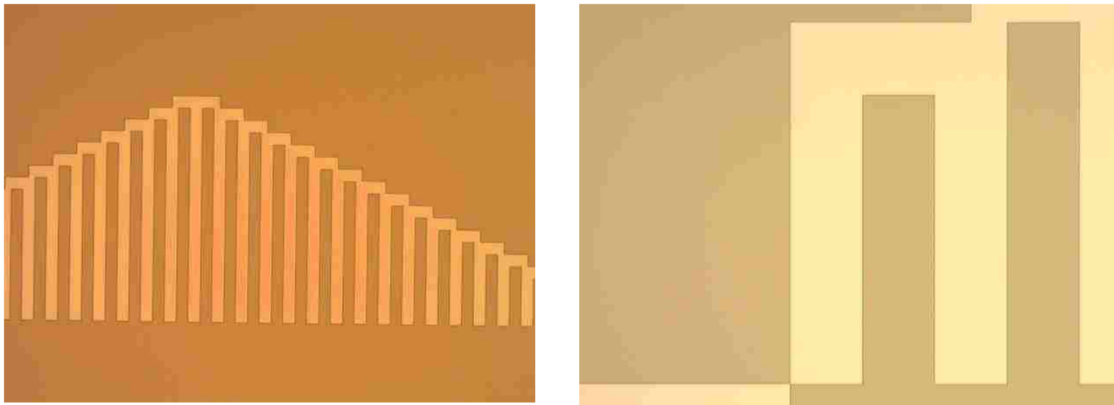

Figure 2.1: Photoresist pattern of cantilever beam

3. Then the Si is etched down to the BOX layer by Reactive Ion Etching process (RIE). With RIE, the plasma is generated by the application of a RF power source across two electrodes separated in a reactive, gaseous chemical mixture of electrons, ions, and free radicals which produce the distinct plasma glow. Initially, the plasma

consists of an equal number of positive and negative charges. Depletion of the charges in the plasma due to diffusion results in a layer of surface charge at the boundary of the plasma. Positive ions are accelerated within the chamber environment and aid in the etching process. The ion bombardment energy is controlled by the plasma potential. The wafer substrate on the lower electrode is exposed to the reactive neutrals and charge species. These species combine with the substrate material and create volatile products that etch the wafer. Since electrons are more mobile that ions, a DC self-bias voltage develops across the electrodes during the etch process to achieve the necessary current continuity. The self-bias voltage accelerates ions towards the wafer surface where they are react, cause various compounds to be desorbed, aid in the formation of polymers and help to facilitate the anisotropic etching. Etching can be attributed to two distinct mechanisms: chemical etching cause by free radicals and physical etching cause by ion bombardment. This process creates a high aspect ratio structure by etching vertically down from the edge of the PR layer.

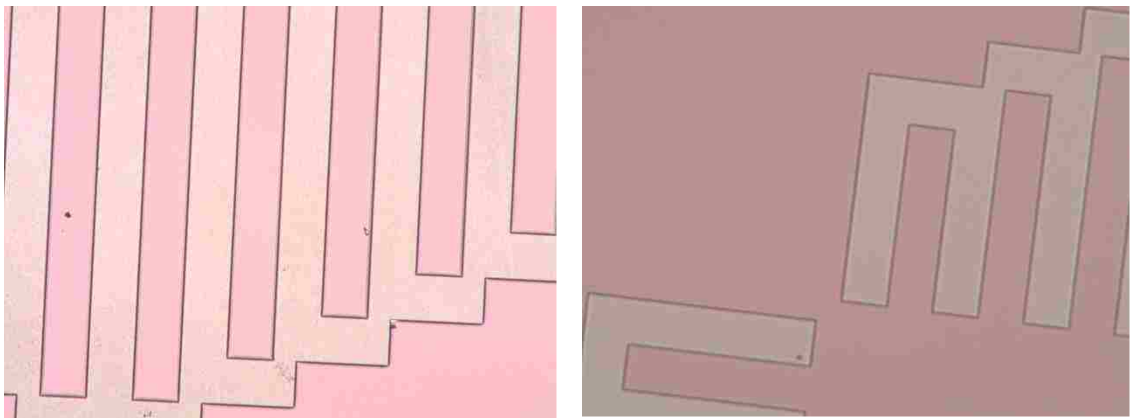

Figure 2.2: Microscopic image after RIE etch

Next, the PR layer is removed using acetone, isopropyl alcohol, and de-ionized water rinses respectively

4. The wafers are then released using Buffered Oxide etch in a 20:1 diluted HF to get the uniform etching all over the area. When the cantilever beam were fully released the wafers are rinsed with DI water and dried for the next step.

5. Next the wafer is coated again with the PR sufficiently thick to cover the entire high aspect ratio structure. The PR is then patterned for the deposition of Aluminum at the free end of the cantilever beam. Aluminum deposition was performed in ultra-high vacuum (<10^{-6} Torr) using a e-beam source with a constant deposition rate of 2A˚/s. 80nm thickness of the Aluminum layer was confirmed with profilometer. Then the wafers were submerged in a acetone remove the access Aluminum from the other area by removing the PR and this process is commonly known as 'lift-off' process. Then the wafers ere rinsed with IPA and water and dried.

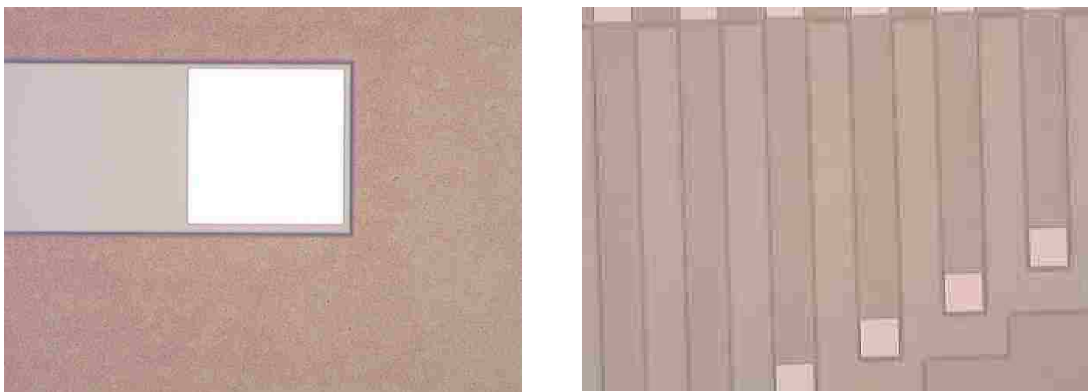

Figure 2.3: Microscopic Al pad deposition and lift off

6. After the samples were released, they were immersed into Critical Point Dryer for a full cycle with IPA to avoid any stiction failure of the devices.

7. As soon as the sample were prepared it was diced into small pieces and the substrate from the back of the cantilever beam were cleaved precisely to be able install in the vacuum chamber and for both directional probing along the beam.

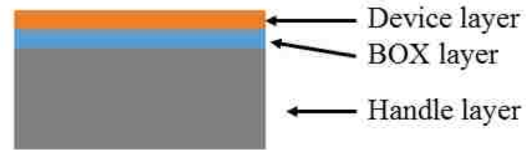

(a) SOI Wafer

(b) Patterned and etched device layer

(c) Metal pad deposition and lift-off

(d) BOX layer etch

(a)

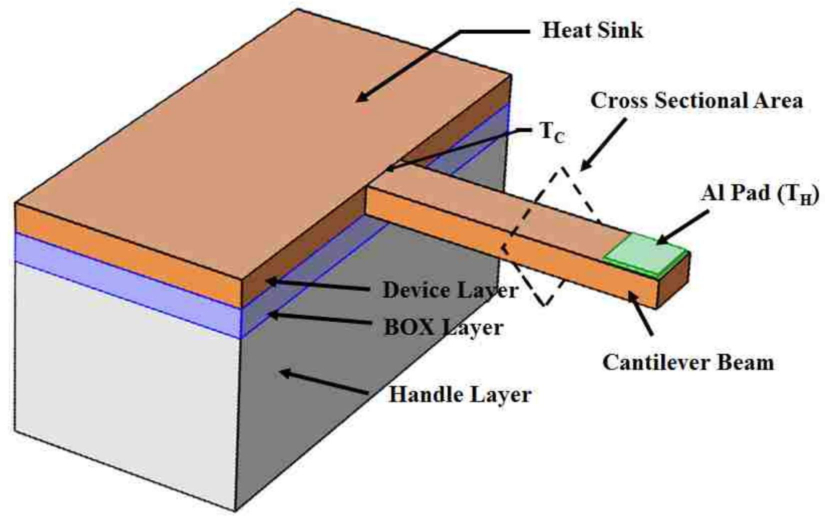

(b)

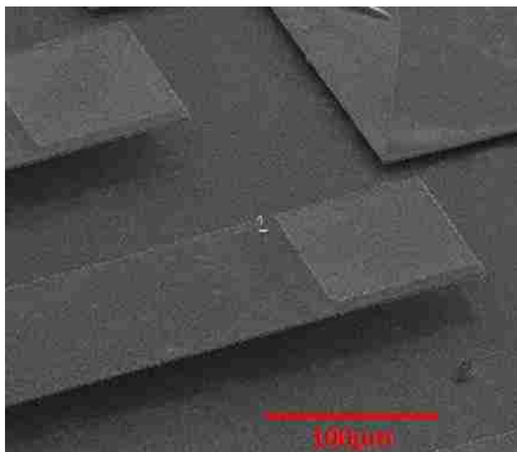

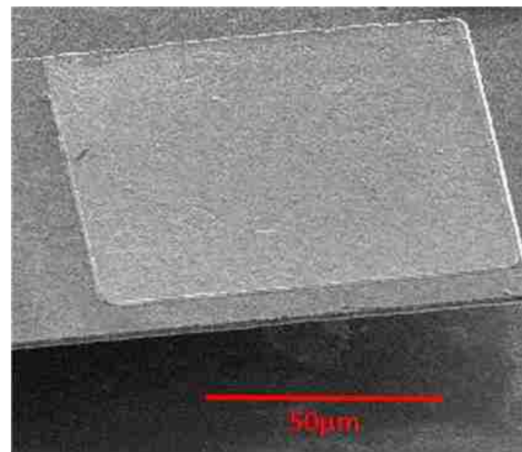

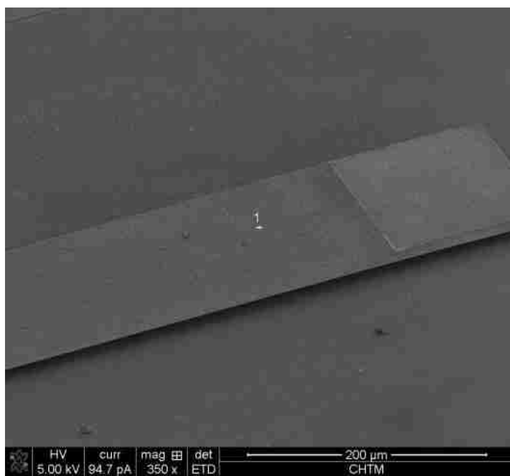

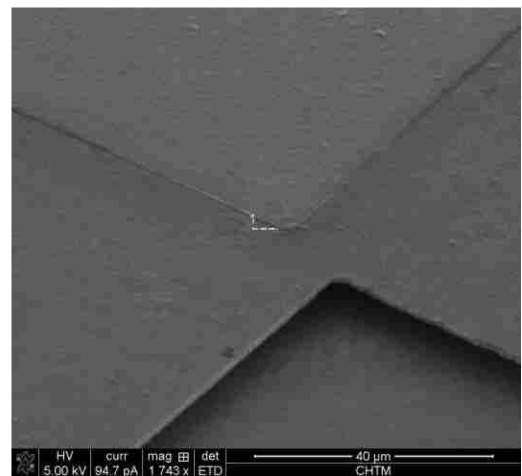

(c)

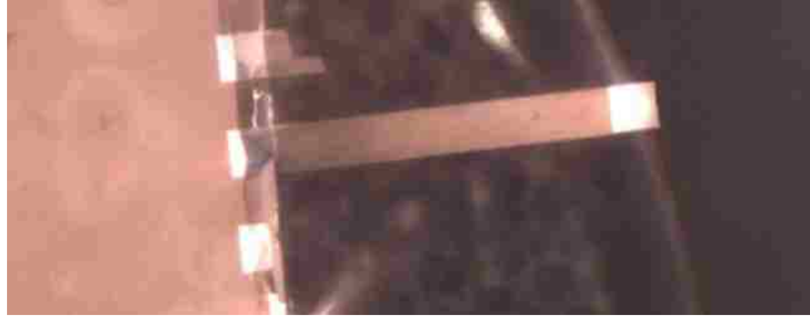

(d)

Figure 2.4: (a) Fabrication Steps; (b) Device Structure; (c) SEM images; (d) cleaved sample

ii. Semi-infinite Sample:

Second set of samples were fabricated depositing Aluminum film on bare Si wafer maintaining all the evaporation parameters of the cantilever beam's Al pad. The bare Si wafer's specification of resistivity, orientation kept similar to the device layer of the SOI wafers that were used to fabricate the cantilever beams. These planar structure sample is been used to measure the thermoreflectance coefficient of the Aluminum film (80nm) which needed to be applied on the measurement of the cantilever beam thermal properties.

Chapter 3

Steady State Analysis

Steady state conduction is the form of conduction that happens when the temperature difference(s) driving the conduction are constant, so that (after an equilibration time), the spatial distribution of temperatures in the conducting object does not change any further. Thus, all partial derivatives of temperature with respect to space may either be zero or have nonzero values, but all derivatives of temperature at any point with respect to time are uniformly zero. In steady state conduction, the amount of heat entering any region of an object is equal to amount of heat coming out.

Fourier's law can be applied in the steady state condition as there is only one free parameter ,thermal conductivity need to be measured and it does not have any heat capacity involved with the equation. For a linear material in a cantilever beam if one end of the beam is pumped with heat, the temperature drop across the beam will be linear and it will constantly reduce with the ration of thermal conductivity. The relationship of Fourier's law to the heat conduction equation has been described at the section 1.1.

3.1 Theory:

For the steady state case all assumption are applied for analysis and those are

- Heat transfer mechanism is only due to conduction
- 1 directional flow of heat transfer, Bounding surfaces are isothermal in character that is constant and uniform temperatures are maintained at the two faces
- Isotropic and homogeneous material and thermal conductivity 'k' is constant

- Constant temperature gradient and linear temperature profile.

3.1.1 Measurement of Thermoreflectance Coefficient of Aluminum for Semi-infinite Structure:

Thermoreflectance coefficient of Aluminum film varies due to its deposition technique, source material being deposited, deposition pressure etc. For this it is very essential that the thermoreflectance coefficient of Aluminum is been measured and calibrated for the experiments, otherwise erroneous result lead into erroneous measurement of the thermal properties in all steps. 80 nm of aluminum was deposited on the topside of the cantilever beam structures at the free end to enhance the absorption of the pump laser. The thermoreflectance coefficient, C_{TR}, of aluminum films vary due to deposition parameters, source material being deposited, deposition pressure etc.[38,39,42] Therefore it is essential to accurately measure the thermoreflectance coefficient of Al for the exact film deposited in a given set of experiments..[6,7]

$$\Delta T = \frac{P_{abs}}{2\sqrt{\pi} r_{spot} \kappa_{bulk}} \tag{3.1}$$

Where, P_{abs} is the absorbed power calculated from the incident and reflected power, r_{spot} is the pump and probe beam radius incident on the sample and κ_{bulk} is the thermal conductivity of bulk Silicon. Change of reflectivity from the sample is directly proportional to the change of temperature and can be expressed by the eqn. 3.2.[36,37,43–46]

$$\frac{\Delta R}{R} = \left(\frac{1}{R}\frac{\partial R}{\partial T}\right)\Delta T = C_{TR}\Delta T \tag{3.2}$$

where, R is the reflectivity from the cantilever beam is not heated and ΔR is the change of reflectivity due to heating, C_{TR} is the thermoreflectance coefficient of Al.

3.1.2 Steady State Analysis for Cantilever Beam:

A pump probe technique with steady heat flux generated by a Continuous Wave Laser is used for the measurement of thermal conductivity of free-standing thin Si film. For Steady state 1D heat flux,

$$q'' = -\kappa \frac{\partial T}{\partial x} \tag{3.3}$$

Where q'' is heat flux, T is the temperature and k is thermal conductivity of the thin film. Which gives the solution for thermal conductivity for temperature difference of ΔT and the beam length is L, [47]

$$\kappa = \frac{q''}{\Delta T}(L - x) \tag{3.4}$$

In this experiment, thermoreflectance response were measured along the beam length (backside technique) and the thermoreflectance response is extracted for the position of tip with Al pad. Using the front side technique ΔT is measured at the tip and C_{tr} of Si is extracted from the backside ΔR/R values at tip with eqn. 3.2.

The temperature profile along the beam length is obtained using the Silicon's thermoreflectance Coefficient and ΔR/R with eqn. 3.2. This temperature distribution and absorbed heat flux used with eq. 3.4 to get the thermal conductivity of Si.

3.2 Experimental Setup:

The experimental analysis has been established using two CW laser one as the heating pump beam at the wavelength of 670nm and the other one is for the probing at the

wavelength of 532nm. In this study the pump beam power has been varied for different analysis but the probe beam power kept constant and which is very small(<1% of the pump power) comparing the pump beam power and does not have any effect on the rise of temperature. The pump and probe laser connected to laser diode controller and temperature controller. The temperature of the laser diodes were kept in the range of 20°C to 25°C. Laser diode temperature in the operating range is very important as the Laser power oscillates at higher temperature. The pump and probe beam passes thru to separate wavelength isolator to prevent reflection reaches laser which can impact on the laser lifetime and can cause undesired heating of the laser from the reflected beam. A regular experimental setup for the steady state measurement is shown in figure 4 for a demonstration purpose but the setup has been used in a different arrangement for the backside temperature profile measuring which has been described later.

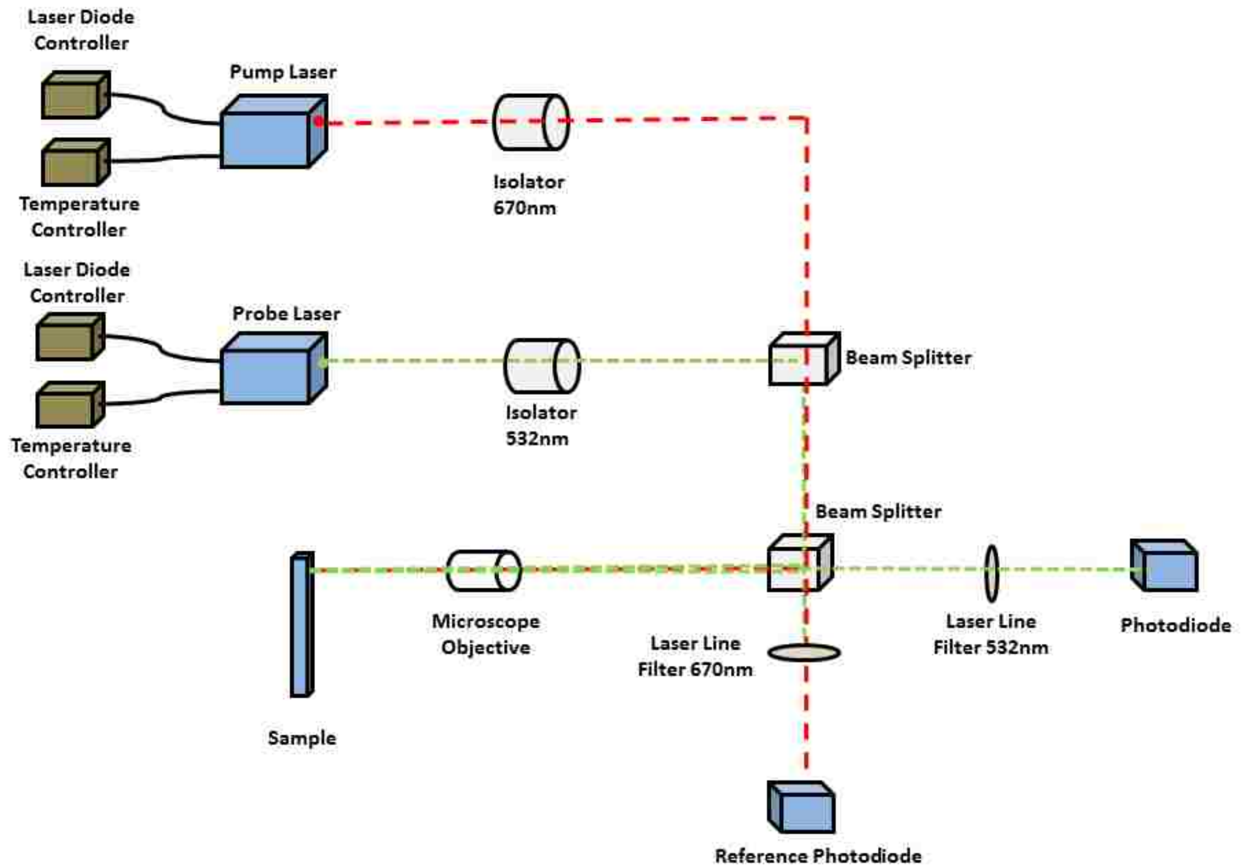

Figure 3.1: Basic Steady State Thermoreflectance Measurement Setup

The samples were placed in a vacuum chamber with a turbo molecular pump and roughing pump for a high vacuum up to $1X10^{-7}$ Torr to prevent convective loss and the radiation loss was also minimized by cleaving the substrate from the cantilever beam.

3.2.1 Spot Size Measurement:

Spot size of the pump and probe beam were measured using a CCD camera showed in fig. 3.2 and the image thru a thin film membrane of the spot size radius were calibrated for different focal length of the lens and the smallest pump and probe beam was measured to the $1/e^2$ value of 5.92 µm.

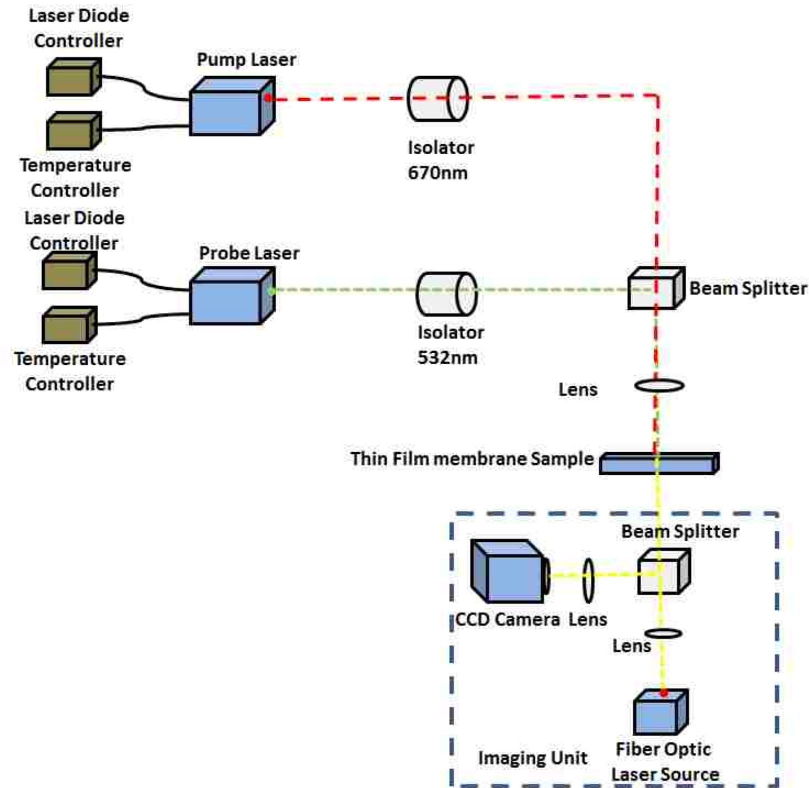

Figure 3.2: Spot size imaging setup

For the measurement of the laser spot size thin film membrane with substrate etched from the backside of the wafer was used. Thin film membrane had metal strip lines of 30μm width as a reference to measure the actual size of the spot size reflecting from the surface of the film. The focal length of the length before the sample to be incident has been calibrated for different spot sizes. An image from the CCD camera of the spot size (a) and calibrated spot size with reference to the metal strip lines (b) are shown in fig. 3.3.

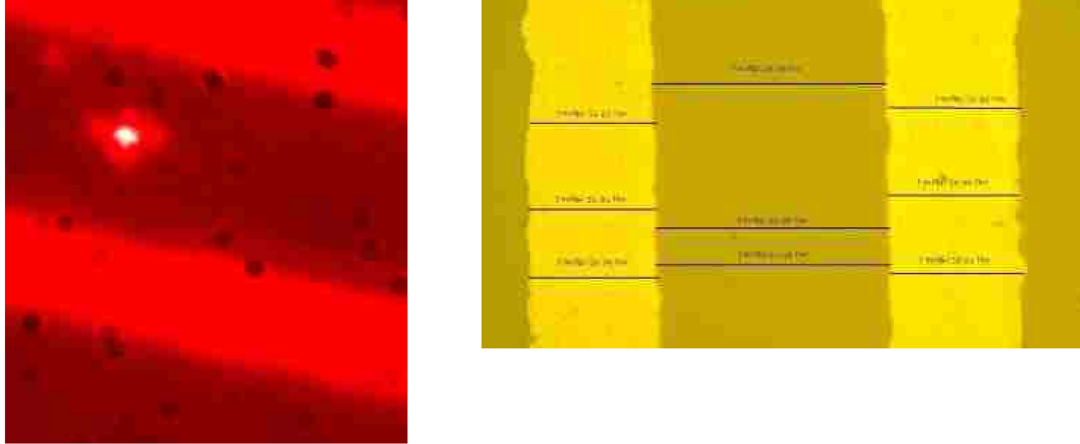

Figure 3.3: Spot Size Imaging Setup; (b) Spot size image

3.2.2 Vacuum Chamber Fabrication:

Two types of vacuum chamber were fabricated for the cantilever beam thermoreflectance measurement which are shown in fig. 3.4. The vacuum chamber shown in fig. 3.4 is comparatively small with both glass view port with the capability of installing free standing cantilever beam in a stage. The chamber is capable of being attached to optical stage easily for x,y,z direction calibration during measurement. The design of the chamber from the one side of glass to the other side of the glass were maintained with the focal length of the lens from the both side. The chamber is capable of holding pressure in the 10^{-7} Torr with very low leak rate. The chamber was connected to the pump using flexible vacuum line to avoid any kind of vibration and gate valve has been used to isolate the chamber portion from the pump during the measurement.

The other type of vacuum chamber is shown chapter 6 which is primarily designed for low temperature application. The chamber has two different compartment inside and outside

chamber to be filled with liquid nitrogen and the sample compartment is installed with two view port capable of pumping down to 10^{-7} Torr. The chamber was tested for liquid Nitrogen temperature (77K) and the inside compartment can be filled with liquid Helium for lower temperature (upto 3mK) application. Comsol simulation has been done on the entire design to make sure the whole system work up to liquid nitrogen temperature and shown in chapter 6.

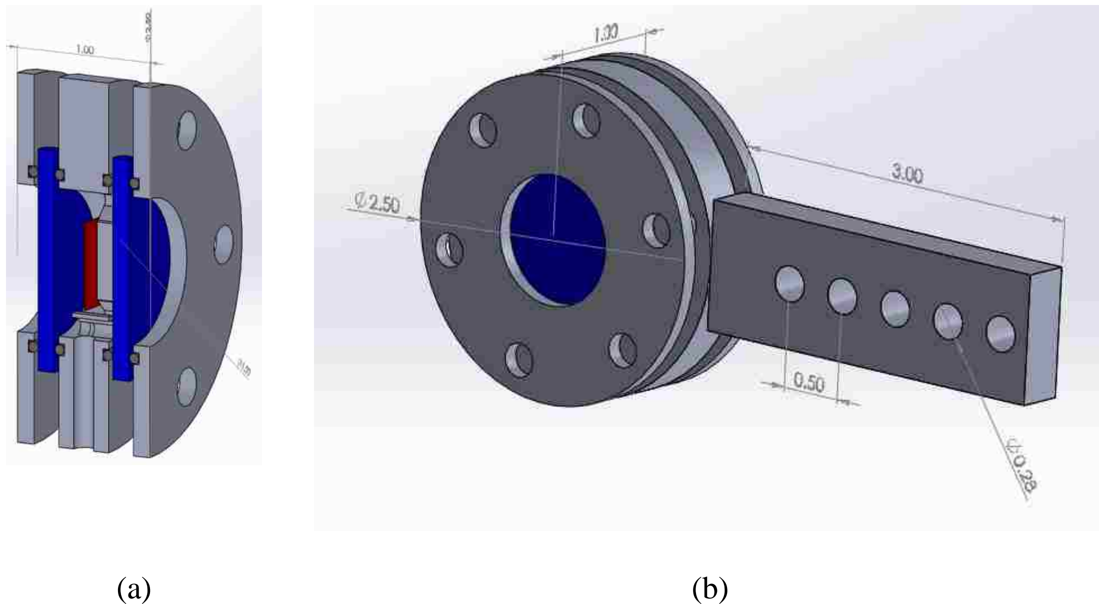

(a) (b)

Figure 3.4: High Pressure small vacuum chamber for thermoreflectance measurement; the cross section of the chamber is shown in (a) and chamber with a handle to be attached to the optical stage is shown in (b)

3.2.3 Topside probing:

Fig. 3.6 shows the experimental setup for pump-probe thermoreflectance measurements for topside probing of semi-infinite substrates and the topside of the cantilever beams. Aluminum was deposited on the tip of the cantilevers due to its

compatibility with Si and for its absorption at the pump wavelength. A 670 nm pump laser (CW) first travels through an optical isolator which prevents back-reflection. The 532 nm probe laser (CW) passes through its own optical isolator before the beam sampler. The beam sampler is aligned such that it co-aligns the beams then passes through a beam splitter and allows the pump and probe beams to continue travelling towards the sample. An objective lens was used to focus the pump beam's diameter to 20µm (for semi-infinite measurements) and to the width of the Al pad for the measurement of the cantilever beam structure. The probe beam was always kept to a spot size of 6µm (1/e value) for all experiments. The reflected probe beam is passed thru a laser line filter and travels toward a photodiode. Depending on the change of the temperature induced by the pump beam, the reflectivity of the sample changes and it is detected at the photodiode.[6,7,41] The reference photodiode is used to measure the incident pump beam's power. However the reflected pump beam's power can be measured using a 670 nm laser line filter placed in front of the photodiode instead of a 532 nm laser line filter.

By measuring the incident and reflected beam powers the absorbed power can be determined by using A = I-R, where I is incident pump power and R is the reflected pump power. Note that there is no transmission.

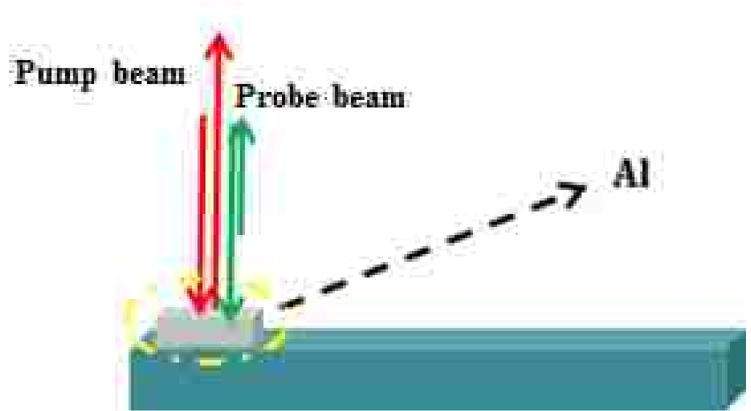

Figure 3.5: Top side measurement beam incident on cantilever beam

The topside thermoreflectance technique is also utilized to measure the thermoreflectance coefficient of the Al films deposited on the semi-infinite Si wafer to use as the coefficient of thermoreflectance.

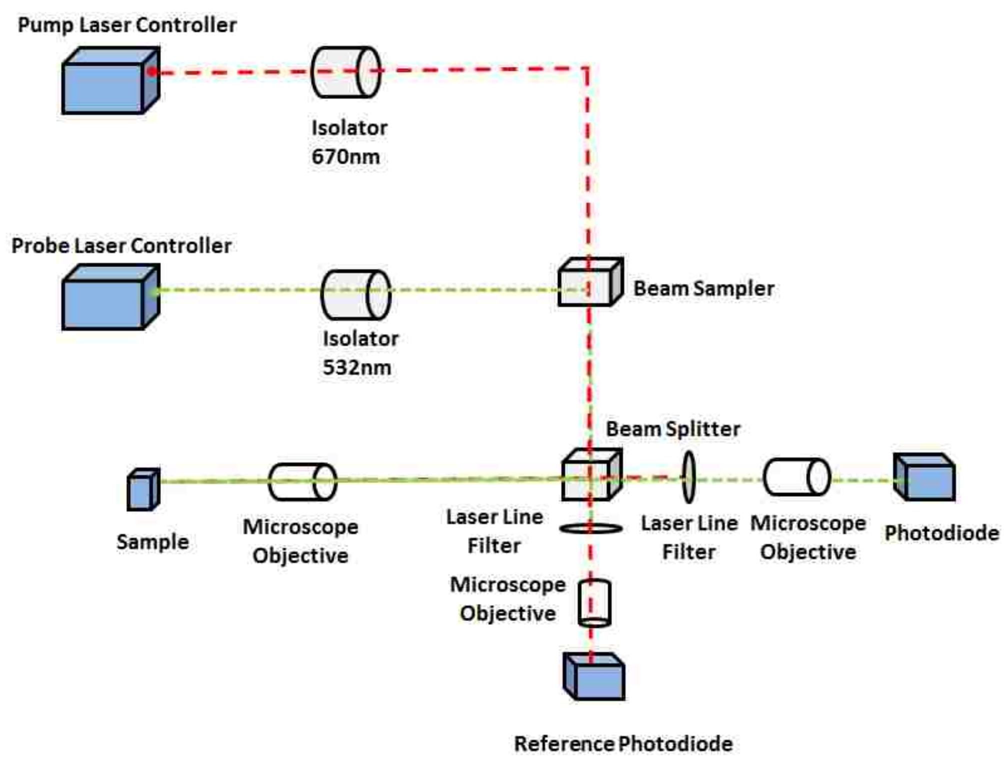

Figure 3.6: Transducer side thermoreflectance measurement setup for Semi-infinite and cantilever beam at tip The front side thermoreflectance technique is used to measure the

thermoreflectance coefficient of Al film deposited on the semi-infinite Si wafer and the change of reflectivity from Al pad tip of the cantilever beam.

3.2.4 Thermal Gradient Probing:

In figure 3.8 experimental setup for thermoreflectance measurement is shown labeling all the components. In this experiment the probe beam incident on the cantilever beam's backside to measure the reflectivity along the beam length for calculating the thermal conductivity of the structure.[6,7,48] The substrate were cleaved for the free suspension of the cantilever beam.

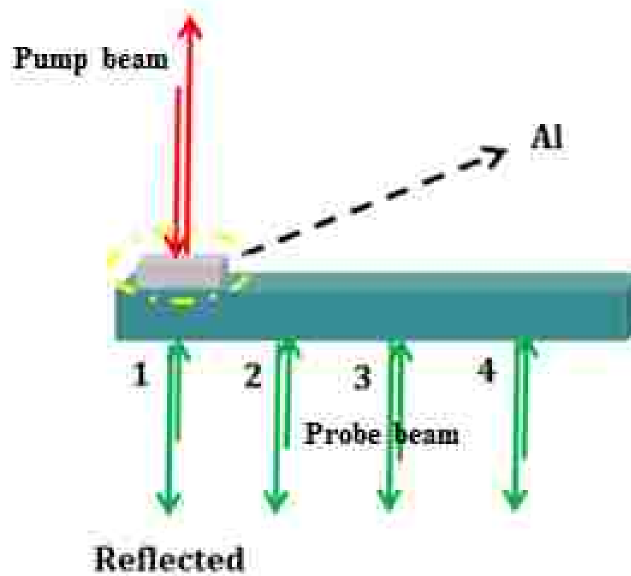

Figure 3.7: Thermal gradient measurement architecture along the cantilever beam.

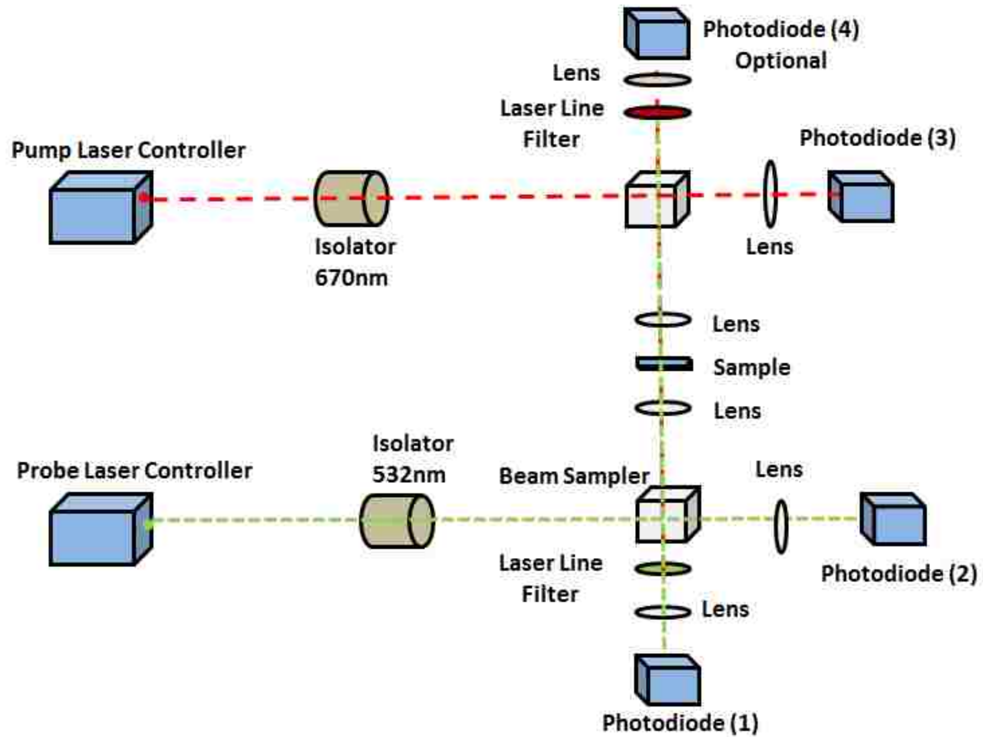

Figure 3.8: Thermal gradient measurement setup for thermoreflectance along the cantilever beam.

The change of thermoreflectance needs to be correlated with the photodiode measured voltage

The measured voltage by a photodiode is a representation of photocurrent which is converted to voltage and correlated with the responsivity of photodiode and which is directly proportional to the reflectance from the sample. The measurement also needs to be calibrated for the responsivity of the photodiode at that particular frequency. The measured output voltage of a photodiode is related with the transimpedance gain and the responsivity of the photodiode. The photodiode responsivity for a particular wavelength can be found from the product data sheet.

$$Out\ Put\ \left({}^{V}/_{W}\right) = Transimp.Gain\ \left({}^{V}/_{A}\right) \times Responsivity\ \left({}^{A}/_{W}\right) \qquad (3.5)$$

3.3 Results:

Experimental measurement for steady state analysis has been demonstrated in this section by step by step analysis. It starts with calibrating the Aluminum thermoreflectance coefficient on a semi-infinite sample and measure it for range of incident laser power. Then apply the value of Al thermoreflectance coefficient for cantilever beam to get the reference temperature point at the free end of cantilever. Then it continuous by measuring thermoreflectance coefficient of Si by measuring the change of reflectance along the beam and use that to extract the temperature gradient and the find thermal conductivity for Si. All the measurements are demonstrated in this section with necessary description.

3.4.1 Thermorfeflectance Coefficient of Aluminum Measurement:

The semi-infinite Al on bulk Si sample were used to measure the thermoreflectance coefficient of Al to be able to use it for further analysis on cantilever beam structure. Using the technique described at section 3.3.1 and the experimental setup of transducer side setup to measure the thermoreflectance coefficient of Al where the pump spot size was kept to 20.5μm and the thermal conductivity of bulk Si were used 113.5 W/m-K[28] which was confirmed using a TDTR technique. The thermoreflectance plot of planar Al on Si is shown in fig. 3.9 and the thermoreflectance Coefficient of Al is measured to be $2.7 \times 10^{-4} K^{-1}$.[38,39,42]

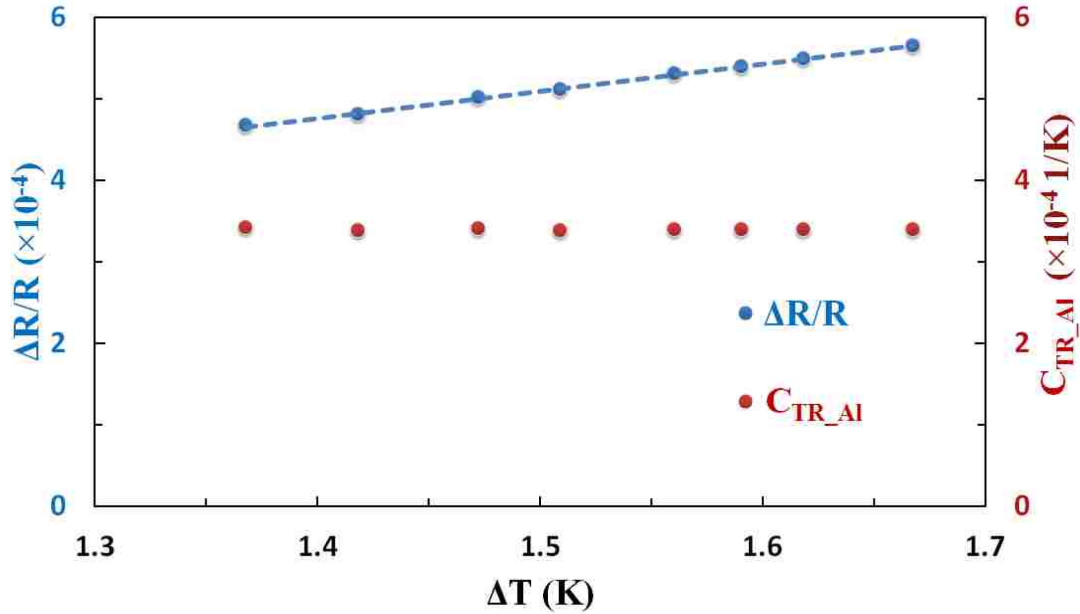

Figure 3.9: Aluminum Thermoreflectance Coefficient for different incident power level

3.4.2 Cantilever beam tip temperature measurement:

With the help of eqn. 3.2 and the transducer side setup described at section 3.4.1 with the knowledge of the thermoreflection coefficient of Aluminum of $2.7 \times 10^{-4} K^{-1}$, the temperature of the free end of the cantilever beam can be known my measuring the change of reflectance for different incident pump power. In this experiment the incident pump power, reflected pump power were also measured using photodiode and transmitted power is negligible thru the Al transducer layer comparing to the incident or reflected pump power.

3.4.3. Change of reflectance along the beam measurement:

Thermoreflectance response of a Cantilever beam of 100μm width and 400μm long for different input flux at high vacuum ($1X10^{-7}$ Torr) shown in fig. 3.10. In this pressure, heat

is only transported due to conduction and this experiment was conducted on different length beam keeping the width fixed and changing the width as well, in all cases the thickness of the cantilever beam were constant to be 1.29μm. In this experiment the change of reflectance were measured at least 50μm away from the end of the Al pad which was $90\mu m \times 90\mu m$ at the free end of the cantilever beam to avoid any kind of effect non parallel isotherm along the width close to the pump spot.

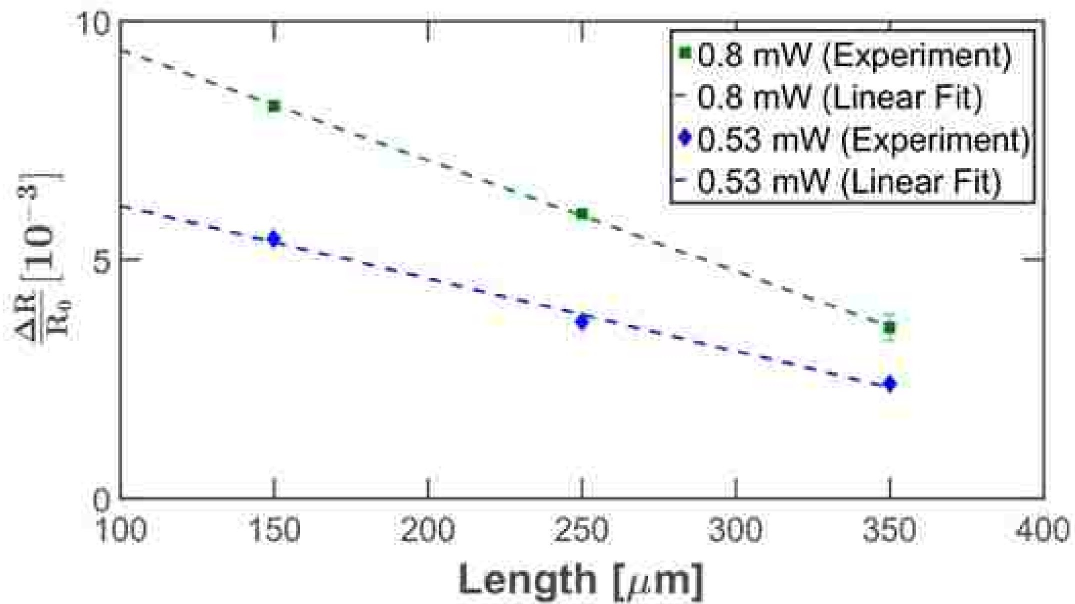

Figure 3.10: Change of reflectance along the beam length of a cantilever beam from the free end to the anchored side. Different power level of incident pump beam is shown to illustrate how the profile is changing.

3.4.4 Measurement of Thermoreflectance Coefficient of Si:

By extracting linear fit value of the $\frac{\Delta R}{R}$ to the position of the pump spot at the Al pad, with the knowledge of temperature at that point described at section 3.3.2 and using eqn. 3.2 the

thermoreflectance coefficient of Si can be measured and the measured value of thermoreflectance coefficient (C_{TR_Si}) of Si is $5.1 \times 10^{-4} K^{-1}$.

3.4.5 Thermal Gradient profile extraction along the beam:

The temperature profile of the cantilever beam along the beam length can be extracted by knowing the thermoreflectance coefficient of Si, change of reflectance $\frac{\Delta R}{R}$ from section 3.4.3 and using the thermoreflectance eqn. 3.2. Which is the essential part of the thermal conductivity measurement in steady state condition using Fourier's law. The temperature gradient profile along the cantilever beam is shown in fig. 3.11.

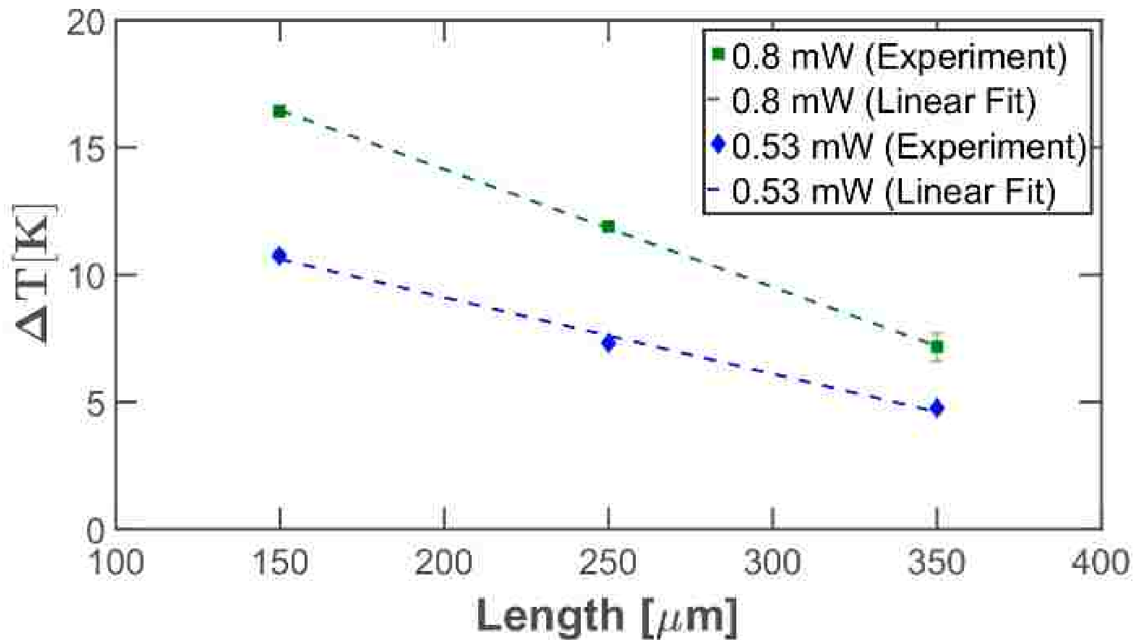

Figure 3.11: Temperature profile along the beam length extracted from the thermoreflectance measurement.

3.4.6 Thermal Conductivity of Si cantilever Beam:

Using temperature gradient in Fourier's law (eqn. 3.3) obtained from the previous part the thermal conductivity can be measured for the cantilever beam. The unknown term in this equation is the flux of pump laser. The absorbed power was measured by measuring the incident, reflected and the transmitted power using photodiode. The transmitted power was negligible comparing to the incident or the reflected power. Measuring the absorbed power for all the beam separately and the measuring all the temperature gradient for beam width of 100µm and 150µm and length of 400µm, 500µm and 750µm, 1050µm respectively the thermal conductivity was measured to be $96.9 \pm 1.76\, Wm^{-1}K^{-1}$.The thermal conductivity value for 10 different measurement is shown in fig. 3.12.

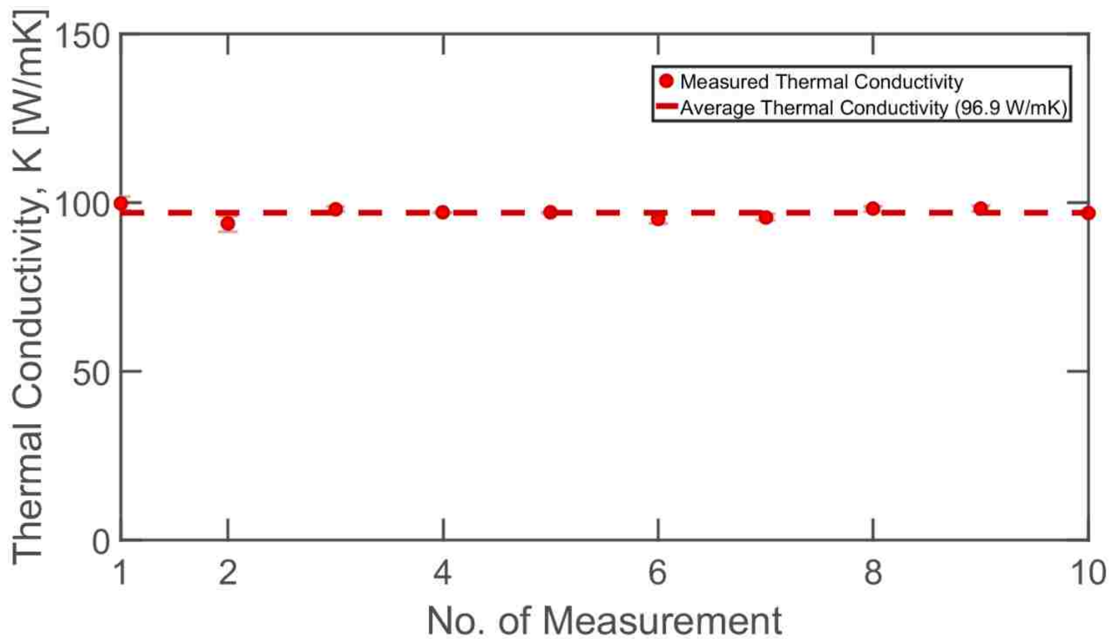

Figure 3.12: Thermal Conductivity of at different power levels of the incident pump beam.

3.5 Constraint Validation:

3.5.1 1D Heat Transfer Validation:

FEM simulations were conducted to establish the constant isotherm for differential heat flow in the beam length direction. Simulation result for the single beam of 50μm width is shown in figure 3.13(a) and the result for nanowire like structure is shown in figure 3.13(b).

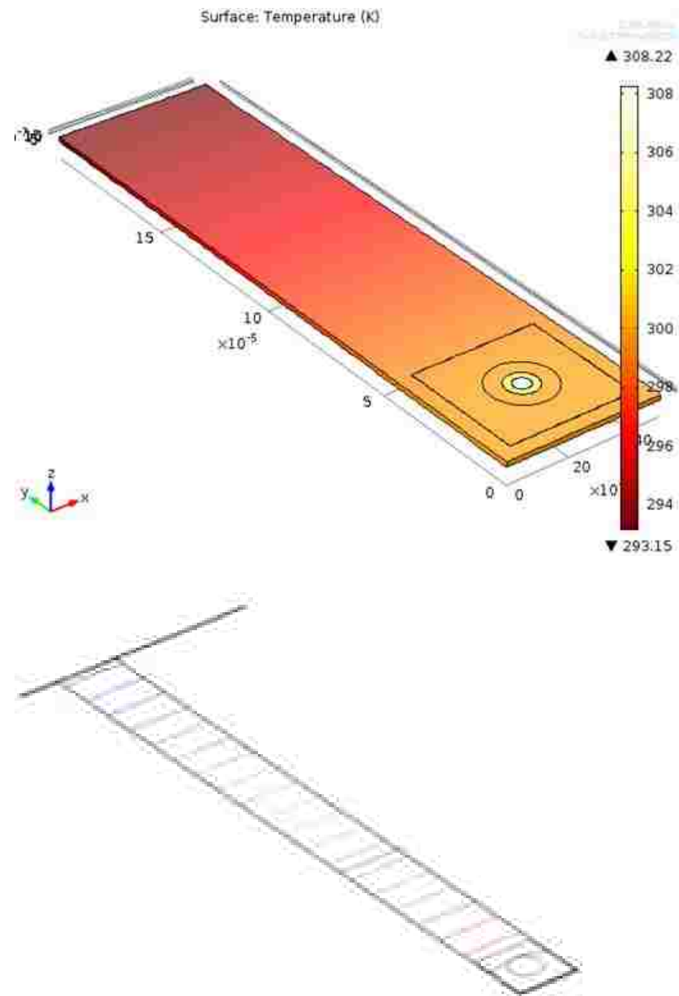

Figure 3.13: Heat flux FEM simulation results for slab structure; (b) heat flux FEM simulation results for isotherm analysis of cantilever beam.

In this study, Isotherm becomes constant or negligible amount of change below 5% of the temperature change from the center to the edge with in the 5% of the length of the beam starting from the edge of the Aluminum pad. Constant isotherm of 95% of the beam length proves the 1D heat flow along the beam length.

There were other different studies were performed to see how the isotherm effects along the beam length if the pump beam spot is not centered or even smaller. In these cases isotherm starts to deviate more than the placed at center of the pad and covered the whole Al pad. In our experiment, we always maintain the pump spot cover the whole pad to avoid these issues.

3.5.2 Temperature Boundary condition Validation

The cantilever beams reflectivity from the tip were analyzed to characterize the boundary condition limitation. Thermoreflectance from the tip is linear at moderate incident pump power shown as common input power operating zone in the figure and reflectivity changes linearly. As the input power goes high we observe transition period of the reflectivity and beyond that the reflectivity increases. The transition period occurs at different input power for different cantilever beam length which is a sign of elevation of the base temperature from the room temperature of heat sink.

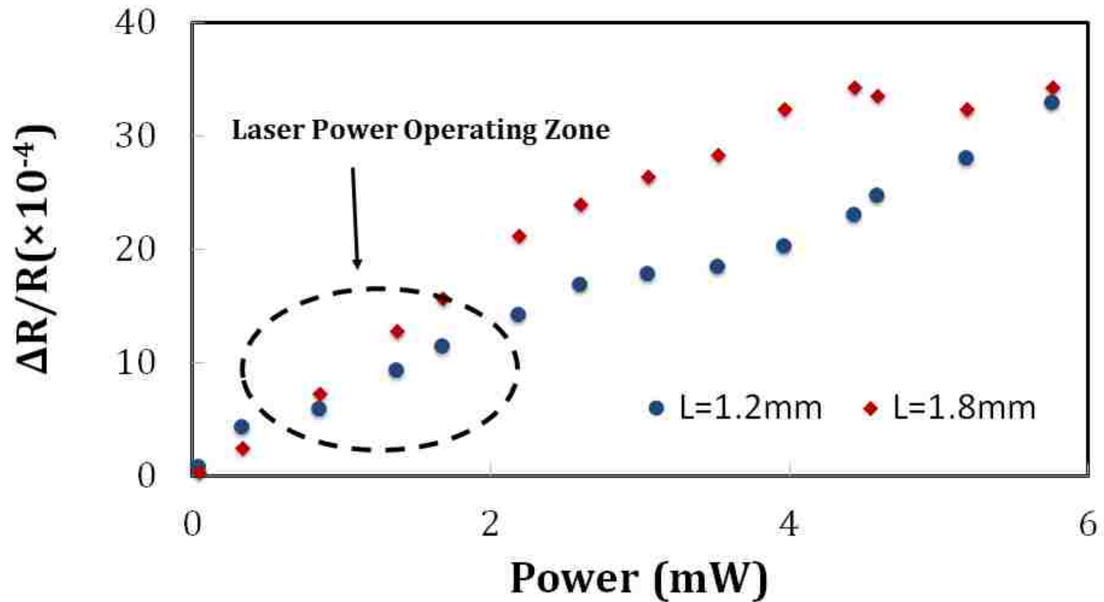

Figure 3.14: Thermoreflectance from cantilever beam tip for varying power, higher incident power induces non continuity of the linear response of thermoreflectance.

To maintain the boundary condition the experiments needed to conduct in the incident laser power regime showed in fig. 3.14 with circled region. Incidence of higher laser power can cause damage to the Al pad which can change the thermoreflectance property of Al as Aluminum is a low melting point metal and erroneous result can baffle the experiment. The incident laser power has a lower limit too where the emitting laser power is not linear with the applied current in this portion of the laser operation laser power can fluctuate over time ending up in less consistency.

3.6 Validation of only Conduction

3.6.1 Convective Loss:

Convective heat loss along the beam length is an important factor in the steady state condition of the thermoreflectance analysis. As our experiment is not conducted using a

ultra-short heat pulse, the convective loss can play an important role measuring thermal properties of the cantilever beam. The samples were placed in a vacuum chamber with a turbo molecular pump and roughing pump for a high vacuum up to $1X10^{-7}$ Torr to prevent convective loss. The experiments were conducted in different pressure from the atmospheric pressure to $1X10^{-7}$ Torr. The pump beam was incident on a part of Silicon and the probe beam was 100μm distant from the beam and the change of reflectivity with pressure is measured. As the pressure goes down below 10^{-4} Torr, the change of reflectivity saturates in higher value and the measurement in this range will have less error in results for conductive heat transfer. For the atmospheric and low vacuum condition heat loss was observed from the thermoreflectance data with different pressure is shown in fig. 3.15. The heat loss due to convection can be avoided in high vacuum condition observed from the thermoreflectance data.

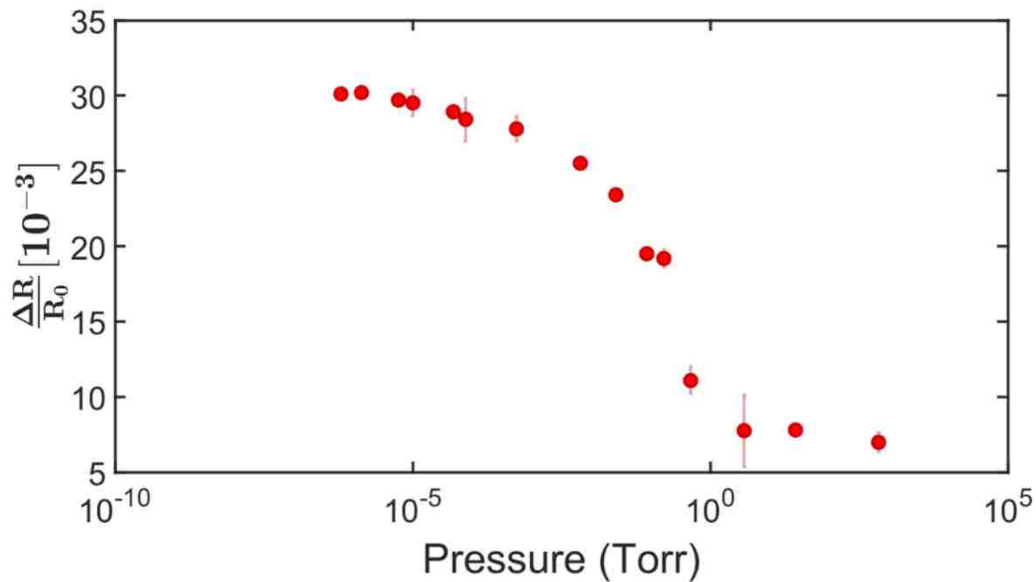

Figure 3.15: Thermoreflectance response of a constact pump and probe beam displacement for a 2.4 mm cantilever beam from atmospheric pressure to $1X10^{-7}$ Torr.

3.6.2 Radiative Loss:

The radiation loss was minimized first of all by releasing the devices from the substrate and later the substrate from the underneath of the cantilever beam were cleaved and minimizing any kind of radiative loss from the measurement. The input power were also maintained in lower regime to prevent radiative loss.

Chapter 4

Harmonic Analysis

4.1 Theory:

4.1.1 Semi Infinite Frequency Domain Thermoreflectance Analysis:

Harmonic analysis needs to be performed using a lock-in amplifier which measures the fundamental harmonic component of the probe signal at the modulation frequency and rejects all other components. The output of the lock in amplifier consists of amplitude A and phase (φ) with respect to the reference wave of the fundamental component of the probe signal with respect to the reference wave. Mathematically, the solution can be expressed as,[11,12,41,48]

$$Ae^{i(\omega_0 t+\varphi)} = Z(\omega_0)e^{i\omega_0 t} \tag{4.1}$$

In case of cw laser the solution is in the form,

$$Z(\omega_0) = \beta H(\omega_0) \tag{4.2}$$

In the frequency domain, temperature (θ) and heat flux (f) of the top and bottom side can be related as,

$$\begin{bmatrix}\theta_b \\ f_b\end{bmatrix} = \begin{bmatrix} cosh(qd) & \frac{-1}{\sigma_z q} sinh(qd) \\ -\sigma_z q\ sinh(qd) & cosh(qd)\end{bmatrix}\begin{bmatrix}\theta_t \\ f_t\end{bmatrix} \tag{4.3}$$

Here d is the layer thickness, σz the cross-plane thermal conductivity and

$$q^2 = \frac{\sigma_r k^2 + \rho c i\omega}{\sigma_z} \tag{4.4}$$

where ρ is the density, c is the specific heat capacity, and σ_r is the radia thermal conductivity and and σ_z is the cross-plane thermal conductivity. Hankel transform of a Gaussian spot

with power A_0 and $1/e^2$ radius w_0, The heat flux boundary condition at the top layer f_t is given by,

$$f_t = \frac{A_0}{2\pi} exp(\frac{-k^2 {w^2}_0}{8}) \tag{4.5}$$

Multiplying the matrices for individual layers together

$$\begin{bmatrix} \theta_b \\ f_b \end{bmatrix} = M_n M_{n-1} \ldots . M_1 = \begin{bmatrix} A & B \\ C & D \end{bmatrix} \begin{bmatrix} \theta_t \\ f_t \end{bmatrix} \tag{4.6}$$

where **M**n is the matrix for the bottom layer. In the limit of the heat capacity of a layer approaches zero (G=z /d) and the bottom surface of the nth layer is adiabatic or semi-infinite, then in both cases eqn. 4.6 reduces to $C_t + Df_t = 0$ and the surface temperature will be in the form of, [9,41]

$$\theta_t = \frac{-D}{C} f_t \tag{4.7}$$

The final frequency response H (ω) in real space is found by taking the inverse Hankel transform of eqn. 4.7,

$$H(\omega) = \frac{A_0}{2\pi} \int_0^\infty k(\frac{-D}{C}) exp[\frac{-k^2({w^2}_0 + {w^2}_1)}{8}] dk \tag{4.8}$$

Solving eqn. 4.8 analytically and using eqn. 4.1 and 4.2 the phase response in the frequency domain can be achieved.

4.1.2 1D Harmonic Thermoreflectance for Free Standing Structure:

The phase-shift method has been widely used to measure the thermal diffusivity of thin-film materials. A sinusoidal heat flux is generated by applying a modulated pump laser beam at the pad of the cantilever beam in fig. 4.1. The 1D transient heat conduction can be formulated as,

$$\frac{\partial T}{\partial t} = \alpha \frac{\partial^2 T}{\partial x^2} \tag{4.9}$$

with an initial condition and boundary conditions,

$$T(x,0) = T_0$$

$$T(L.t) = T_0$$

$$-k \frac{\partial T}{\partial x}\bigg|_{x=0} = T_1 Sin\omega t$$

Using Complex Temperature Method the solution of eqn. 8 will be,

$$T(x,t) = T_0 + T_1 sin(\omega t - x\sqrt{\frac{\omega}{2\alpha}})e^{-x\sqrt{\omega/2\alpha}} \tag{4.10}$$

Phase difference along the beam, $|\Delta\emptyset| = \sqrt{\frac{\omega}{2\alpha}}x$

Using finite element method for the solution of the eqn. 4.9. The analytical and numerical solution are shown in fig 4.1.

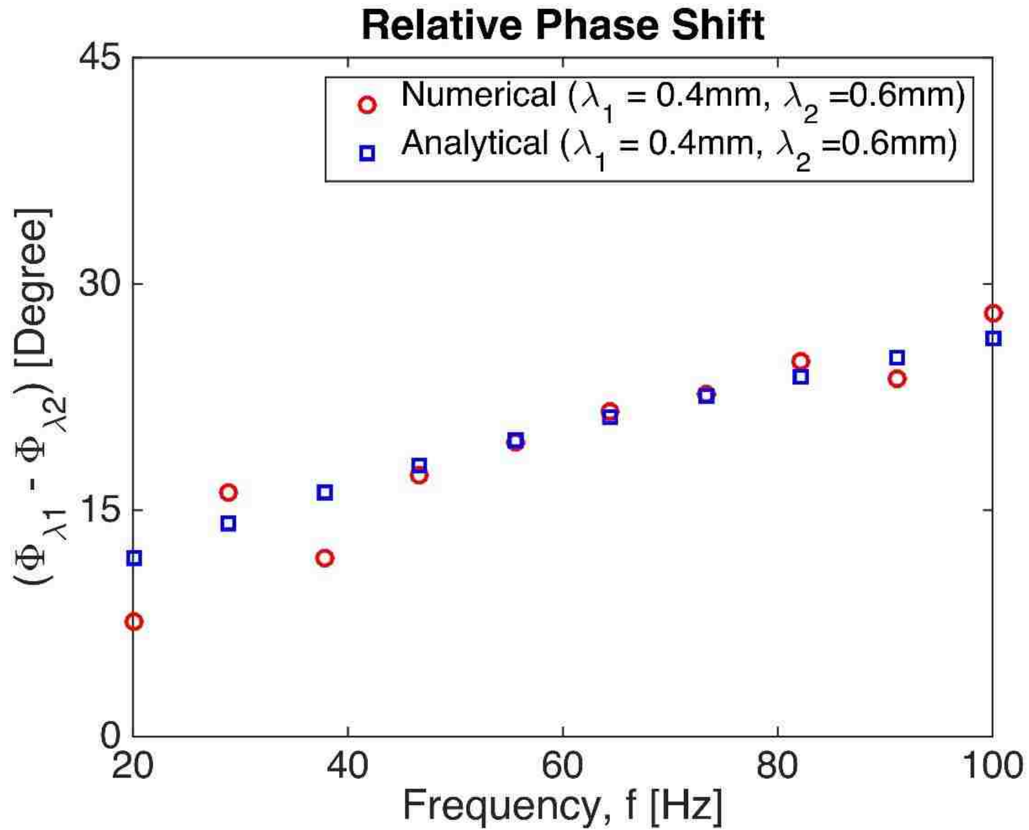

Figure 4.1: Analytical and Numerical analysis result of cantilever beam in harmonic case from the frequency ranging from 10 Hz to 100Hz

4.2 Experimental Setup:

In fig. 4.4 experimental setup for thermoreflectance measurement is shown labeling all the components. In this experiment the probe beam is modulated by an electro-optic modulator after it passes through the isolator. The signal generator is to generate sinusoidal signal and the Lock in Amplifier measures the amplitude and the phase of the signals. [6,7,48]The experimental setup was designed in such a way that the input pump beam travel towards the Al tip from the front side passing through isolator, EOM, beamplitter and probe beam comes from the back of the cantilever beam and when it reflects back due to the temperature oscillation the reflected beam end up being modulated and detected in the photodiode. With

reference to the input pump beam the phase change of the probe beam can be measured using Lock in Amplifier.

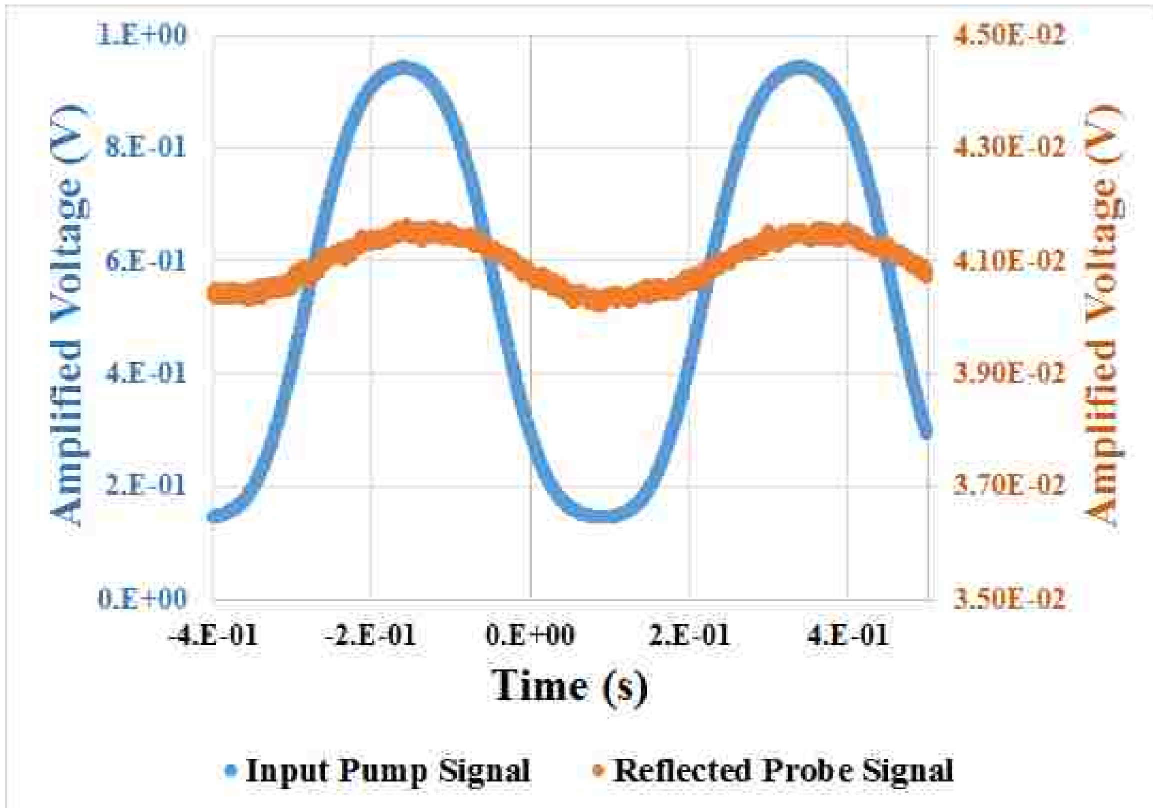

Figure 4.2: Modulated Incident pump beam and thermally modulated reflected probe beam for harmonic analysis

Lock in Amplifier is an essential equipment in harmonic analysis due to its capability of detecting signal buried under the noise. As our measurement is in the range of nano volts, it is necessary to extract the change of voltage signal rejecting all the noise contributing due to electronic noise, vibration, laser oscillation etc. Precautionary measure were taken to eliminate all the noise source can affect the measurement. Lock-in amplifier measures signal at a reference frequency feed as input from the signal generator which is the frequency of the laser that is oscillating as an input to the cantilever beam. The lock in Amplifier only can detect signal at this frequency other frequency oscillation are eliminated

by Phase Locked Loop circuitry. In the following diagram, the reference signal is a square wave at frequency ω_r. This might be the sync output from a function generator. If the sine output from the function generator is used to excite the experiment, the response might be the signal waveform shown below. The signal is $V_{sig}\sin(\omega_r t + \theta_{sig})$ where $V_{sig}$the signal amplitude is, ω_r is the signal frequency, and θ_{sig} is the signal's phase. Lock-in amplifiers generate their own internal reference signal usually by a phase-locked-loop locked to the external reference. In the diagram, the external reference, the lock-in's reference, and the signal are all shown. The internal reference is $V_L\sin(\omega_L t + \theta_{ref})$

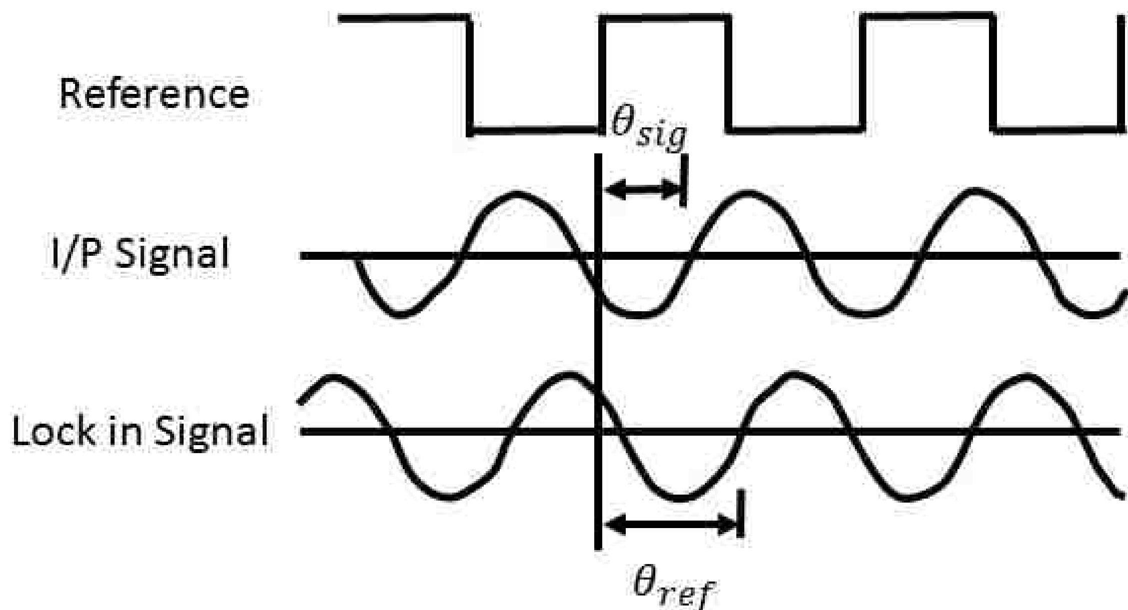

Figure 4.3: Lock in Amplifier operation with respect to reference signal to measure the real signal's phase shift[49]

The lock-in amplifies the signal and then multiplies it by the lock-in reference using a phase-sensitive detector or multiplier. The output of the PSD is simply the product of two Sine waves.

$$V_{psd} = V_{sig}V_L \sin(\omega_r t + \theta_{sig}) \sin(\omega_L t + \theta_{ref})$$

$$= \frac{1}{2} V_{sig}V_L \cos([\omega_r - \omega_L]t + \theta_{sig} - \theta_{ref}) - \frac{1}{2} V_{sig}V_L \cos([\omega_r + \omega_L)t + \theta_{sig} + \theta_{ref})$$

If the PSD output is passed through a low pass filter, the AC signals are removed. And in this case, the filtered PSD output will be:

$$V_{psd} = \frac{1}{2} V_{sig}V_L \cos(\theta_{sig} - \theta_{ref})$$

If second PSD multiplies the signal with the reference oscillator shifted by 90°, i.e. $V_L \sin(\omega_L t + \theta_{ref} + 90^o)$, its low pass filtered output will be:

$$V_{psd2} = \frac{1}{2} V_{sig}V_L \sin(\theta_{sig} - \theta_{ref})$$

$$V_{psd2} \sim V_{sig} \sin\theta$$

Now we have two outputs: one proportional to $\cos\theta$ and the other proportional to$\sin\theta$. If we call the first output X and the second Y,

$X = V_{sig}\cos\theta; Y = V_{sig}\sin\theta$

these two quantities represent the signal as a vector relative to the lock-in reference oscillator. X is called the 'in-phase' component and Y the 'out of phase' component. This is because when θ = 0, X measures the signal while Y is zero.

By computing the magnitude (R) of the signal vector, the phase dependency is removed.

$$R = \sqrt{X^2 + Y^2} = V_{sig}$$

R measures the signal amplitude and does not depend upon the phase between the signal and lock-in reference. A dual-phase lock-in has two PSDs with reference oscillators 90° apart, and can measure X, Y and R directly. In addition, the phase (θ) between the signal and lock-in is defined as:[49,50]

$$\theta = tan^{-1}(\frac{Y}{X})$$

Characterize the thermoreflectance behavior for micro and nano scale cantilever beam structures. The width of the beams are 50µm, 100µm, 150µm, 200µm, 250µm, 300µm and the minimum length is of the beams are four times of the corresponding width length. The resistivity of the of the device layer were kept in the range of 1-20 Ω-cm with 100 crystal orientation and the box layer thickness were in between 1-2µm.

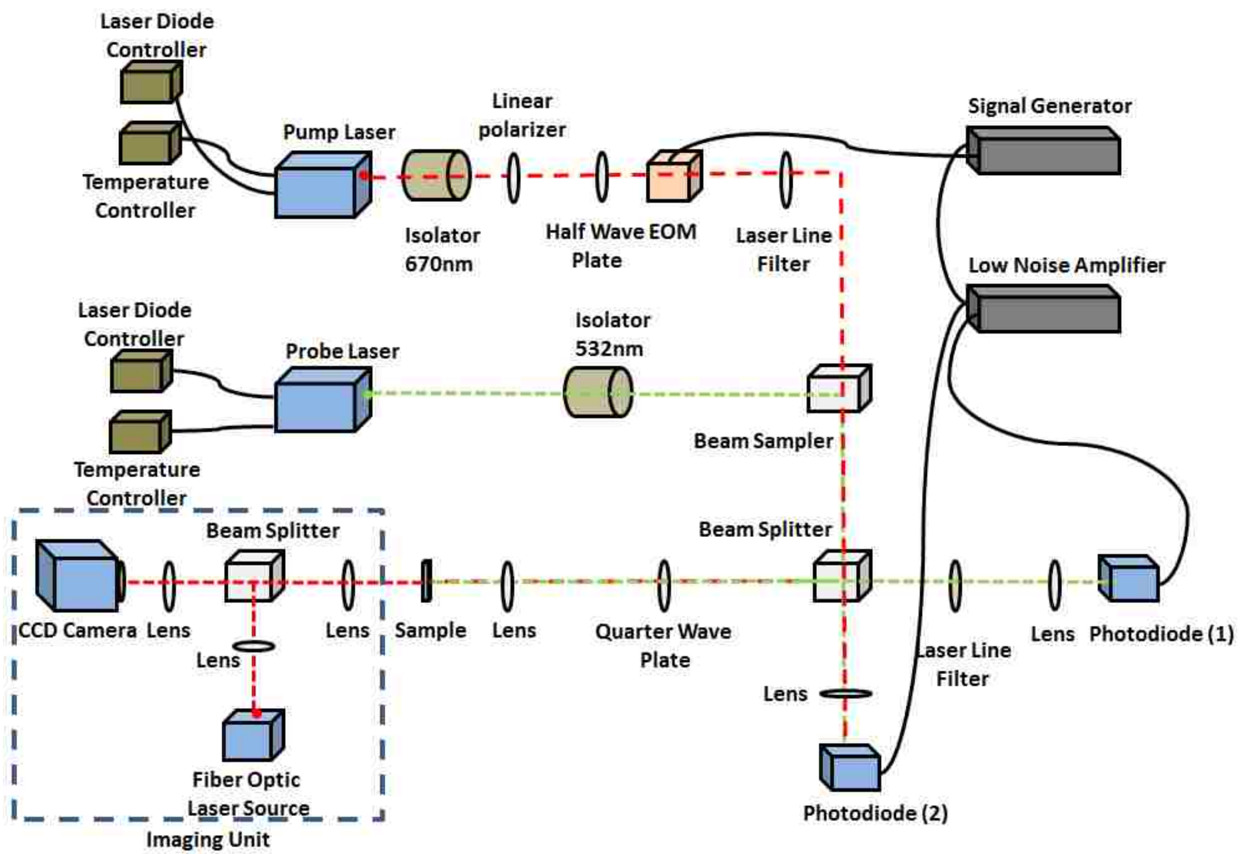

Figure 4.3: Harmonic analysis setup for topside thermoreflectance measurement

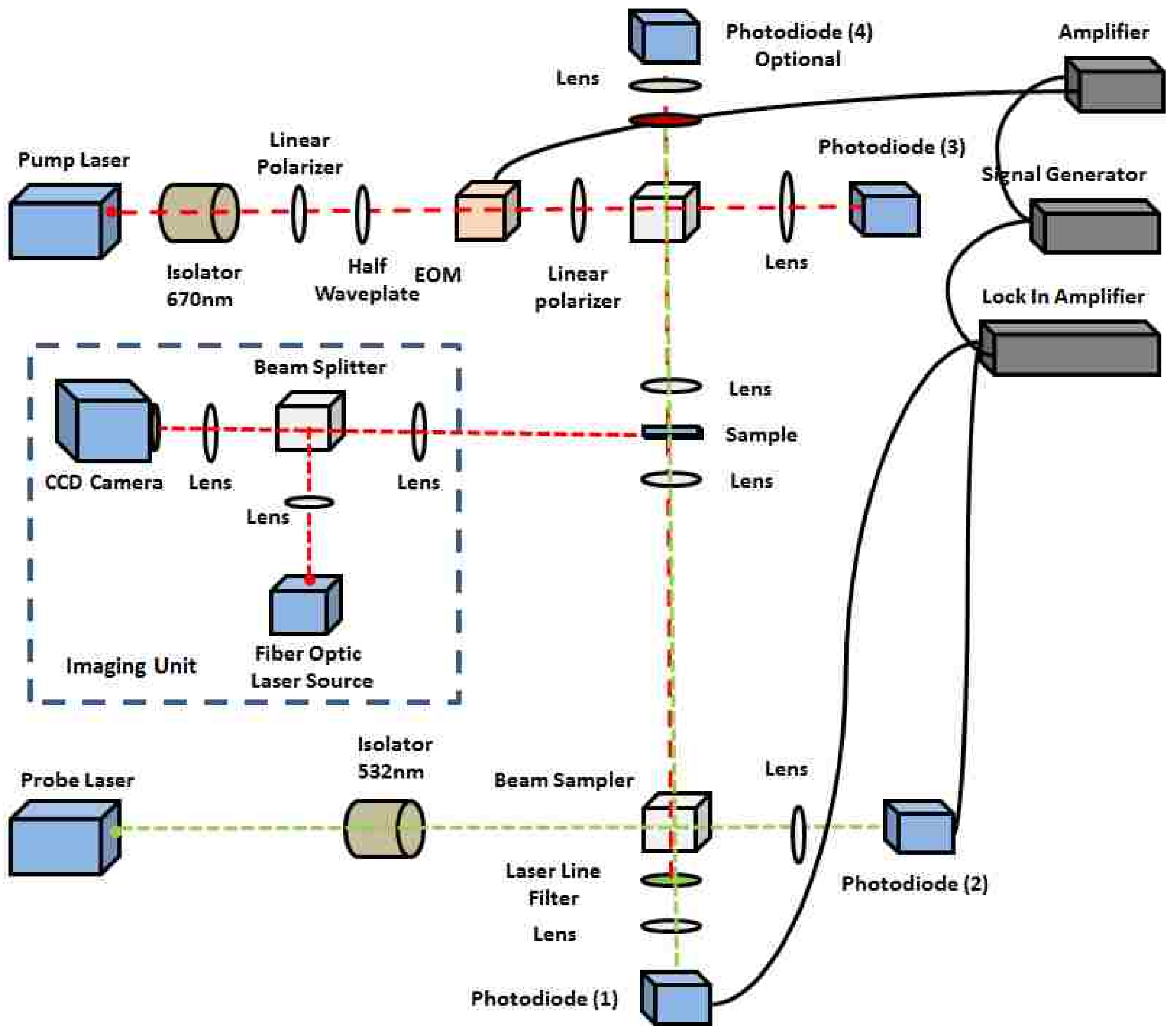

Figure 4.4: Setup for harmonic analysis setup for backside thermoreflectance

4.3 Results:

The experimental analysis of harmonic analysis were performed first of all validating the setup with Malen et. al.[6] with their measurement of semi-infinite bulk measurement and then Aluminum of 80nm film were deposited on top of bulk to Si to validate the result

using TDTR technique. After validating both of the results, experiment on cantilever beam were conducted and those are described below in different section.

4.3.1: Semi Infinite Sample Result validation:

Harmonic thermoreflectance setup for semi-infinite sample shown in fig. 4.4. The experimental data is in good agreement with the theory for the fitting parameter of thermal conductivity with the value of 117 W/m-K shown in fig. 4.7. The phase response for the bulk Si was validated with malen et al shown in fig. 4.6.[6]

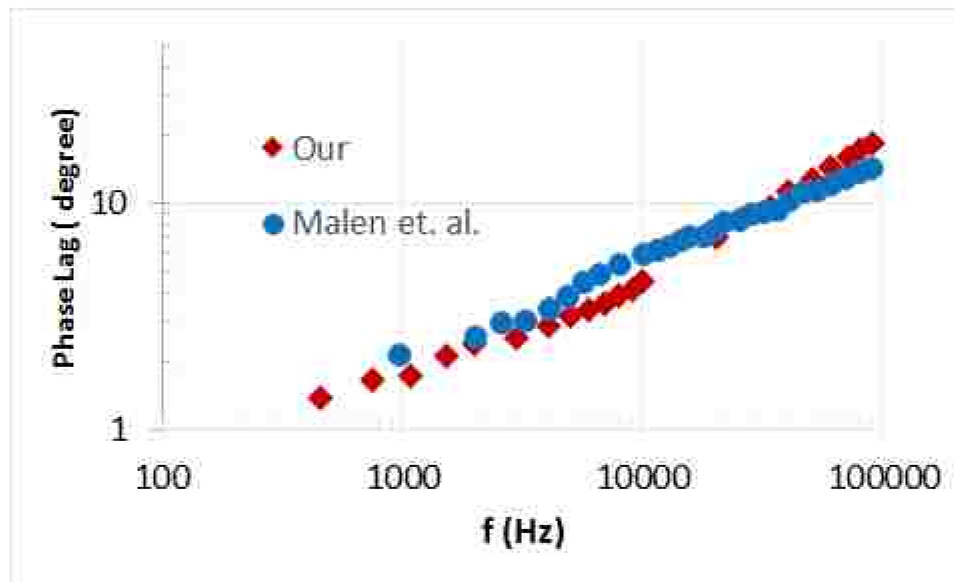

Figure 4.5: Semi-infinite sample result validation with malen et at. [6]

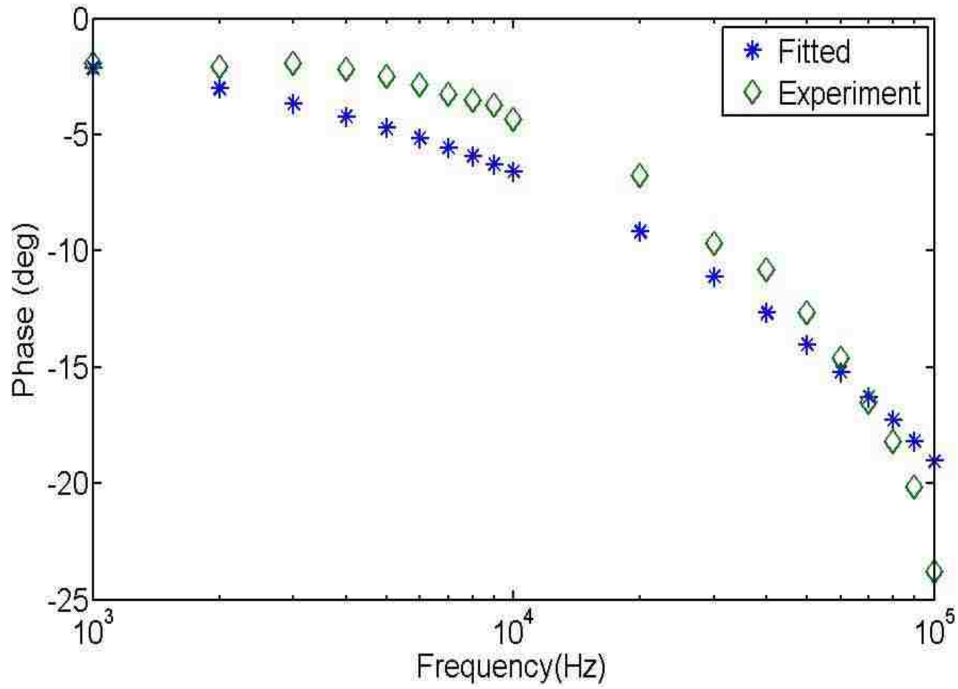

Figure 4.6: Semi-infinite result fit with the analytical analysis

4.3.2 Cantilever Beam Phase Response:

Phase response of a cantilever beam was measured along the length of the cantilever beam and the phase difference between two pints 400μm and 600μm are well fitted with the analytical result shown in fig. 4.8. In the frequency range of 10-50 Hz the heat capacity $764\, Jkg^{-1}K^{-1}$ has been measured. Higher frequency oscillation has effect of resonance and the time constant of the structure which prevents high frequency operation of the beam.

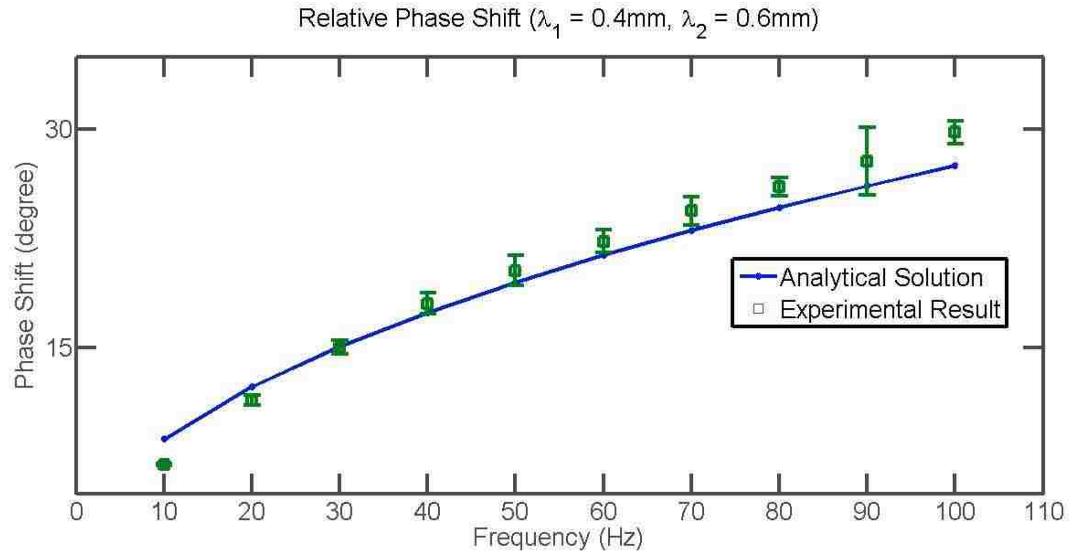

Figure 4.7: Cantilever beam phase response between 400μm and 600μm from the center of the Aluminum pad of the free end of the cantilever beam.

Chapter 5

Transient Analysis

5.1 Theory

In cartesian coordinate, the heat equation can be expressed as below,

$$\frac{\partial T}{\partial t} = \alpha \frac{\partial^2 T}{\partial x^2} \tag{5.1}$$

where, α is the thermal thermal diffusivity and expressed in terms of thermal conductivity

κ, heat capacity C and density ρ as $\alpha = \frac{\kappa}{\rho C}$.

with an initial condition and boundary conditions,

$$T(x, 0) = T_0$$

$$T(L. t) = T_0$$

$$-k \frac{\partial T}{\partial x}\bigg|_{x=0} = \begin{cases} T_1, 0 < t < t_0 \\ 0, t > t_0 \end{cases}$$

The solution can be derived in the form of,

$$T(0, t) = T_0 + T_1(1 - \exp^{-t}/_{\tau}) \tag{5.2}$$

Where, the time constant for the temperature rise and decay for 1D structure can be approximated as, $\tau = \frac{L^2}{\alpha}$ here L is denoted as the cantilever beam length and heat capacity can be extracted by inserting the value of thermal conductivity measured from the steady state technique.

For the transient analysis of cantilever beam numerical analysis were performed and the result of numerical analysis follows closely to the analytical value obtained from the experiment below.

5.2 Experimental Setup:

The experimental setup was kept similar as of the harmonic analysis shown in figure 5.1, in this case low frequency pulse function was generated using the function generator passing thru the EOM to modulate the pump beam, and the probe beam was used from the bottomside of the sample to measure the transient change in the thermoreflectance. All the measurement were performed at the pressure 1×10^{-7}Torr where convection does not have any impact on the result.

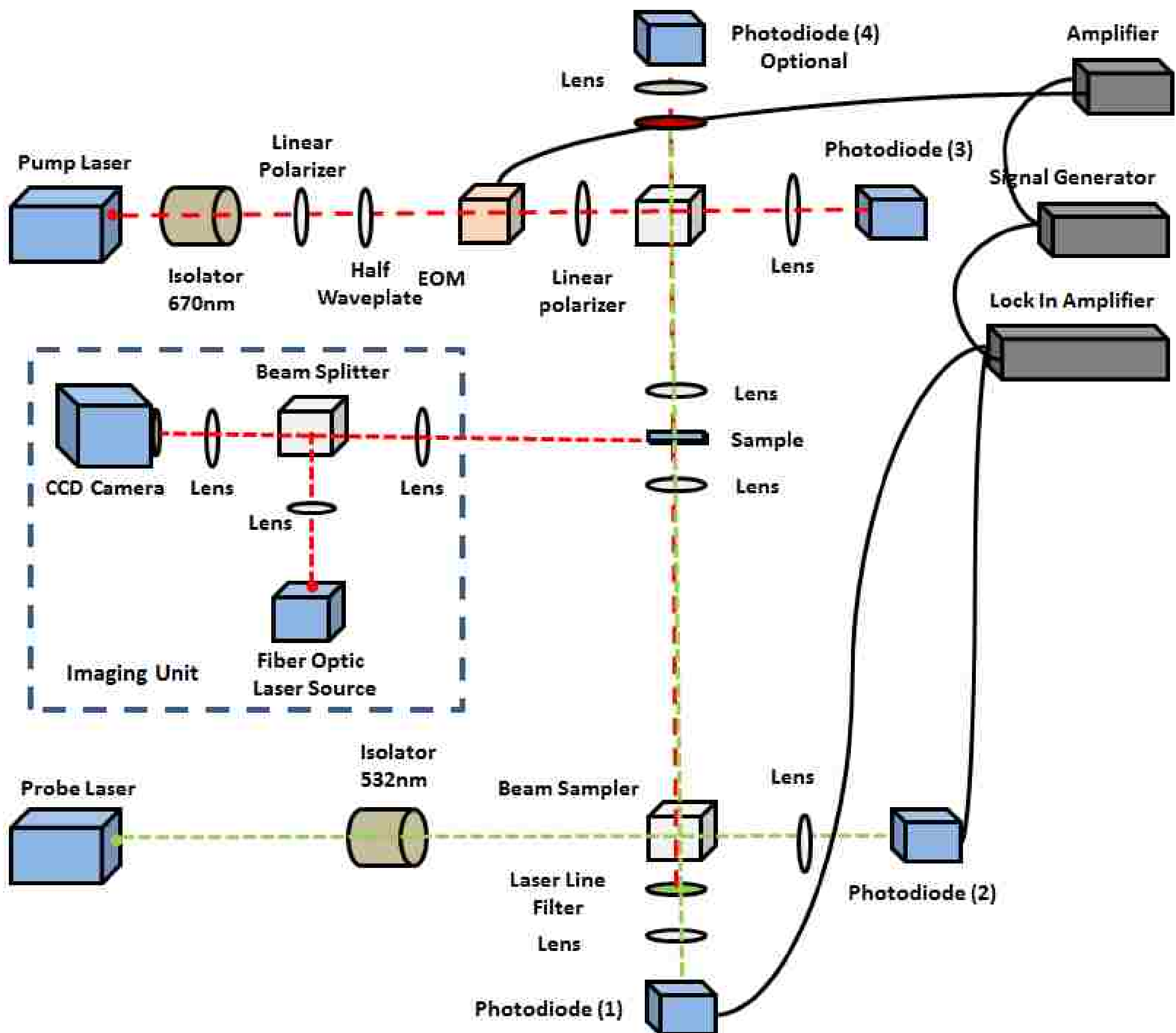

Figure 5.1: Setup for harmonic analysis setup for backside thermoreflectance

5.3 Results:

Pulse input of a transient pump beam incident on cantilever beam and the change of reflectivity due to temperature rise is analyzed and measured time constant were fitted for the extraction of specific heat capacity using the thermal conductivity measured in the steady state analysis. In this experiment the EOM modulation with other optical component such as wave plate, linear polarizer were monitored very carefully to make sure the pulse reaches its peak value or decay its lowest value without effecting the rise or fall time. Longer pulse duty cycle were chosen to make the saturated value is long enough and does not impact the time constant. On the other hand, it is very import to look after if the photodiode is getting saturated or not. The pump or probe power kept small enough or using Neutral Density filter to cut off the power before reaching to the photodiode and does not saturate. Saturated photodiode can produce erroneous measurement data hence erroneous time constant. For this region lower frequency pulse cycle were chose due to fact that cantilever beam reaches to its resonance frequency in higher frequency range which does not provide any result for the transient analysis. The pump and probe beam transient analysis result shown in figure 5.2.

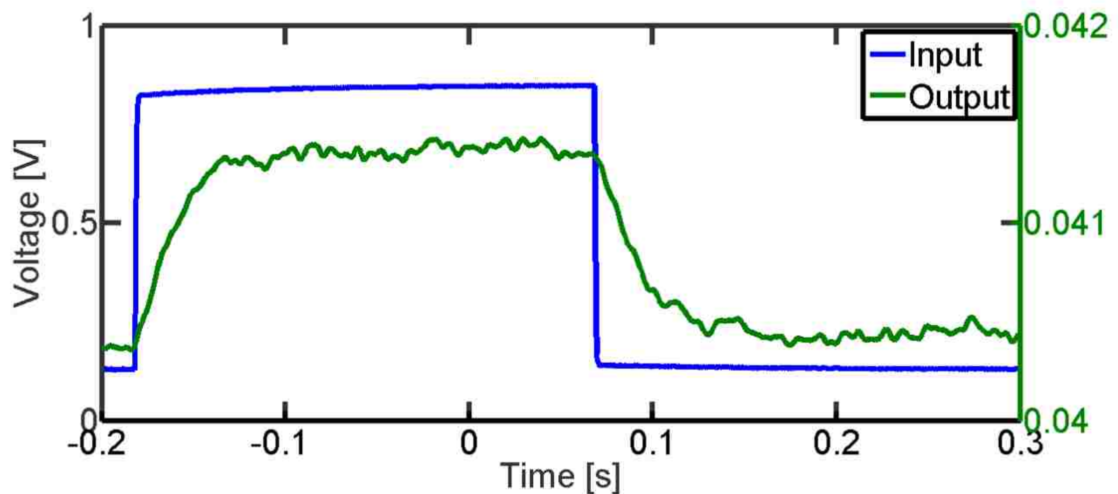

Figure 5.2: Transient temperature response using pump probe technique on cantilever beam

Several measurements were performed in this analysis with different input power and the rise time and the fall time were measured for the cantilever beam. The rise and fall time were very in close proximity and their results are shown in figure 5.3.

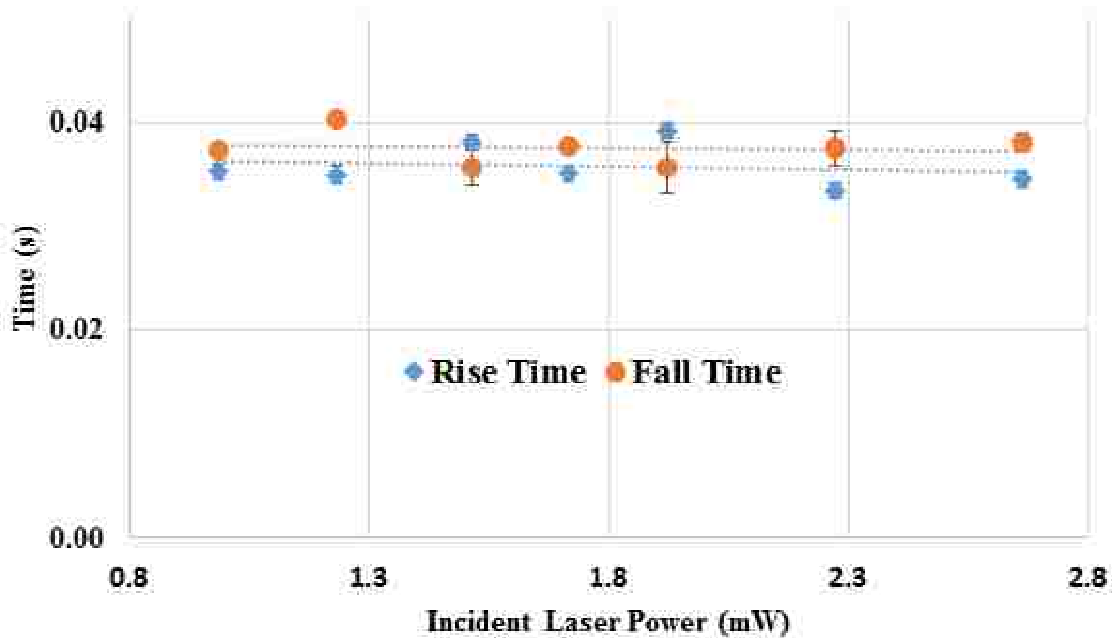

Figure 5.3: Analysis of rise and fall time with different incident laser power

The average value of rise and fall time of 35.5ms for 1.4mm long cantilever beam was measured and the thermal conductivity measured using steady state technique of 96.9 $Wm^{-1}K^{-1}$ has been used to measure the heat capacity at, $\tau = \frac{L^2}{\alpha}$; the heat capacity of Si has measured to be 753 $JKg^{-1}K^{-1}$. Which is very close to the value that we have measured using harmonic analysis.

Chapter 6

Conclusion and Future Work

The pump-probe thermoreflectance technique was demonstrated in steady state, harmonic and transient conditions for thermoreflectance coefficient, thermal conductivity, specific heat capacity measurement of free standing Si cantilever beams. Measurements were conducted in high vacuum to avoid convective losses and with no substrate to minimize radiative losses. Temperature gradients were minimized such that linear thermoreflectance response can be related to the measurements of thermal conductivity. Four cantilever beams 1.29 µm thick were measured and determined to have an average thermal conductivity of 96.9 ± 1.76 $Wm^{-1}K^{-1}$, which is a ~30% reduction from bulk values and applying harmonic and transient analysis of 1D free standing beam specific capacity also deduced with a value of $760\ JKg^{-1}K^{-1}$ which does not have much changes from its bulk.

So far we have able to establish a way to measure thermal conductivity at steady state condition for cantilever beam, harmonic and transient analysis to extract heat capacity using the thermal conductivity achieved from the steady state condition. For the establishment of the work, all the parameters of the experiment spot size, 1D heat conduction validation using FEM, convection effect on the thermoreflectance, radiation, boundary condition were analyzed step by step and demonstrated throughout the manuscript.

Several measurement analysis can be extended using this study for future research.

1. Analysis of thermal Conductivity with Various Film Thickness:

The main goal would be to apply these three technique for different thickness of Si cantilever beams and extrapolate the variation of thermal conductivity and heat capacity with the film thickness and demonstrate size effect variation from the bulk.[3,43,51]

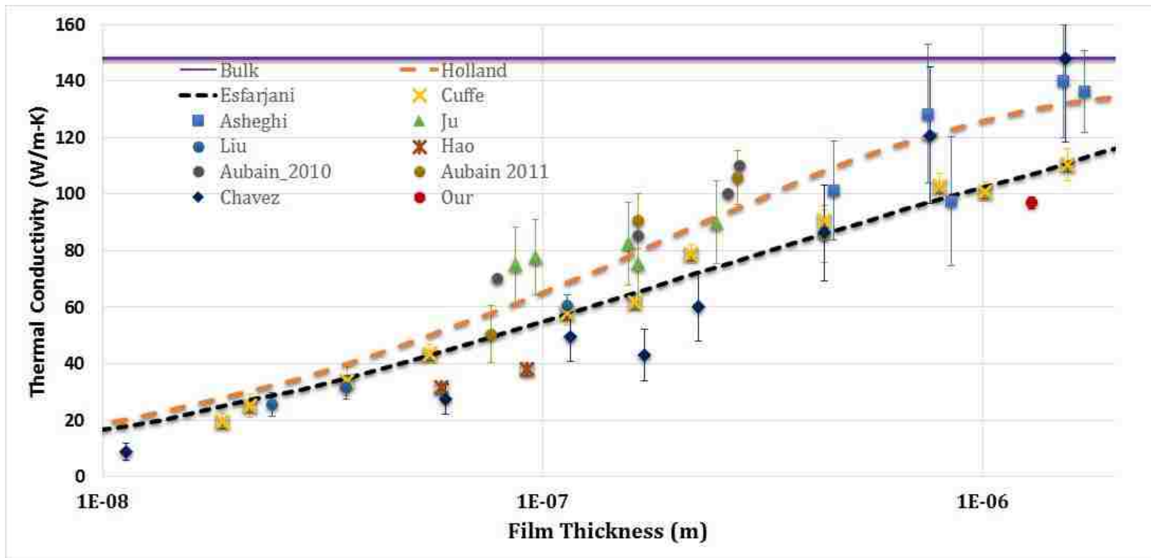

Figure 6.1: Thermal conductivity variation with film thickness extracted from different author and comparison to our analysis

2. Measurement at Cryogenic:

The setup for the cryogenic measurement is shown in figure 6.2 and 6.3. The cryo set up needs to be designed in such a way that the sample can be easily placed in the chamber without having any interference from the liquid nitrogen or helium pouring in to the chamber. The chamber also needed to be designed in such a way that the chamber have optical view port from both of the direction to allow laser beam to be accessible in the chamber to the cantilever beam. Using this technique the variation of thermal properties of different films at low temperature can be demonstrated and the identify size effect of microscale scale structure in the variation of thermal properties from the bulk and which is

necessary to measure accurately for low temperature device application or for thermoelectric materials.

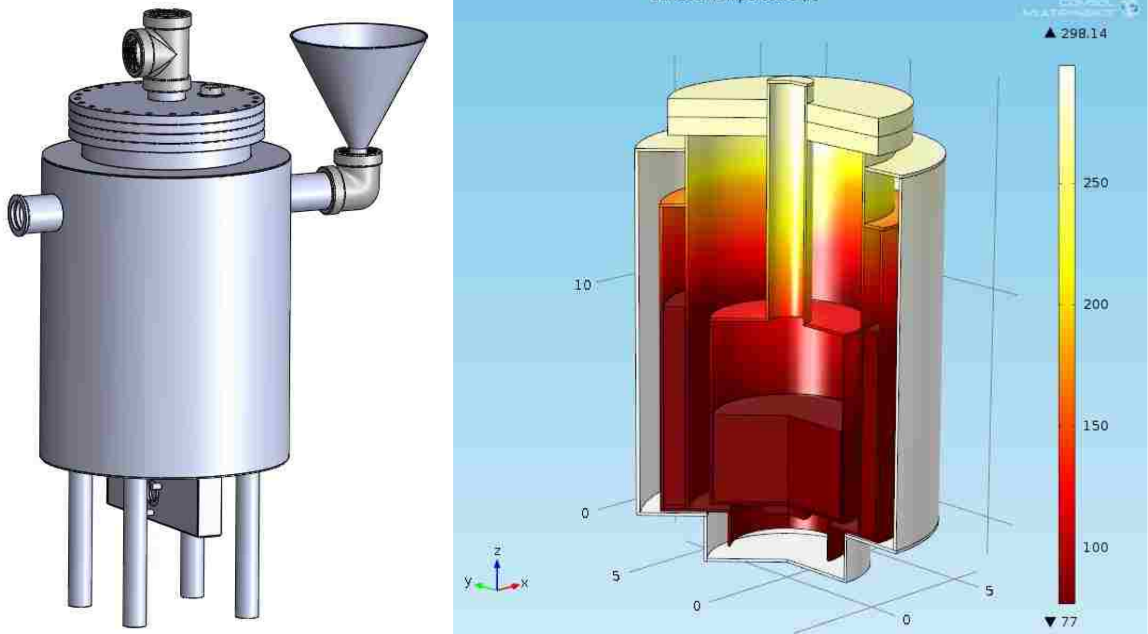

Figure 6.2: Cryogenic setup design for low temperature application

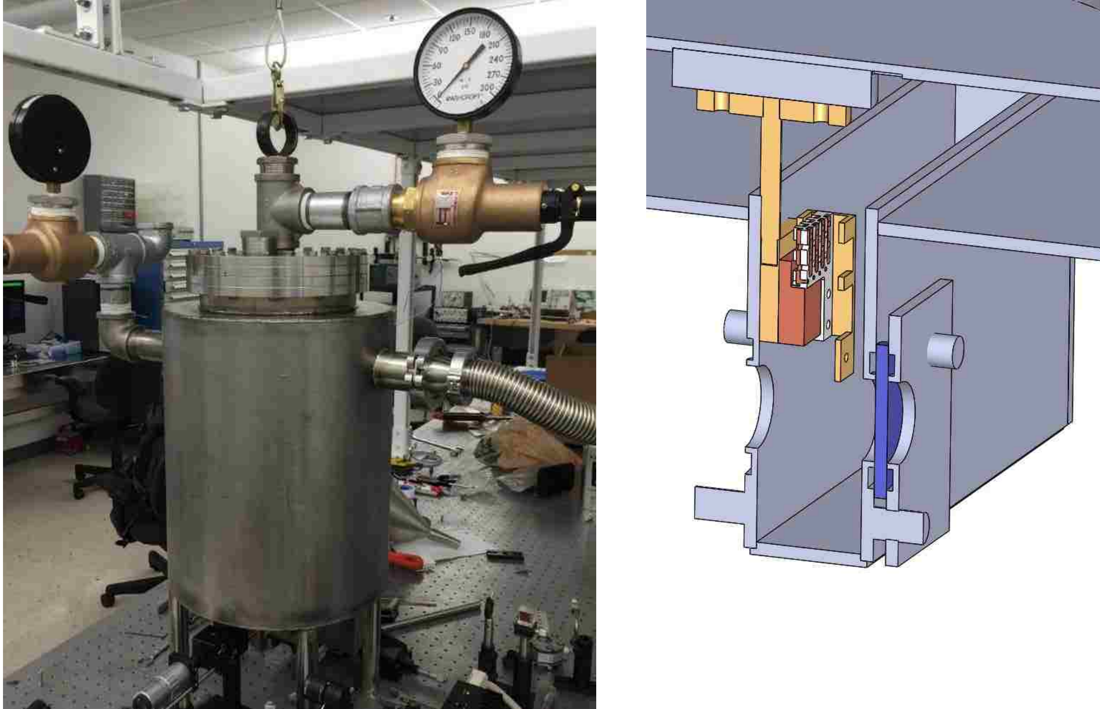

Figure 6.3: installation of Cryogenic Setup for low temperature measurement application

3. Phononic Crystal Structure Measurement:

The analysis of different thickness of Si cantilever beam will give a better insight of the variation of thermal conductivity and heat capacity. And applying it to phononic crystal structure provide better insight of thermal property variation due to the change phonon mean free path. Phononic device structure is constructed in such a way that air holes are fabricated intentionally in a materials where the dimensions are smaller than the mean free path of phonon which introduces more scattering in heat conduction and effect the material property which are useful for low temperature application and also to manipulate for wideband gap phononic structure devices.

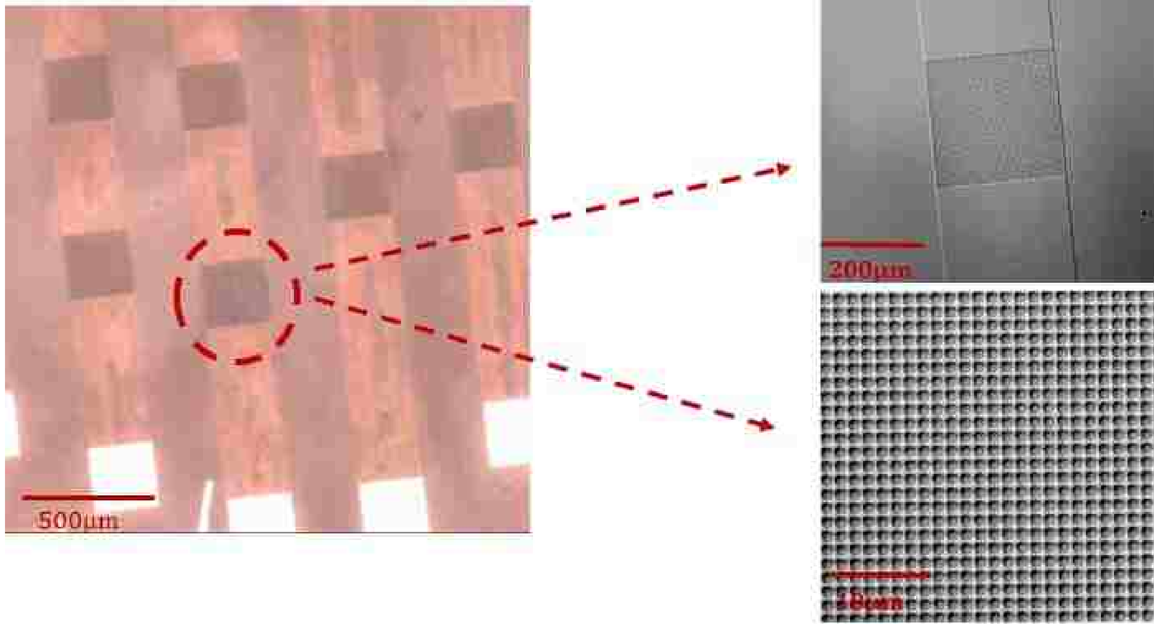

Figure 6.4: Phononic Crystals along the slab of cantilever beam to compare thermal conductivity variation with their slab counterpart.

References

[1] D.G. Cahill, Rev. Sci. Instrum. **61**, 802 (1990).

[2] K.T. Regner, D.P. Sellan, Z. Su, C.H. Amon, A.J.H. McGaughey, and J. Malen, Nat. Commun. **4**, 1640 (2013).

[3] J. Cuffe, J.K. Eliason, A.A. Maznev, K.C. Collins, J.A. Johnson, A. Shchepetov, M. Prunnila, J. Ahopelto, C.M. Sotomayor Torres, G. Chen, and K.A. Nelson, Phys. Rev. B - Condens. Matter Mater. Phys. **91**, 1 (2015).

[4] H.A. Weakliem and D. Redfield, J. Appl. Phys. **50**, 1491 (1979).

[5] M. Asheghi, M.N. Touzelbaev, K.E. Goodson, Y.K. Leung, and S.S. Wong, J. Heat Transfer **120**, 30 (1998).

[6] J. a. Malen, K. Baheti, T. Tong, Y. Zhao, J. a. Hudgings, and A. Majumdar, J. Heat Transfer **133**, 081601 (2011).

[7] K.T. Regner, S. Majumdar, and J. a Malen, Rev. Sci. Instrum. **84**, 064901 (2013).

[8] P.E. Hopkins, J.R. Serrano, and L.M. Phinney, Int. J. Thermophys. **31**, 2380 (2010).

[9] D.G. Cahill, Rev. Sci. Instrum. **75**, 5119 (2004).

[10] D.G. Cahill, P. V. Braun, G. Chen, D.R. Clarke, S. Fan, K.E. Goodson, P. Keblinski, W.P. King, G.D. Mahan, A. Majumdar, H.J. Maris, S.R. Phillpot, E. Pop, and L. Shi, Appl. Phys. Rev. **1**, 011305 (2014).

[11] A. Schmidt, M. Chiesa, X. Chen, and G. Chen, Rev. Sci. Instrum. **79**, (2008).

[12] A.J. Schmidt, X. Chen, and G. Chen, Rev. Sci. Instrum. **79**, 1 (2008).

[13] S. Torii and W.J. Yang, Int. J. Heat Mass Transf. **48**, 537 (2005).

[14] A.A. Joshi and A. Majumdar, J. Appl. Phys. **74**, 31 (1993).

[15] M.I. Flik, B.I. Choi, and K.E. Goodson, J. Heat Transfer **114**, 666 (1992).

[16] G. Chen and a. Shakouri, J. Heat Transfer **124**, 242 (2002).

[17] F. Yang and C. Dames, Phys. Rev. B - Condens. Matter Mater. Phys. **87**, 1 (2013).

[18] J.P. Freedman, J.H. Leach, E. a Preble, Z. Sitar, R.F. Davis, and J. a Malen, Sci. Rep. **3**, 2963 (2013).

[19] W.J. Parker, R.J. Jenkins, C.P. Butler, and G.L. Abbott, J. Appl. Phys. **32**, 1679 (1961).

[20] N.O. Birge and S.R. Nagel, Rev. Sci. Instrum. **58**, 1464 (1987).

[21] D.G. Cahill, Rev. Sci. Instrum. **61**, 802 (1990).

[22] C.A. Paddock and G.L. Eesley, J. Appl. Phys. **60**, 285 (1986).

[23] W.S. Capinski and H.J. Maris, Rev. Sci. Instrum. **67**, 2720 (1996).

[24] Y. Wang, J.Y. Park, Y.K. Koh, and D.G. Cahill, J. Appl. Phys. **108**, 1 (2010).

[25] J.L. Battaglia, A. Kusiak, C. Rossignol, and N. Chigarev, Phys. Rev. B - Condens. Matter Mater. Phys. **76**, 1 (2007).

[26] T. Borca-Tasciuc, A.R. Kumar, and G. Chen, Rev. Sci. Instrum. **72**, 2139 (2001).

[27] N. Taketoshi, T. Baba, and A. Ono, Meas. Sci. Technol. **12**, 2064 (2001).

[28] J.L. Braun, C.H. Baker, A. Giri, M. Elahi, K. Artyushkova, E. Thomas, P.M. Norris, Z.C. Leseman, J.T. Gaskins, and P.E. Hopkins, Phys. Rev. B **140201**, 1 (2016).

[29] R. Cheaito, J.C. Duda, T.E. Beechem, K. Hattar, J.F. Ihlefeld, D.L. Medlin, M.A. Rodriguez, M.J. Campion, E.S. Piekos, and P.E. Hopkins, Phys. Rev. Lett. **109**, 1 (2012).

[30] G.R. Stewart, Rev. Sci. Instrum. **54**, 1 (1983).

[31] B.L. Zink, B. Revaz, R. Sappey, and F. Hellman, Rev. Sci. Instrum. **73**, 1841 (2002).

[32] P.F. Sullivan and G. Seidel, Phys. Rev. **173**, 679 (1968).

[33] L. Steele, Rev. … **39**, 588 (1993).

[34] F. Fominaya, J. Chaussy, and P. Gandit, Rev. Sci. Instrum. **69**, 168 (1998).

[35] G. Ventura and M. Perfetti, Spiringer (2014).

[36] M. Farzaneh, K. Maize, D. Lüerßen, J.A. Summers, P.M. Mayer, P.E. Raad, K.P. Pipe, A. Shakouri, R.J. Ram, and J.A. Hudgings, J. Phys. D. Appl. Phys. **42**, 143001 (2009).

[37] R. Weil, Proc. Phys. Soc. **60**, 8 (1948).

[38] T. Favaloro, J.H. Bahk, and A. Shakouri, Rev. Sci. Instrum. **86**, (2015).

[39] P.E. Raad, P.L. Komarov, and M.G. Burzo, Electron. Cool. **v. 14**, (2008).

[40] M. Aubian, Determination of the Thermal Conductivity of Dielectric Thin Films through Experimental Measurement and Crystallographic Analysis, 2013.

[41] A.J. Schmidt, R. Cheaito, and M. Chiesa, **094901**, (2009).

[42] C. Pradere, J. Caumes, S. Benkhemis, G. Pernot, S. Dilhaire, J. Batsale, C. Pradere, J. Caumes, S. Benkhemis, G. Pernot, and E. Palomo, (2015).

[43] R. Chavez, S. Angst, K. Maize, A. Gondorf, G. Schierning, D.E. Wolf, and A. Lorke, **083705**, 1 (2012).

[44] M.G. Burzo, P.L. Komarov, and P.E. Raad, **28**, 637 (2005).

[45] J. Christofferson and A. Shakouri, IEEE Semicond. Therm. Meas. Manag. Symp. 271 (2004).

[46] S. Dilhaire, S. Grauby, and W. Claeys, Appl. Phys. Lett. **84**, 822 (2004).

[47] X. Zhang and C.P. Grigoropoulosa, Rev. Sci. Instrum. **66 (2)**, 1115 (1995).

[48] J. Liu, J. Zhu, M. Tian, X. Gu, A. Schmidt, and R. Yang, Rev. Sci. Instrum. **84**, 034902 (2013).

[49]Appl. Note 1 (2011).

[50] S. Bhattacharyya, R.N. Ahmed, B.B. Purkayastha, and K. Bhattacharyya, J. Phys. Conf. Ser. **759**, 012096 (2016).

[51] K. Esfarjani, G. Chen, and H.T. Stokes, Phys. Rev. B - Condens. Matter Mater. Phys. **84**, 1 (2011).

Appendix

Appendix A: Fabrication Process Flow

Process Sheet Cantilever Beam

Wafer Specs:

Type: SOI <100> n-type

Device: 1.29um; BOX: 500nm; Handle: 525um

Front: Polished Back: Polished

Process:

HF Cleaning

Process Step	*Tool*	*Parameters*		*Comments*
BHF Cleaning	Acid Bench	6:1 BOE	60 sec	6 Pts 40% NH_4F; 1 Pt 49% HF Acid
QDR	Caustic Bench	5 cycles		
Spin Rinse Dryer	Verteq	Resistivity DI water: 15 - 18 mega ohm		
Dehydration Bake	Hot Plate	200° C, 5 min		

Cantilever
Beam
Pattern
(Mask 1)

Process Step	*Tool*	*Parameters*		*Comments*
HMDS Spin	HMDS Vapor Coating	100°C	60s	
PR Spin	CEE Coater	500 rpm, 5 sec	5000 rpm, 20 sec	AZ1518 Single Dispense of 10ml
Soft Bake	Hot Plate	115° C, 90 s		
Expose	Karl Suss	Mask: Cantilever Beam Pattern, Exp: 12 sec		
Develop	Caustic Bench	3 mins AZ300MIF		with slight agitation
QDR	Caustic Bench	5 cycles		
Spin Rinse Dryer	Verteq	Resistivity DI water: 15 - 18 mega ohm		
Inspection	Nikon Microscope			

RIE Etch (Device) &
Cleaning

Process Step	*Tool*	*Parameters*		*Comments*
RIE Etch	March Plasma RIE	125W, SF6, CHF_3, O_2	300nm/min	
Ashing	March RIE Etcher	600 watt; 100mTorr, 60 sec, 4 times	86% O_2 (Gas 4)	Rotate wafer 180° and repeat for uniform cleaning

Metal Pad
Pattern
(Mask 2)

Process Step	*Tool*	*Parameters*		*Comments*
HMDS Spin	HMDS Vapor Coating	100°C	60s	
PR Spin	CEE Coater	500 rpm, 5 sec	5000 rpm, 20 sec	AZ15 18 Single Dispense of 10ml
Soft Bake	Hot Plate	115° C, 90 s		
Expose	Karl Suss	Mask: Metal Pad Pattern, Exp: 15 sec		
Develop	Caustic Bench	2 mins AZ300MIF		with slight agitation
QDR	Caustic Bench	5 cycles		
Spin Rinse Dryer	Verteq	Resistivity DI water: 15 - 18 mega ohm		
Inspection	Nikon Microscope			

Al Pad
Metal
Deposition
& Lift off

Process Step	*Parameters*	*Comments*
Metal Evaporation	250A, 1A/s	80nm
Acetone Soak	10 min	
IPA Rinse	2 min	

QDR	5 Cycles	
Spin Rinse Dryer	Resistivity DI water: 15 - 18 mega ohm	

Al Pad Protect Layer (Mask 1)

Process Step	*Tool*	*Parameters*		*Comments*
HMDS Spin	CEE Coater	500 rpm, 5 sec	5000 rpm, 30 s	HMDS single Dispense with repeater setting 3ml
PR Spin	CEE Coater	500 rpm, 5 sec	5000 rpm, 20 sec	AZ15 18 Single Dispense of 10ml
Soft Bake	Hot Plate	115° C, 90 s		
Expose	Karl Suss	Mask: Cantilever Beam Pattern, Exp: 15 sec		
Develop	Caustic Bench	2 mins AZ300MIF		with slight agitation
QDR	Caustic Bench	5 cycles		
Spin Rinse Dryer	Verteq	Resistivity DI water: 15 - 18 mega ohm		
Inspection	Nikon Microscope			

HF Release & PR Strip

Process Step	*Tool*	*Parameters*		*Comments*
Hard Bake	Hot Plate	120˚C	2 min	

6:1 BOE	Acid Bench	5-10 hours depending on device dimensions		Slight agitation time to time
DI Water Clean	Solvent Bench			Slight agitation
N_2 Dry	Solvent Bench			Blow slowly
Acetone Soak		10 min		
IPA Rinse	Solvent Bench	2 min		
DI Water Clean	Solvent Bench			Slight agitation
N_2 Dry	Solvent Bench			Blow slowly

Appendix B: Supporting Experimental Data

Thermoreflectance and temperature of different beams, supporting figures for thermal conductivity measurement.

Steady State Supporting Measurement: Thermoreflectance Data for different beams:

i. Width 100µm and length 400µm.

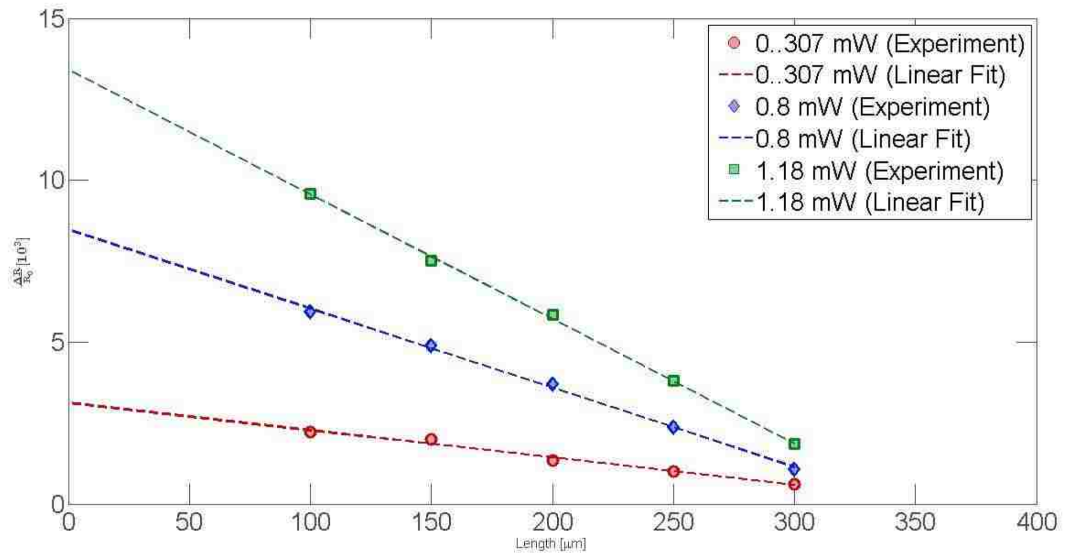

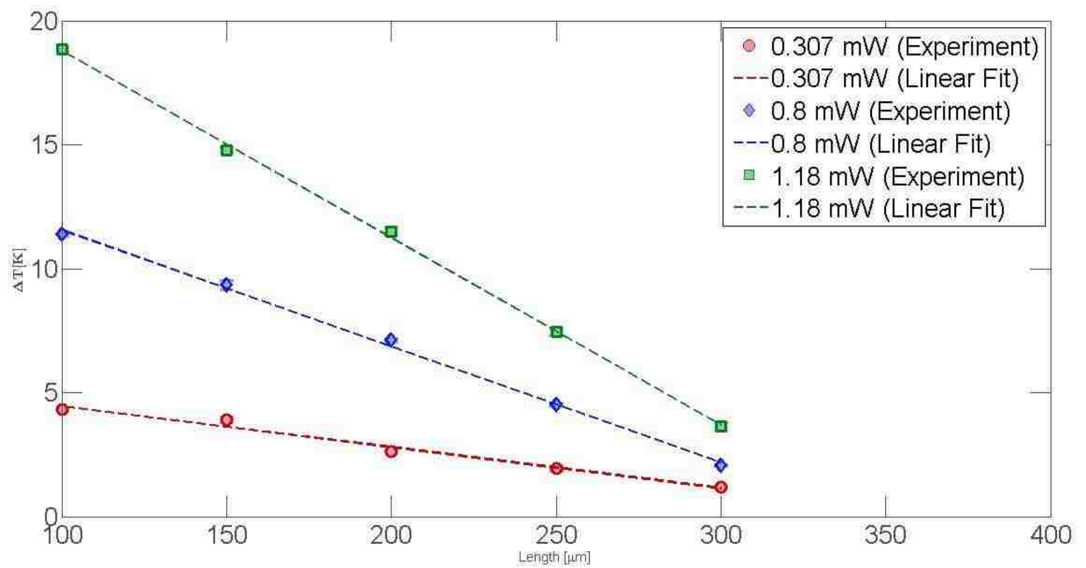

ii. Width 150µm and length of 750µm

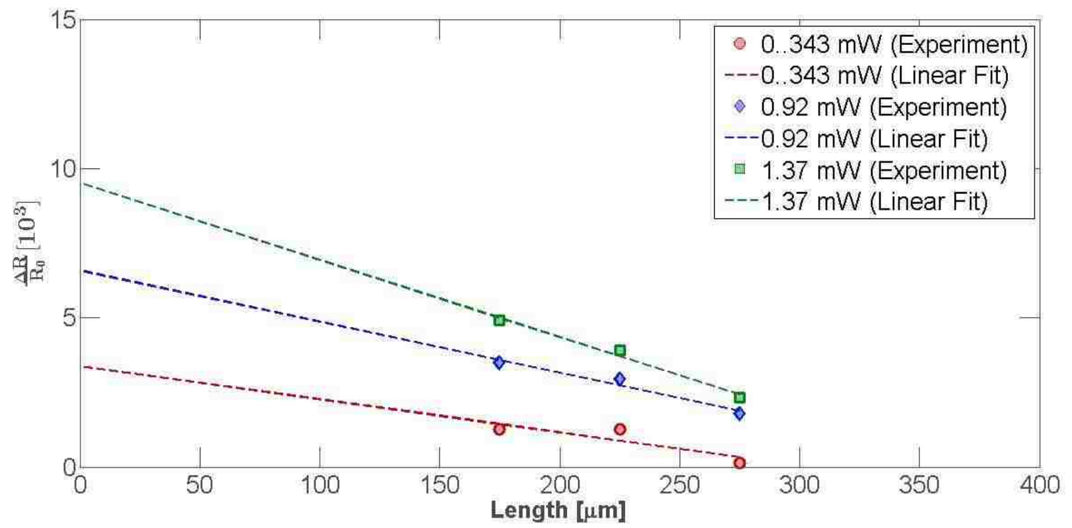

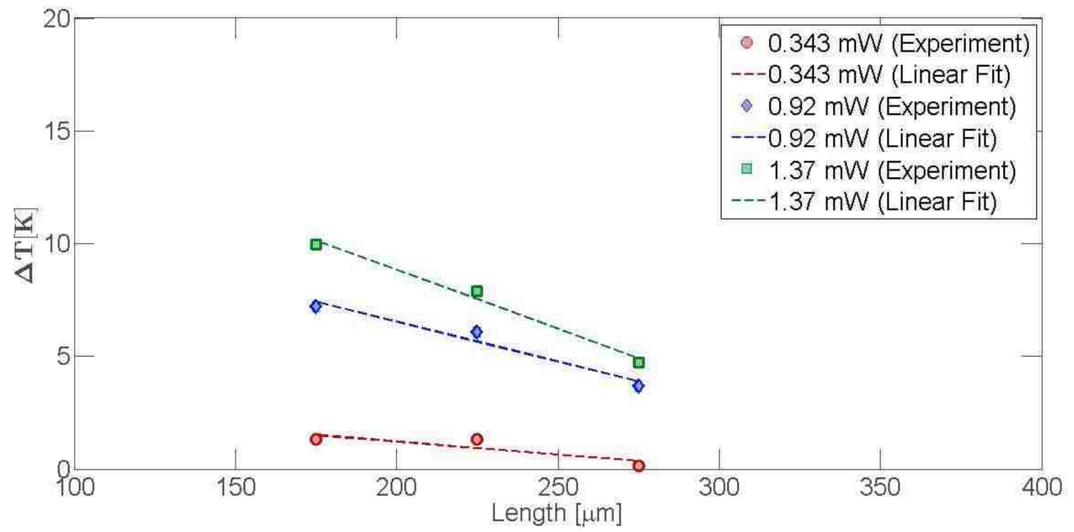

iii. Width 150µm and Length of 1050µm:

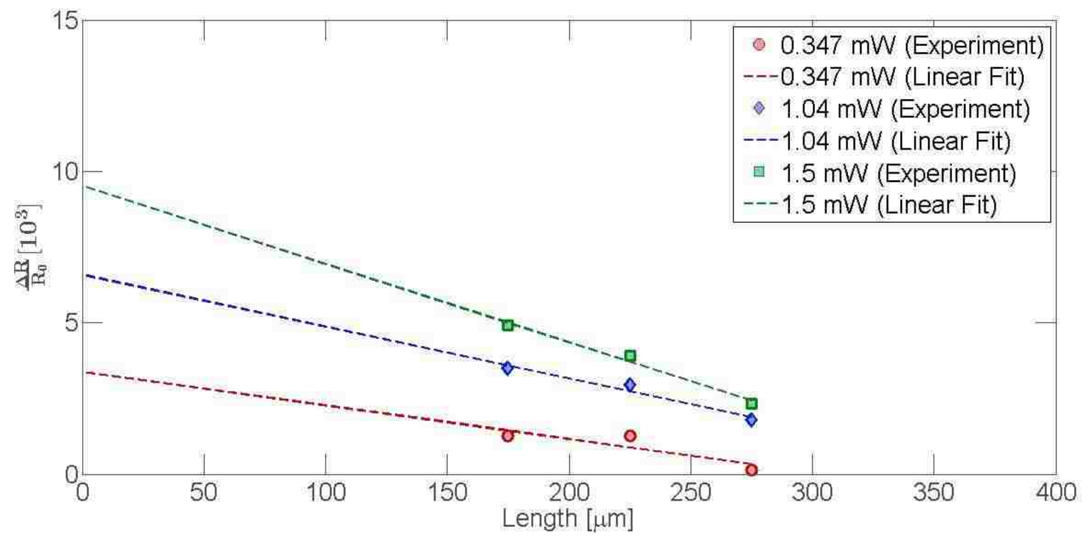

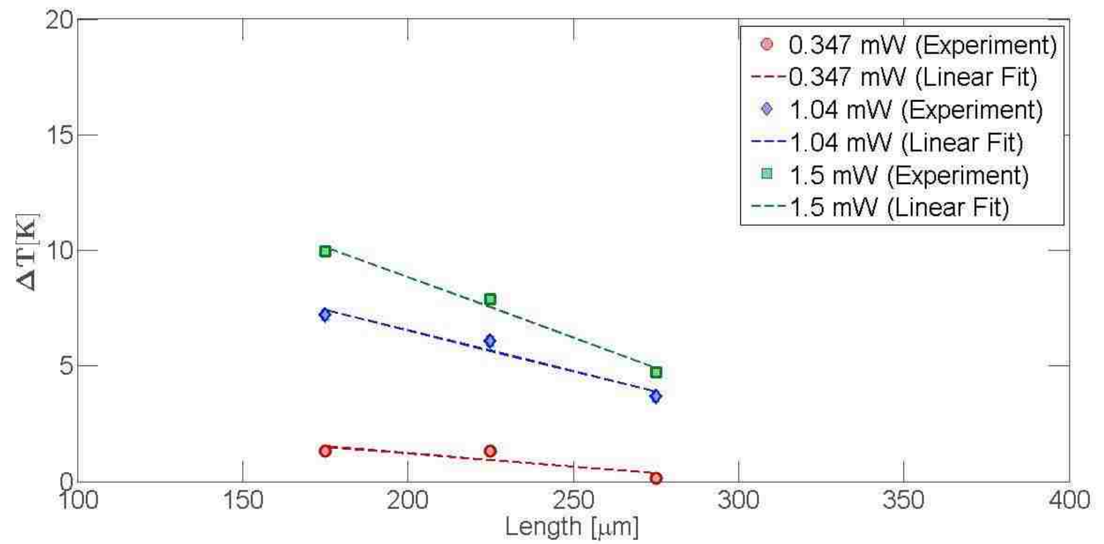

Appendix C: Matlab Script

1. Steady State:

```
clear all;
close all;
clc;

%%%%%%%%%%%%%%%%% Steady State Calculation
%%%%%%%%%%%%%%%%%%%%%%%%%%%%%%%%%

%% import data
fileName = 'Steady_State_Datav1.0.xlsx';
BeamParam = importBeamParam(fileName, 'Beam parameters'  );
FrontSideParam = importFrontSide(fileName, 'Front Side'  );
BackSide_425_param = importBackSide(fileName, 'Backside(425)'  );
BackSide_450_param = importBackSide(fileName, 'Backside(450)'  );
BackSide_475_param = importBackSide(fileName, 'Backside(475)'  );



%% 425
BackSide_425_param = processSteadyState( BackSide_425_param, FrontSideParam.dTK(1),
FrontSideParam.FluxWm2(1) );
%% 450
BackSide_450_param = processSteadyState( BackSide_450_param, FrontSideParam.dTK(2),
FrontSideParam.FluxWm2(2) );
%% 475
BackSide_475_param = processSteadyState( BackSide_475_param, FrontSideParam.dTK(3),
FrontSideParam.FluxWm2(3) );

K_Average = ( BackSide_425_param.K_thrmlCond + BackSide_450_param.K_thrmlCond +
BackSide_475_param.K_thrmlCond )/3
  %% plot dR/R0
  width = 3.39;     % Width in inches
  golden_mean = (sqrt(5)-1.0)/2.0;    % Aesthetic ratio
  height = width*golden_mean;    % Height in inches
  alw = 0.5;    % AxesLineWidth
  fsz = 11;      % Fontsize
  lw = 2.5;      % LineWidth
  msz = 10;       % MarkerSize

  h = figure;
  pos = get(gcf, 'Position');
  posNew = [pos(1) pos(2) width*100, height*100];
  set(gcf, 'Position', posNew); %<- Set size
  set(h, 'Renderer', 'painters');
  set(gca, 'FontSize', fsz, 'LineWidth', alw); %<- Set properties
  markerEdgeColor = [ 205 1 1;
                  2 32 218;
                  1 127 26 ]/255;
  markerFaceColor = [ 223 161 161;
                  148 158 222;
                  134 209 149]/255;
```

```
   errorbar( BackSide_425_param.xm/1E-6, BackSide_425_param.dRR0*1E3,
BackSide_425_param.dRR0_errorBar*1E3,  'o', 'LineWidth', lw, 'MarkerSize', msz,  'MarkerFaceColor',
markerFaceColor(1,:), 'MarkerEdgeColor',  markerEdgeColor(1,:), 'Color',  markerFaceColor(1,:)  );
   hold on;
   plot( BackSide_425_param.linearFit_xm/1E-6, BackSide_425_param.linearFit_dRR0*1E3, '--
','LineWidth', lw/1.2, 'MarkerSize', msz,  'Color',  markerEdgeColor(1,:) );
   hold on;
   errorbar( BackSide_450_param.xm/1E-6, BackSide_450_param.dRR0*1E3,
BackSide_450_param.dRR0_errorBar*1E3, 'd', 'LineWidth', lw, 'MarkerSize', msz,  'MarkerEdgeColor',
markerEdgeColor(2,:), 'MarkerFaceColor',  markerFaceColor(2,:), 'Color',  markerFaceColor(2,:) );
   hold on;
   plot( BackSide_450_param.linearFit_xm/1E-6, BackSide_450_param.linearFit_dRR0*1E3, '--
','LineWidth', lw/1.2, 'MarkerSize', msz,  'Color',  markerEdgeColor(2,:) );
   hold on;
   errorbar( BackSide_475_param.xm/1E-6,
BackSide_475_param.dRR0*1E3,BackSide_475_param.dRR0_errorBar*1E3,  's', 'LineWidth', lw,
'MarkerSize', msz,  'MarkerFaceColor',  markerFaceColor(3,:), 'MarkerEdgeColor',  markerEdgeColor(3,:),
'Color',  markerFaceColor(3,:));
   hold on;
   plot( BackSide_475_param.linearFit_xm/1E-6, BackSide_475_param.linearFit_dRR0*1E3, '--
','LineWidth', lw/1.2, 'MarkerSize', msz,  'Color',  markerEdgeColor(3,:) );



   ttltext = sprintf( 'Title (place your own)' );
   title(ttltext);
   lgnd1 = sprintf( '425 mA (Experiment)');
   lgnd11 = sprintf( '425 mA (Linear Fit)');
   lgnd2 = sprintf( '450 mA (Experiment)' );
   lgnd22 = sprintf( '450 mA (Linear Fit)');
   lgnd3 = sprintf( '475 mA (Experiment)');
   lgnd33 = sprintf( '475 mA (Linear Fit)');
   set(gca, 'YTick', 0:5:15, ...
         'TickLength'  , [.02 .02] , ...
         'XColor', [.3 .3 .3], ...
         'YColor', [.3 .3 .3], ...
         'XMinorTick', 'off', ...
         'YMinorTick', 'off');
   legend(lgnd1, lgnd11, lgnd2, lgnd22, lgnd3, lgnd33);
   xlabel('Length [\mum]');
   ylabel('$\mathbf{\frac{dR}{R_0} [10^3]}$','Interpreter','LaTex');
   ylim([0, 15]);
   xlim([0, 350]);
   set(gca, 'fontsize', 20);
   % Save the file as PNG
   FileName = 'SteadyState_drR0';
   print(FileName,'-dpng','-r600');


   %% plot dT
   width = 3.39;     % Width in inches
   golden_mean = (sqrt(5)-1.0)/2.0;    % Aesthetic ratio
   height = width*golden_mean;    % Height in inches
   alw = 0.5;    % AxesLineWidth
```

```
fsz = 11;     % Fontsize
lw = 2.5;     % LineWidth
msz = 10;      % MarkerSize

h = figure;
pos = get(gcf, 'Position');
set(gcf, 'Position', [pos(1) pos(2) width*100, height*100]); %<- Set size
set(h, 'Renderer', 'painters');
set(gca, 'FontSize', fsz, 'LineWidth', alw); %<- Set properties
markerEdgeColor = [ 205 1 1;
                2 32 218;
                1 127 26 ]/255;
markerFaceColor = [ 223 161 161;
                148 158 222;
                134 209 149]/255;

errorbar( BackSide_425_param.xm/1E-6, BackSide_425_param.TempProf_dT,
BackSide_425_param.TempProf_dT_errorBar, 'o', 'LineWidth', lw, 'MarkerSize', msz,  'MarkerFaceColor',
markerFaceColor(1,:), 'MarkerEdgeColor',  markerEdgeColor(1,:), 'Color',  markerFaceColor(1,:)  );
hold on;
plot( BackSide_425_param.xm/1E-6, BackSide_425_param.linearFit_dT, '--','LineWidth', lw/1.2,
'MarkerSize', msz,  'Color',  markerEdgeColor(1,:) );
hold on;
errorbar( BackSide_450_param.xm/1E-6, BackSide_450_param.TempProf_dT,
BackSide_450_param.TempProf_dT_errorBar, 'd', 'LineWidth', lw, 'MarkerSize', msz,  'MarkerEdgeColor',
markerEdgeColor(2,:), 'MarkerFaceColor',  markerFaceColor(2,:), 'Color',  markerFaceColor(2,:)  );
hold on;
plot( BackSide_450_param.xm/1E-6, BackSide_450_param.linearFit_dT, '--','LineWidth', lw/1.2,
'MarkerSize', msz,  'Color',  markerEdgeColor(2,:) );
hold on;
errorbar( BackSide_475_param.xm/1E-6, BackSide_475_param.TempProf_dT,
BackSide_475_param.TempProf_dT_errorBar, 's', 'LineWidth', lw, 'MarkerSize', msz,  'MarkerFaceColor',
markerFaceColor(3,:), 'MarkerEdgeColor',  markerEdgeColor(3,:), 'Color',  markerFaceColor(3,:) );
hold on;
plot( BackSide_475_param.xm/1E-6, BackSide_475_param.linearFit_dT, '--','LineWidth', lw/1.2,
'MarkerSize', msz,  'Color',  markerEdgeColor(3,:) );


ttltext = sprintf( 'Title (place your own)' );
title(ttltext);
lgnd1 = sprintf( '425 mA (Experiment)');
lgnd11 = sprintf( '425 mA (Linear Fit)');
lgnd2 = sprintf( '450 mA (Experiment)' );
lgnd22 = sprintf( '450 mA (Linear Fit)');
lgnd3 = sprintf( '475 mA (Experiment)');
lgnd33 = sprintf( '475 mA (Linear Fit)');
set(gca,'YTick', 0:5:20, ...
      'TickLength'  , [.02 .02] , ...
       'XColor', [.3 .3 .3], ...
       'YColor', [.3 .3 .3], ...
       'XMinorTick', 'off', ...
       'YMinorTick', 'off');
legend(lgnd1, lgnd11, lgnd2, lgnd22, lgnd3, lgnd33);
xlabel('Length [\mum]');
ylabel('$\mathbf{dT [K]}$','Interpreter','LaTex');
```

```
ylim([0, 20]);
xlim([100, 350]);
set(gca, 'fontsize', 20);
% Save the file as PNG
FileName = 'SteadyState_dT';
print(FileName,'-dpng','-r600');


%% plot dT
width = 3.39;    % Width in inches
golden_mean = (sqrt(5)-1.0)/2.0;   % Aesthetic ratio
height = width*golden_mean;   % Height in inches
alw = 0.5;   % AxesLineWidth
fsz = 11;     % Fontsize
lw = 2.5;     % LineWidth
msz = 10;      % MarkerSize

h = figure;
pos = get(gcf, 'Position');
set(gcf, 'Position', [pos(1) pos(2) width*100, height*100]); %<- Set size
set(h, 'Renderer', 'painters');
set(gca, 'FontSize', fsz, 'LineWidth', alw); %<- Set properties
markerEdgeColor = [ 205 1 1;
                2 32 218;
                1 127 26 ]/255;
markerFaceColor = [ 223 161 161;
                148 158 222;
                134 209 149]/255;
ThermalCondVec = [BackSide_425_param.K_thrmlCond, BackSide_450_param.K_thrmlCond,
BackSide_475_param.K_thrmlCond]';
plot( FrontSideParam.LaserCurrentmA, ThermalCondVec, 'o', 'LineWidth', lw, 'MarkerSize', msz,
'MarkerFaceColor',  markerFaceColor(2,:), 'MarkerEdgeColor',  markerEdgeColor(2,:)  );


ttltext = sprintf( 'Title (place your own)' );
title(ttltext);
set(gca,'YTick', 0:50:150, ...
      'XTick', 400:25:500, ...
      'TickLength'  , [.02 .02] , ...
       'XColor', [.3 .3 .3], ...
       'YColor', [.3 .3 .3], ...
       'XMinorTick', 'off', ...
       'YMinorTick', 'off');
xlabel('Laser Current [mA]');
ylabel('Thermal Conductivity, K [W\mum^{-1}K^{-1}]');

ylim([0, 150]);
xlim([400, 500]);
set(gca, 'fontsize', 20);
% Save the file as PNG
FileName = 'SteadyState_K';
print(FileName,'-dpng','-r600');
```

2. Hermonic Analysis:

```
clear all;
close all;
clc

parameters = [];
%% Freq and measurement points
   fmin = 10;
   fmax = 100;
   delf = 10;

   Cpmin = 700;
   Cpmax = 800;
   delCp = 1;

   xMeasurement_1 = 400;              % [um]
   xMeasurement_2 = 600;              % [um]
%% Import Exp data
   expData = importPhaseChange( '10freq_phase.xlsx' );
%% Specify the physical constants for this heat trasnsfer problem
   parameters.w = 200;          % Beam Width          [um]
   parameters.d = 1.29;         % Beam thickness      [um]
   parameters.k = 113E-6;       % Thermal conductivity  [W/umK]
   parameters.rho = 2300E-18;   % Density             [kg/m3]
   parameters.Cp = 710;         % Thermal Capacity     [J/kgK]
   parameters.L = 1.4E3;        % Cantilever Beam length[um]
%% Define the problem
   parameters.Troom = 300;                    % Room Temp           [K]
   parameters.Toffset = 10;                   % DC value of the input [K]
   parameters.ACAmp = parameters.Toffset;          % AC Amplitude of input [K]
   parameters.delx = 10;                      % gradient in x direction [um]
   parameters.Nt = 10000;                     % No of points in t
   parameters.tmin = 0;

%% Solve the problem

   freqVec = fmin : delf : fmax;
   Cpvec = Cpmin : delCp : Cpmax;
   delPhaseShift = zeros(1, length(freqVec));
   delPhaseShiftAna = zeros(1, length(freqVec));
   isFigure = false;
   Error = zeros( length(Cpvec), length(freqVec) );
   minError = 1E20;
   matchCpIndex = 0;
%% Extract the first solution component as u.  This is not necessary
   for iCp = 1 : length(Cpvec)

      parameters.Cp = Cpvec(iCp);
      for iFreq = 1 : 4
         parameters.f = freqVec(iFreq);
         phaseShiftAna_1 = calculateAnaPhaseShift( parameters.k , parameters.rho, parameters.Cp,
parameters.f, xMeasurement_1 );
```

```
            phaseShiftAna_2 = calculateAnaPhaseShift( parameters.k , parameters.rho, parameters.Cp,
parameters.f, xMeasurement_2 );
            delPhaseShiftAna(iCp, iFreq) = abs( phaseShiftAna_1 - phaseShiftAna_2 );
            indexExpData = find( expData.freq == freqVec(iFreq) );
            Error( iCp, iFreq ) = ( abs(delPhaseShiftAna(iCp, iFreq) - expData.Phasechange(indexExpData,1))
)^2;
        end
        % minm Error Calculation
        tempMinmError = sum( Error(iCp, :) );
        if tempMinmError < minError
            minError = tempMinmError;
            matchCpIndex = iCp;
        end
    end
    CpFit = Cpvec(matchCpIndex)
    parameters.Cp = CpFit;
    fprintf('Fiting Complete, C_p = %0.1f J//kgK\n', CpFit);


    delPhaseShift = zeros(1, length(freqVec));
    delPhaseShiftAna = zeros(1, length(freqVec));
    for iFreq = 1 : length(freqVec)
        parameters.f = freqVec(iFreq);                          % Frequency of input    [Hz]
        parameters.tmax = 31 * (1/parameters.f);
        [uAC, uDC, u, x, t, TimePeriod] = solveCantiliver( parameters, isFigure );
        tmin = 20*TimePeriod : TimePeriod : 30*TimePeriod;
        tmax = zeros(1, length(tmin));
        phaseShift_1 = 0;
        phaseShiftAna_1 = 0;
        phaseShift_2 = 0;
        phaseShiftAna_2 = 0;

        for j = 1: length(tmin)
            tmax(j) = tmin(j) + TimePeriod;

            [T_x_0, tvec0, xNewMeasurement_0] = cutxt(u, x, t, tmin(j), tmax(j), 0);
            [T_x_measurement_1, tvec1, xNewMeasurement_1] = cutxt(u, x, t, tmin(j), tmax(j),
xMeasurement_1);
            [T_x_measurement_2, tvec2, xNewMeasurement_2] = cutxt(u, x, t, tmin(j), tmax(j),
xMeasurement_2);

            phaseShift_1 = calculatePhaseShift( T_x_0, T_x_measurement_1, tvec1, TimePeriod ) +
phaseShift_1;
            phaseShiftAna_1 = calculateAnaPhaseShift( parameters.k , parameters.rho, parameters.Cp,
parameters.f, xNewMeasurement_1 ) + phaseShiftAna_1;

            phaseShift_2 = calculatePhaseShift( T_x_0, T_x_measurement_2, tvec2, TimePeriod ) +
phaseShift_2;
            phaseShiftAna_2 = calculateAnaPhaseShift( parameters.k , parameters.rho, parameters.Cp,
parameters.f, xNewMeasurement_2 ) + phaseShiftAna_2;

        end
        count = length(tmin);
        delPhaseShift(iFreq) = abs( phaseShift_1/count - phaseShift_2/count );
```

```
        delPhaseShiftAna(iFreq) = abs( phaseShiftAna_1/count - phaseShiftAna_2/count );
        fprintf('%0.1f%% Complete\n', iFreq*100/length(freqVec));
    end

     %% export mat file

        freqVec = freqVec';
        delPhaseShiftFit = delPhaseShift' * 180 /pi;
        delPhaseShiftAnaFit = delPhaseShiftAna' *180 /pi;
        delPhaseShiftExp = expData.Phasechange *180/pi;
        delPhaseShiftExpErrorBar = expData.Errorbarindeg*180/pi;
        save('data_RelativePhaseShift.mat', 'CpFit','freqVec', 'delPhaseShiftFit', 'delPhaseShiftAnaFit',
'delPhaseShiftExp', 'delPhaseShiftExpErrorBar');

    %% Plot
    % Defaults for this blog post
    width = 3.39;     % Width in inches
    golden_mean = (sqrt(5)-1.0)/2.0    % Aesthetic ratio
    height = width*golden_mean;    % Height in inches
    alw = 0.5;    % AxesLineWidth
    fsz = 11;      % Fontsize
    lw = 2.5;      % LineWidth
    msz = 10;       % MarkerSize

    h = figure;
    pos = get(gcf, 'Position');
    set(gcf, 'Position', [pos(1) pos(2) width*100, height*100]); %<- Set size
    set(h, 'Renderer', 'painters');
    set(gca, 'FontSize', fsz, 'LineWidth', alw); %<- Set properties
    markerEdgeColor = [ 205 1 1;
                    2 32 218;
                    1 127 26 ]/255;
    markerFaceColor = [ 223 161 161;
                    148 158 222;
                    134 209 149]/255;
    plot(freqVec, delPhaseShiftFit, '-o', 'LineWidth', lw/1.2, 'MarkerSize', msz/3, 'Color',
markerEdgeColor(1,:), 'MarkerFaceColor',  markerEdgeColor(1,:));

    hold on;
    plot(freqVec, delPhaseShiftAnaFit, '-d', 'LineWidth', lw/1.2, 'MarkerSize', msz/3, 'Color',
markerEdgeColor(2,:), 'MarkerFaceColor',  markerEdgeColor(2,:) );
    hold on;
    h_errorBar = errorbar( expData.freq, delPhaseShiftExp, delPhaseShiftExpErrorBar,  's', 'Color',
markerEdgeColor(3,:), 'MarkerEdgeColor', markerEdgeColor(3,:) , 'LineWidth', lw/1.3, 'MarkerSize', msz
);
    % Plot Properties
    ttltext = sprintf( 'Relative Phase Shift (\\lambda_1 = %0.1fmm, \\lambda_2 = %0.1fmm)',
xMeasurement_1/1E3, xMeasurement_2/1E3 );
    title(ttltext);
    lgnd1 = sprintf( 'Numerical');
    lgnd2 = sprintf( 'Analytical' );
    lgnd3 = sprintf( 'Experiment');
    set(gca, 'YTick', 0:15:45, ...
          'TickLength'  , [.02 .02] , ...
          'XColor', [.3 .3 .3], ...
```

```
        'YColor', [.3 .3 .3], ...
        'XMinorTick', 'off', ...
        'YMinorTick', 'off');
    legend(lgnd1, lgnd2, lgnd3);
    xlabel('Frequency, f [Hz]');
    ylabel('(\Phi_{\lambda2} - \Phi_{\lambda1}) [Degree]');
    ylim([0, 45]);
    xlim([0, 110]);
    set(gca, 'fontsize', 20);
    % Save the file as PNG
    FileName = 'PhaseShiftExp';
    print(FileName,'-dpng','-r600');
```

3. Transient Analysis:

```
clear all;
close all;
clc;

%filename1 = 'scope_trn2_tip_550.csv';
%expData = importStep( filename1, 2 , 2001 );
filename1 = 'ref_400um_sq_600.xlsx';
filename2 = 'ref_600um_sq_575.xlsx';
filename3 = 'ref_700um_sq_600.xlsx';
sheetname1 = 'ref_400um_sq_600';
sheetname2 = 'ref_600um_sq_575';
sheetname3 = 'ref_700um_sq_600';
expData  = importLN( filename2, sheetname2 );

%plot(expData.Times, smooth( smooth(expData.VoltV) ), 'o');
% NormInPow = expData.InputVoltage - min(expData.InputVoltage);
% NormInPow = NormInPow / max(NormInPow);
NormInPow = expData.Input;
%expData.OutWsmooth = smooth( expData.OutputVoltage );
windowSize = 1;
expData.OutWsmooth = filter(ones(windowSize, 1)/windowSize, 1, expData.Output);
% NormOutPow = expData.OutWsmooth - min(expData.OutWsmooth);
% NormOutPow = NormOutPow / max(NormOutPow);
for i = 1 : 4
    expData.OutWsmooth = smooth( expData.OutWsmooth );
end
NormOutPow = expData.OutWsmooth;
%% Plot
    width = 3.39;                          % Width in inches
    golden_mean = (sqrt(5)-1.0)/2.0;       % Aesthetic ratio
    height = width*golden_mean;            % Height in inches
    alw = 0.5;                             % AxesLineWidth
    fsz = 11;                              % Fontsize
    lw = 2.5;                              % LineWidth
    msz = 10;                              % MarkerSizedes

    h = figure;
```

```
    pos = get(gcf, 'Position');
    set(gcf, 'Position', [pos(1) pos(2) width*100, height*100]); %<- Set size
    set(h, 'Renderer', 'painters');
    set(gca, 'FontSize', fsz, 'LineWidth', alw);    %<- Set properties
    markerEdgeColor = [ 205 1 1;
                   2 32 218;
                   1 127 26 ]/255;
    markerFaceColor = [ 223 161 161;
                   148 158 222;
                   134 209 149]/255;

%     yyaxis left
%     plot(expData.second1, NormInPow/10, 'Color', markerEdgeColor(1, :), 'linewidth', lw );
%
%     yyaxis right
%     plot(expData.second1, NormOutPow, 'Color', markerEdgeColor(2, :), 'linewidth', lw  );
    [hAx,hLine1,hLine2] = plotyy(expData.second1, NormInPow, expData.second1, NormOutPow );
    lgnd1 = sprintf( 'Input');
    lgnd2 = sprintf( 'Output');
    legend( lgnd1, lgnd2 );
    ylabel(hAx(1),'Voltage [V]') % left y-axis
    %ylabel(hAx(2),'Output Voltage [V]') % right y-axis
    hLine1.Color = markerEdgeColor(1, :);
    hLine1.LineWidth = lw;
    hLine2.Color = markerEdgeColor(2, :);
    hLine2.LineWidth = lw;
    ttltext = sprintf( 'Title (place your own)' );
    %title(ttltext);
    set(gca, 'TickLength'  , [.02 .02] , ...
          'XColor', [.2 .2 .2], ...
           'YColor', [.2 .2 .2], ...
           'XMinorTick', 'off', ...
           'YMinorTick', 'off');
    xlabel('Time [s]');
    % X limit
    xlimit = [-0.21 0.33]
    hAx(1).XLim = xlimit;
    hAx(2).XLim = xlimit;
    %ylim([0, 1.3]);
    set(gca, 'fontsize', 20);
    hAx(2).FontSize = 20;
    hAx(1).YColor = markerEdgeColor(1, :);
    hAx(2).YColor = markerEdgeColor(2, :);
    hAx(1).TickLength = [.02 .02];
    hAx(2).TickLength = [.02 .02];
    % Save the file as PNG
    FileName = 'InOut2';
    print(FileName,'-dpng','-r600');
```